The Role of Glutaredoxin-2 in the Modulation of Mitochondrial Bioenergetics in Female Mice Fed a High-Fat Diet

By ©Robert Gill, B.Sc. (Honours) A thesis submitted

to the school of graduate studies in partial fulfilment of the

requirements for the degree of

Master of Science, Department of Biochemistry, Faculty of Science

Memorial University of Newfoundland

May 2020

St. John's Newfoundland and Labrador

Abstract

Our group recently observed that male mice containing a deletion for the gene encoding the thiol oxidoreductase glutaredoxin-2 (GRX2) were protected from diet-induced obesity (DIO) and the development of related disorders (e.g. fatty liver disease). This effect was associated with increased fuel combustion in muscles. In the present study, I assessed if deleting the *Grx2* gene protected female mice from DIO. Unlike male mice, in this study female wild-type (WT) littermates were completely resistant to developing DIO and related co-morbidities. Additionally, deletion of the *Grx2* gene did not alter the weight gain profiles, adiposity, intrahepatic fatty acid and glycogen levels, or circulating triglycerides in these mice. Furthermore, while differences in reactive oxygen species generation in liver mitochondria were observed, this trend was not present in muscle mitochondria. Mitochondrial bioenergetics data revealed no differences in mitochondrial respiration between WT and GRX2-deficient female mice fed a control or high-fat diet.

Acknowledgments

Firstly, I would like to acknowledge the contributes of my supervisor Dr. Ryan J. Mailloux to this thesis and my continued learning. His approach to scientific research and great mentorship will not be forgotten. I would like to thank my supervisory committee consisting of Dr. Scott Harding and Dr. Robert Bertolo for their constructive feedback and many suggestions that improved this project and thesis. I would like to thank my lab mates; Adrian Young, Katie Oldford, Nidhi Kuksal, Ibrahim Dogar, and Sarah Mallay for aiding in conducting my experiments. Especially Adrian, who provided me with continued support, training, and answers to countless questions. Lastly I would like to acknowledge my family and friends that have been supportive throughout my whole education and journey in science.

Table of Contents

List of Tables

List of Equations

List of Figures

List of Abbreviations and Symbols

ADP	Adenosine diphosphate
ANOVA	Analysis of variance
ANT	Adenine nucleotide transporter
AMP	Adenosine monophosphate
ATP	Adenosine triphosphate
AUR	Amplex UltraRed
BM	Basic medium
bp	Base pairs
BSA	Bovine serum albumin
CAC	Carnitine/acylcarnitine carrier
cAMP	Cyclic AMP
CD	Control diet
CoA	Coenzyme A
Cys	Cysteine
DIO	Diet-induced obesity
DMSO	Dimethyl sulfoxide
DNA	Deoxyribonucleic acid
DNP	Dinitrophenyl
DNPH	2,4-dinitrophenylhydrazine
DTNB	5,5'-dithiobis (2-nitrobenzoic acid)
EGTA	ethylene glycol-bis (β-aminoethyl ether)-N,N,N',N'- tetraacetic acid

eIF4E	Eukaryotic initiation factor 4F complex
ETC	Electron transport chain
ETFQO	Electron transferring flavoprotein: ubiquinone oxidoreductase
FAD	Flavin adenine dinucleotide
$FADH_2$	Flavin adenine dinucleotide reduced
Fe-S	Iron-sulfur
FMN	Flavin mononucleotide
GK	Glycerol kinase
GLUT	Glucose transporter
GPO	Glycerol-3-phosphate oxidase
GPX	Glutathione peroxidase
GR	Glutathione reductase
GRX2	Glutaredoxin-2
GSH	Glutathione
GSSG	Glutathione disulfide
GTP	Guanosine-5'-triphosphate
H&E	Hematoxylin and eosin
H^+	Proton
H_2O_2	Hydrogen peroxide
HCl	Hydrogen chloride
HEPES	4-(2-hydroxyethyl)-1-piperazineethanesulfonic acid
HFD	High-fat diet
HM	Homogenizing medium

HMMPS	N-(3-isopropyl)-3methoxy-5-methylaniline
HRP	Horseradish peroxidase
IMS	Intermembrane space
KCl	Potassium chloride
KEAP1	Kelch-like ECH-associated protein 1
KGDH	α-ketoglutarate dehydrogenase
KMV	α-keto-β-methyl-n-valeric acid
LDL	Low-density lipoprotein
LPL	Lipoprotein lipase
MESH	Mannitol/EGTA/Sucrose/HEPES buffer
$MgCl_2$	Magnesium chloride
MIM	Mitochondrial inner membrane
mM	millimolar
MPC	Mitochondrial pyruvate carrier
mtDNA	Mitochondrial DNA
NAD^+	Nicotinamide adenine dinucleotide
NADH	Nicotinamide adenine dinucleotide reduced
$NADP^+$	Nicotinamide adenine dinucleotide phosphate
NADPH	Nicotinamide adenine dinucleotide phosphate reduced
NDUFS1	NADH:Ubiquinone Oxidoreductase Core Subunit 1
NNT	Nicotinamide nucleotide transhydrogenase
Nrf2	NF-E2p45-related factor 2
O_2	Diatomic oxygen

$O_2^{\bullet-}$	Superoxide
$OH^{\bullet}$	Hydroxyl radical
$OHOO^-$	Peroxynitrite
PAS	Periodic Acid-Schiff
PCR	Polymerase chain reaction
PDH	Pyruvate dehydrogenase complex
PKA	Protein kinase A
P_i	Inorganic phosphate
PMF	Proton motive force
PRX	Peroxiredoxin
PSH	Reduced protein
PSSG	Glutathionylated protein
PVDF	Polyvinylidene difluoride
Q	Ubiquinone
QH_2	Ubiquinol
RCR	Respiratory control ratio
RIPA	Radioimmunoprecipitation assay
ROS	Reactive oxygen species
SD	Standard deviation
SeOH	Selenic acid
Se-SG	Selenenyl-glutathione sulfide
SEM	Standard error of the mean

SERCA	Sarco/endoplasmic reticulum Ca2+-ATPase-1
SGLT	Sodium-glucose transporter
SO_2H	Sulfinic acid
SO_3H	Sulfonic acid
SOD	Superoxide dismutase
SOH	Sulfenic acid
STAT5	Signal transducer and activation of transcription 5
TBE	Tris-Borate-EDTA
TCA	Tricarboxylic acid cycle
TNB	5-thio-2-nitrobenzoic acid
TPP	Thiamine pyrophosphate
TR2	Thioredoxin reductase-2
TRX	Thioredoxin
U	Unit
UCP	Uncoupling protein
VLDL	Very low-density lipoprotein
WHO	World Health Organization
WT	Wild type
w/v	Weight by volume

Chapter 1: Introduction

1.1 Energy Metabolism

The "universal energy currency" for cells is commonly known to be adenosine triphosphate (ATP) as it drives almost all physiological processes ranging from the movement of muscles for locomotion to aiding in the transport of molecules into cells via active transport (1). Often mitochondria are referred to as the "powerhouse" for good reason since these double-membraned organelles are responsible for producing ~90% of the ATP in many mammalian cells (1). The superior ATP producing capacity of mitochondria is attributed to its highly-folded and selectively permeable mitochondrial inner membrane (MIM), which allows the conservation of a large amount of energy liberated during fuel metabolism for the production of ATP (2). Additionally, the highly folding nature of the MIM creates deep invaginations called cristae. These cristae are enriched in various enzymes and multi-subunit complexes that are critical for fuel metabolism and ATP production (1). Furthermore, while mammalian mitochondrial DNA (mtDNA) only consists of 15,000-17,000 base pairs (bp) of double stranded DNA, this DNA has been highly conserved with estimations of sequence evolution at 2% per million years (3). This small amount of mtDNA transcribes only 13 protein products that are all involved in the electron transport chain (ETC) and crucial for mitochondrial function (3).

The metabolism of carbon sources, such as glucose, fatty acids, and amino acids, for energy is essential for all mammalian life. Fuel combustion and cellular respiration occurs in mitochondria, subsequently generating a proton-motive force (PMF). This PMF is composed of two components, an electrical ($\Delta\psi_m$) and chemical (ΔpH) gradient, making up the electrochemical gradient. The electrochemical gradient occurs across the MIM with the chemical gradient making up the majority of stored potential energy (4). A description of carbon

oxidation, along with how mitochondria harness potential energy to form ATP, will be conveyed in the following sections.

1.1.1 Glycolysis

The complete oxidation of glucose to carbon dioxide and water results in the release of 2,840 kJ/mol energy (2). Heterotrophs such as herbivores and omnivores meet most of their glucose demands through the consumption of autotrophs (e.g. plants), which utilize solar energy in conjunction with CO_2 and H_2O to form sugars. Carnivores, on the other hand, rely mostly on gluconeogenesis in hepatic tissue to meet their glucose demands, a process that can form glucose from non-carbohydrate molecules such as amino acids and glycerol (2). Use of glucose for the production of ATP depends on its uptake, transformation, and degradation in the cytosol of mammalian cells. Full degradation of glucose by glycolysis yields two pyruvate, which can undergo further oxidation in mitochondria when molecular oxygen is available (aerobic respiration) (2). During low O_2, however, pyruvate is reduced in the presence of NADH by lactate dehydrogenase, forming lactate (2). This is called anaerobic respiration and is vital for maintaining glycolytic flux when O_2 is limiting (2). Glycolysis produces a net yield of 2 ATP per glucose molecule, along with reducing 2 cytosolic NAD^+ (Equation 1.1) (2). Glycolysis utilizes 10 enzymes to generate ATP and pyruvate, which can be divided into two sub-categories (Figure 1.1): the preparatory phase (requires ATP input), and the payoff phase (yields ATP) (2).

Glycolysis takes place in the cytoplasm of mammalian cells, but glucose has to be transported first from the intestinal tract, into the blood stream, and then across the cell membrane. This transport begins in the gut lumen where glucose and galactose are taken up by epithelial cells by glucose transporter-2 (GLUT2) or the symporter, sodium-glucose transporter (SGLT) (2). It is important to recognize that fructose can be taken up into epithelial cells by the

fructose transporter, GLUT5 (2). Once in the epithelial cell, glucose/galactose/fructose can be transported across the basolateral side of the cell by GLUT2, entering the blood stream (2). These molecules then enter the hepatic portal vein with galactose/fructose taken up by the liver and metabolized, while most of the glucose remains in circulation to be taken up by other cells such as myocytes. This uptake of glucose is typically insulin dependent; insulin signalling induces translocation of GLUT4 transporters to the cell membrane allowing glucose uptake (2). It is in this manner that organisms maintain blood glucose homeostasis. Once in the cell, the first step of glucose metabolism is catalysis by hexokinase, which expends ATP to phosphorylate glucose generating glucose-6-phosphate (2). Hexokinase has four isozymes (I to IV) with hexokinase IV differing in kinetic and regulatory properties and often referred to as glucokinase (2). One of the key differences between hexokinase I-III and IV is their affinity for glucose and regulation by glucose-6-phosphate (2). Hexokinase IV has a lower affinity for glucose, with a Km of 5 mM in rats (compared to 0.007-0.045 mM for hexokinase I-III), and is not allosterically inhibited by glucose-6-phosphate (2,5). These characteristics allow the liver to take in large amounts of glucose after a meal for storage. However, when glucose is scarce, it allows for glucose, generated by gluconeogenesis, to leave the cell and be transported to cells such as myocytes (2). Next, the hexose ring of glucose-6-phosphate is rearranged by phosphohexose isomerase, generating fructose-6-phosphate (2). Once formed, fructose-6-phosphate is phosphorylated on the C-1 position by phosphofructokinase-1 in an ATP dependent fashion, yielding fructose-1,6-bisphosphate (2). The next step results in the cleavage of fructose-1,6-bisphosphate into two 3-carbon sugar molecules: glyceraldehyde-3-phosphate and dihydroxyacetone phosphate (2). This step is catalyzed by aldolase and the resulting dihydroxyacetone phosphate is transformed into another glyceraldehyde-3-phosphate molecule

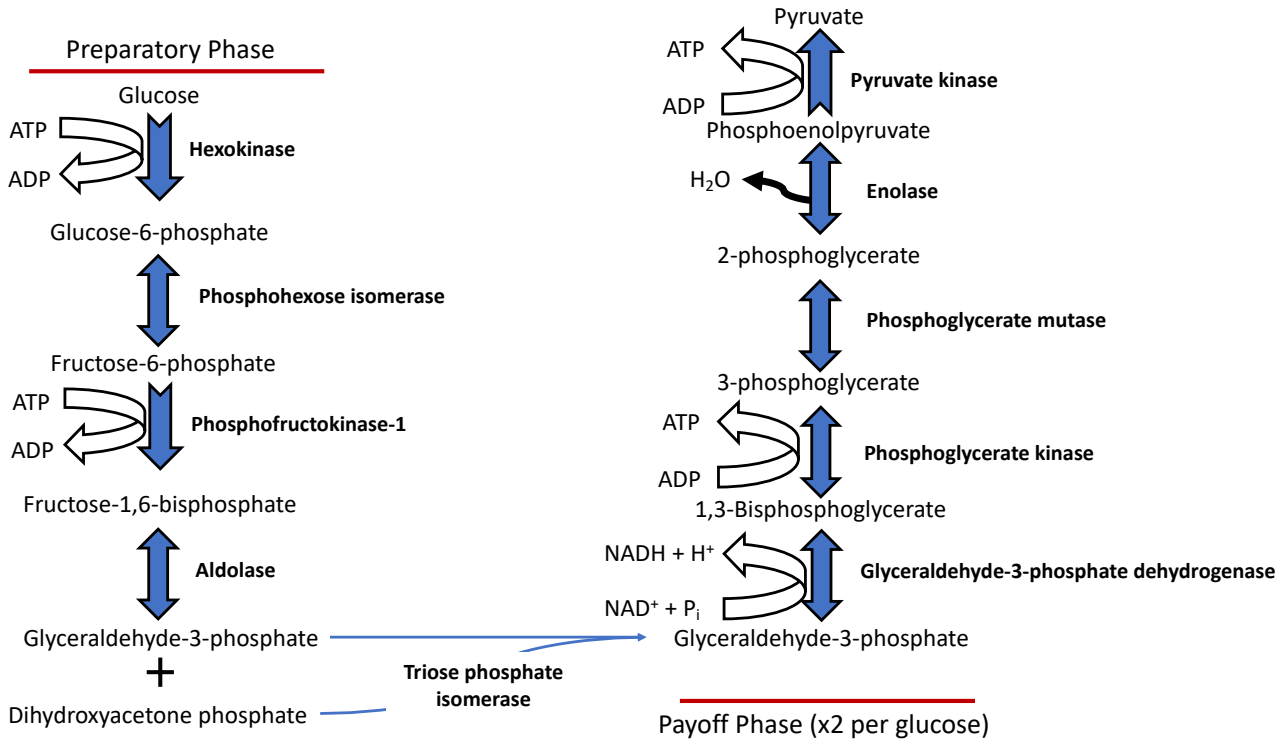

Figure 1.1: Glycolysis.

by triose phosphate isomerase (2). Once formed, the two glyceraldehyde-3-phosphate molecules generated by the preparatory phase are used in the payoff phase.

The payoff phase starts with the phosphorylation of glyceraldehyde-3-phosphate by glyceraldehyde-3-phosphate dehydrogenase (2). Phosphorylation requires inorganic phosphate and is coupled to glyceraldehyde-3-phosphate oxidation, generating 1,3-bisphosphoglycerate and NADH (2). It is important to note that all the steps of the payoff phase occur in duplicate, as one glucose produces 2 glyceraldehyde-3-phosphate molecules. Next, the high energy 1,3-bisphosphoglycerate is utilized to drive the substrate level phosphorylation of ADP, producing ATP and 3-phosphoglycerate, which is catalyzed by phosphoglycerate kinase (2). Following this, phosphoglycerate mutase moves the phosphate from the C-3 position to C-2, producing 2-phosphoglycerate (2). This is achieved through a dehydration reaction which forms a double bond between the C-1 and C-2 positions (2). Finally, phosphoenolpyruvate is then used for the substrate level phosphorylation of ADP, producing ATP, a reaction that is mediated by pyruvate kinase (2). The ATP produced from glycolysis is utilized to do work while the NADH must be shuttled into the mitochondrial matrix to donate its electrons to the ETC.

The MIM is impermeable to NADH; therefore, there are two mechanisms by which this electron carrier donates its electrons to the ETC: 1) the malate-aspartate shuttle and 2) the glycerol-3-phosphate shuttle. The malate-aspartate shuttle works by malate dehydrogenase utilizing NADH to yield malate from oxaloacetate which can be transported across the MIM by the malate-α-ketoglutarate transporter (2). Matrix malate dehydrogenase can then regenerate NADH and oxaloacetate allowing NADH to donate its electrons to complex I (2). Oxaloacetate must then be returned to the cytosol in order to allow the cycle to continue and this is achieved through its conversion to aspartate and shuttling through the glutamate-aspartate transporter (2).

Alternatively, the glycerol-3-phosphate shuttle utilizes cytosolic glycerol-3-phosphate dehydrogenase and NADH to convert dihydroxyacetone into glycerol-3-phosphate (2). An isozyme of glycerol-3-phosphate dehydrogenase, which is bound to the outer face of the MIM, reoxidizes the glycerol-3-phosphate back into dihydroxyacetone. The FAD subunit of the MIM bound glycerol-3-phosphate dehydrogenase accepts the electrons during this reaction and donates them to the Q pool (2). Since the electrons from the glycerol-3-phosphate shuttle bypasses complex I, each NADH only produces ~1.5 instead of ~2.5 ATP (2).

Equation 1.1:

$$\textbf{Glucose} + 2\,\textbf{NAD}^+ + 2\,\textbf{ADP} + 2\,\textbf{P}_i \rightarrow 2\,\textbf{Pyruvate} + 2\,\textbf{NADH} + 2\,\textbf{H}^+ + 2\,\textbf{ATP} + 2\,\textbf{H}_2\textbf{O}$$

1.1.2 Krebs Cycle

The Krebs cycle (citric acid cycle or tricarboxylic acid cycle) is the most central metabolic pathway in all organisms as it is responsible for both the production of ATP and genesis of precursors for the biosynthesis of macromolecules. The cycle is comprised of eight enzymatic steps that couple the oxidation of various substrates to the production of the electron carriers NADH, $FADH_2$, and GTP/ATP (Figure 1.2; Equation 1.3) (2). A number of different fuels, including amino acids, ketone bodies, fatty acids, and many others, can serve as substrates for the Krebs cycle (2). Oxidation of these fuels and the formation of the different electron carriers is coupled to the irreversible production of CO_2. The full oxidation of glucose, when O_2 is available, first requires the production of acetyl-CoA from pyruvate after the import of pyruvate into the mitochondrial matrix. The transport of pyruvate into the mitochondrial matrix is facilitated by mitochondrial pyruvate carrier (MPC) transporters (6). Mitochondria contain two

MPC isoforms, MPC1 and 2, which couple the unfavourable transport of pyruvate to the return of protons into the matrix (6).

Once inside the matrix of the mitochondria, the pyruvate must be converted into acetyl-CoA by pyruvate dehydrogenase (Equation 1.2). The pyruvate dehydrogenase complex (PDH) is made up of three subunits: E1: pyruvate dehydrogenase, E2: dihydrolipoyl transacetylase, and E3: dihydrolipoyl dehydrogenase (2). The E1 subunit is responsible for the release of C-1 of pyruvate as CO_2 and the coupling of C-2 to the thiamine pyrophosphate (TPP) group forming a hydroxyethyl group (2). Step 2 of this reaction oxidizes the hydroxyethyl group to acetate, utilizing the electrons released to reduce the disulfide bond in the lipoyllysine group of E2 (2). The acetyl group from this reaction is then esterified to one of the reduced lipoyl sulfides (-SH) (2). Next, a transesterification reaction occurs that results in the conjugation of Coenzyme A (CoA) to the acetyl group, releasing acetyl-CoA from the complex (2). The E3 subunit of this complex is responsible for the regeneration of the lipoyllysine disulfide, accomplished via two reactions: 1) the reduced lipoyllysine is oxidized by E3-bound FAD to regenerate the disulfide bond and form FADH, and 2) the FADH formed reduces NAD^+ forming NADH and reoxidizes the E3 subunit (2). The NADH formed by PDH can then donate its electrons to complex I yielding ~2.5 ATP (2).

Equation 1.2:

$$\textbf{Pyruvate} + \textbf{NAD}^+ + \textbf{CoA-SH} \rightarrow \textbf{NADH} + \textbf{Acetyl-CoA} + \textbf{CO}_2$$

Following its production, acetyl-CoA is condensed with oxaloacetate by citrate synthase via a Claisen-type condensation reaction to generate citric acid (2). It is important to note that the

initial production of oxaloacetate is produced from pyruvate and a bicarbonate molecule via pyruvate carboxylase and is required to prime the Krebs cycle (2). The next step in the cycle results in the formation of isocitrate from citric acid through the intermediate formation of cis-aconitate via the enzyme aconitase (2). This reaction proceeds through a dehydration reaction followed by a hydration reaction removing the hydroxy group from C-3 and placing it on C-2 (2). In the next step, isocitrate dehydrogenase oxidizes isocitrate using the cofactor NAD^+ to form NADH and the intermediate oxalosuccinate, which undergoes immediate decarboxylation to form α-ketoglutarate and release CO_2 (2). It should be noted that there are two isoforms of isocitrate dehydrogenase present in cells. The NAD^+-requiring form in the Krebs cycle is localized to the mitochondrial matrix. The other form utilizes $NADP^+$ and is present in both the cytosol and mitochondrial matrix and generates NADPH required for reductive reactions, such as maintenance of antioxidant systems (2). Next in the cycle, α-ketoglutarate dehydrogenase catalyzes the conversion of α-ketoglutarate to succinyl-CoA resulting in the reduction of another NAD^+ molecule (2). This reaction requires the cofactor CoA and results in the release of CO_2 (2). Succinyl-CoA has a high energy thioester bond and its breakage releases energy that can be coupled to the formation of ATP/GTP and results in the formation of succinate and release of CoA (2). The enzyme that catalyzes this reaction is succinyl-CoA synthase, of which there are two isozymes in animal cells, either specific for ADP or GDP (2). The GTP formed can be used to form ATP via nucleotide diphosphate kinase by transferring its electrons to ADP (2). Next, succinate is oxidized via succinate dehydrogenase (complex II), which is bound to the inner side of the MIM in eukaryotes (2). This reaction results in the formation of fumarate and the reduction of an FAD molecule within the succinate dehydrogenase; these electrons passed to FAD are then shuttled through iron-sulfur (Fe-S) clusters to the ETC yielding ~1.5 ATP (2). The

fumarate formed by this reaction can then undergo a hydration reaction to form L-malate by fumarase (2). The last reaction of this cycle is the conversion of L-malate to oxaloacetate resulting in the reduction of an NAD^+ molecule (2). This reaction proceeds via L-malate dehydrogenase and the oxaloacetate formed can then restart the cycle by condensing with a new acetyl-CoA molecule (2).

Equation 1.3:

$$\textbf{Acetyl-CoA + 4 NAD}^+ \textbf{ + FAD + GDP + P}_i \rightarrow \textbf{3 CO}_2 \textbf{ + 4 NADH + 4 H}^+ \textbf{ + FADH}_2 \textbf{ + GTP/ATP}$$

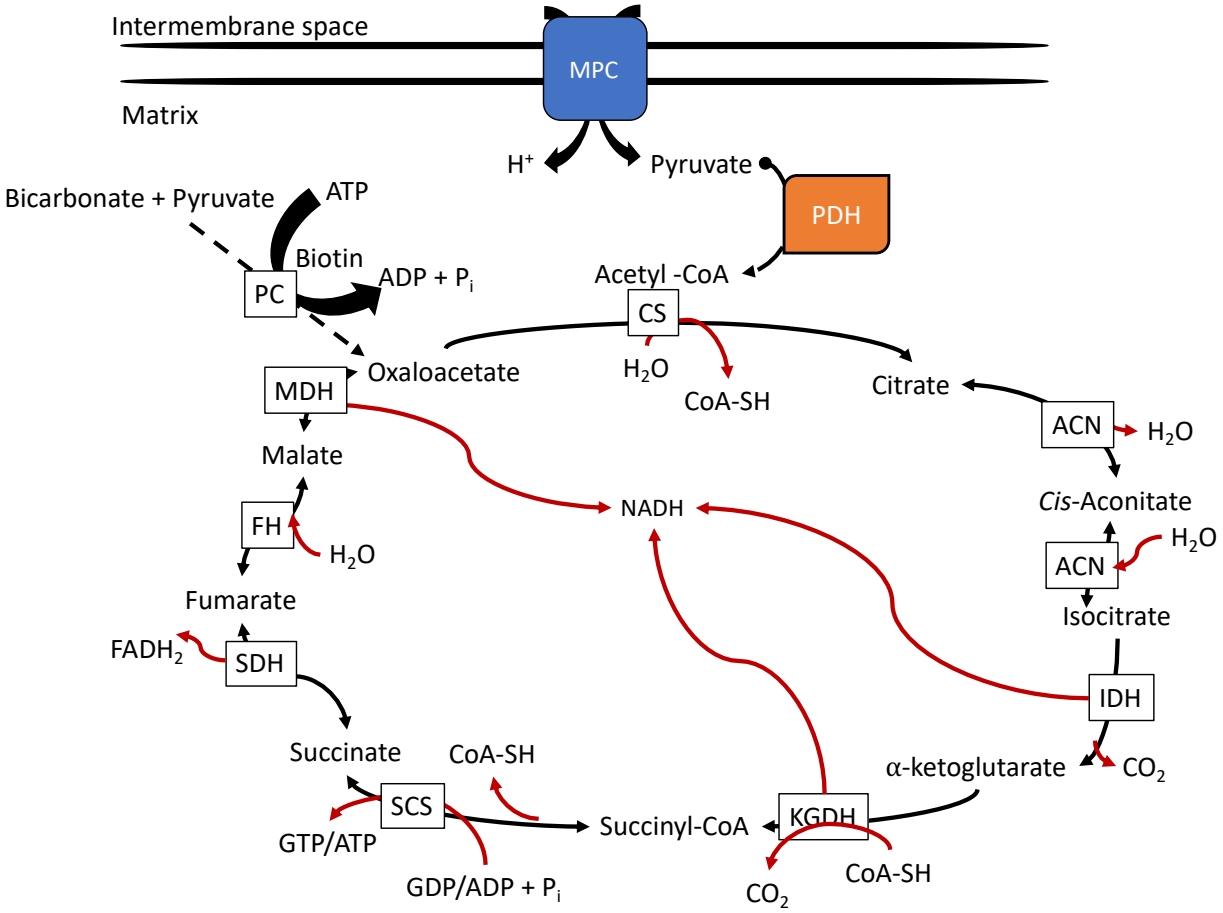

Legend

- PC- Pyruvate Carboxylase
- CS- Citrate Synthase
- ACN- Aconitase
- IDH- Isocitrate Dehydrogenase
- KGDH- α-ketoglutarate Dehydrogenase Complex
- SCS- Succinyl-CoA Synthase
- SDH- Succinate Dehydrogenase
- FH- Fumarase
- MDH- Malate Dehydrogenase
- MPC- Mitochondrial pyruvate carrier
- PDH- Pyruvate dehydrogenase complex

Figure 1.2: Mitochondrial pyruvate import and Krebs cycle pathway.

1.1.3 Lipid Metabolism and β-Oxidation

The ability of animals to store fats provided an evolutionary advantage for maintenance of energy homeostasis during starvation. While lipid storage is possible in all organisms, including prokaryotes, only vertebrates have evolved specialized cells called adipocytes (7). Fatty acids are an important source and major form of storage of energy in mammalian adipocytes; their richness for energy is attributed to two properties: 1) hydrophobicity, which allows the storage of higher quantities of fatty acids in adipocytes, and 2) oxidation of a long chain fatty acid, such as palmitate, yields 108 ATP, whereas glucose oxidation produces only 36 ATP (2). The major product of fatty acid synthesis in mammals is palmitate (16-C chain), which is packaged into cells as triglycerides (2). Triglycerides are the combination of 3 fatty acids attached to a glycerol backbone and a major characteristic of these triglycerides is their hydrophobicity. This hydrophobic nature requires that triglycerides be packaged with proteins into a lipoprotein particle to allow its transport in blood.

In mammals, there are three sources of fatty acids that cells can utilize for fuel. These are fatty acids obtained from diet, fatty acids mobilized from adipose tissue stores, and endogenous fatty acid synthesis by the liver from precursors such as excess carbohydrates (2). Dietary fatty acids are digested and absorbed in the small intestine, involving the secretion of bile from the gallbladder and lipases from the pancreas (2). Bile allows the insoluble fatty acids to form micelles, thereby increasing the fatty acids' exposure to water soluble lipases and aiding in the breakdown of triglycerides into free fatty acids, monoacylglycerol, diacylglycerol, and glycerol. These breakdown products then diffuse into epithelial cells where they become reconstituted into triglycerides by acyl-CoA: monoacylglycerol acyltransferase and acyl-CoA: diacylglycerol acyltransferase (2). Then these reconstituted triglycerides are packaged with cholesteryl esters,

cholesterol, phospholipids, and proteins into lipoprotein particles called chylomicrons, which are released into the lymphatic system (2). The proteins in the chylomicron include apolipoproteins and aid in transport of lipids in the blood (2). Once these lipid particles travel from the lymphatic system into the blood stream, they are carried to either muscle tissue to be used as energy or adipose tissue to be stored as fat. Lipoprotein lipase in the capillaries of these tissues is activated by apoC-II on the lipoprotein's surface, resulting in hydrolysis of triglycerides to fatty acids and glycerol that can be taken up by cells (2). Muscle tissue oxidizes these fatty acids for fuel while adipocytes re-esterify them for storage. The chylomicrons that have been depleted of triglycerides still contain cholesterol and apolipoproteins which are carried in the blood to the liver (2). These chylomicron remnants are taken up by the hepatocyte (receptor-mediated binding to apoE) and the remaining fatty acids are either used for energy or repackaged as very low-density lipoproteins (VLDL) to be released into the blood and transported to adipose tissue (2).

Furthermore, it is important to note that hepatocytes have the ability for *de novo* lipogenesis through fatty acid synthase and a malonyl-CoA molecule. This malonyl-CoA is derived from an acetyl-CoA molecule and acetyl-CoA carboxylase (2). It is key to emphasize here that acetyl-CoA is at the crossroads for both anabolic and catabolic pathways. This relationship is tightly regulated to prevent the formation of a futile cycle and allows acetyl-CoA to be metabolized when the body requires energy, but diverted for fatty acid synthesis and storage when energy demands are met (2). These fatty acids can then be packaged into triglycerides and VLDL for release into the blood stream (2). VLDL transports fatty acids to tissues in the same manner as chylomicrons, and as they lose triglycerides and apolioproteins, they become low-density lipoproteins (LDL) (2). These LDL particles are rich in cholesterol and cholesterol esters and responsible for some of the transport of cholesterol to extrahepatic tissues.

The removal of LDL from circulation is achieved through the LDL receptor, localized in hepatic tissue, that recognizes apoB-100 and through endocytosis engulfs both the LDL particle and receptor (2).

Lastly, adipocytes are the cells responsible for the storage of fats into a lipid droplet which is surrounded by perilipins, proteins responsible for containing the lipids (2). The fats stored in these droplets can be mobilized for energy when blood glucose becomes low or when cells, such as muscle, require excess energy (e.g. during exercise). This mobilization occurs through the release of epinephrine and glucagon which activate surface located adenylyl cyclase on adipocytes (2). Adenylyl cyclase produces cyclic AMP (cAMP), a second messenger that activates cyclic AMP-dependent protein kinase (PKA) (2). PKA then phosphorylates perilipins resulting in a conformational change that exposes the lipid droplet to the rest of the cell (2). PKA also activates hormone-sensitive lipases that make contact with the lipid droplet releasing fatty acids (2). The fatty acids then can pass from the adipocyte into the blood stream where they noncovalently bind serum albumin (2). Serum albumin-bound fatty acids can then be transported to tissues in which they are released and taken up by plasma membrane transporters (2).

Once transported into the cell, fatty acids must become activated as fatty acyl-CoA molecules and then make their way into the mitochondrial matrix to undergo β-oxidation. This is achieved through an outer mitochondrial membrane bound protein, acyl-CoA synthetase, which catalyzes the addition of CoA at the expense of one ATP (2). Next, the transport of acyl-CoA into the mitochondrial matrix occurs in three steps: 1) a carnitine group is exchanged for the CoA group on the fatty acid by the enzyme carnitine acyl transferase-1, 2) the antiporter carnitine/acyl-carnitine carrier moves the acyl-carnitine into the matrix in exchange for a

carnitine molecule, and 3) carnitine acyl transferase-2 in the matrix exchanges the carnitine group for a CoA to regenerate an acyl-CoA molecule (2).

Once into the matrix, the fatty acyl-CoA undergoes β-oxidation (Figure 1.3). The first step involves acyl-CoA dehydrogenase, which oxidizes the fatty acyl-CoA forming a double bond between the α and β carbons (2). Oxidation is coupled to the reduction of FAD in acyl-CoA dehydrogenase. Once formed, $FADH_2$ is oxidized by electron transferring flavoprotein and electron transferring flavoprotein oxidoreductase (ETFQO), resulting in the reduction of ubiquinone (Q) to ubiquinol (QH_2) in the ETC (2). Next, the newly formed enoyl-CoA molecule is hydrated by enoyl-CoA hydratase resulting in hydroxylation of the β carbon, forming β-hydroxylacyl-CoA (2). Then β-hydroxylacyl-CoA dehydrogenase couples the oxidation of β-hydroxylacyl-CoA to the reduction of NAD^+ to NADH (2). The resulting β-ketoacyl-CoA is then cleaved in the presence of CoA by thiolase forming acetyl-CoA and an acyl-CoA molecule that is now 2 carbons shorter (2). For example, oxidation of palmitate, which contains 16 carbons, results in the formation of one acetyl-CoA and a C-14 myristoyl-CoA. Once formed myristoyl-CoA is subjected to further oxidation until the carbon chain has been fully degraded. For palmitoyl-CoA, 7 passes through β-oxidation is required for full degradation to 8 acetyl-CoA, 7 $FADH_2$, and 7 NADH molecules (Equation 1.4) (2). NADH and $FADH_2$ donate their electrons to the ETC resulting in a yield of 28 ATP. The 8 acetyl-CoA molecules can undergo further oxidation by the Krebs cycle, resulting in a yield of 80 ATP, making a total of 108 ATP formed from palmitoyl-CoA.

Equation 1.4:

$$\textbf{Palmitoyl-CoA + 7 CoA + 7 FAD + 7 NAD}^{+}\textbf{ + 7 H}_2\textbf{O} \rightarrow \textbf{8 acetyl-CoA + 7 FADH}_2\textbf{ + 7 NADH + 7 H}^{+}$$

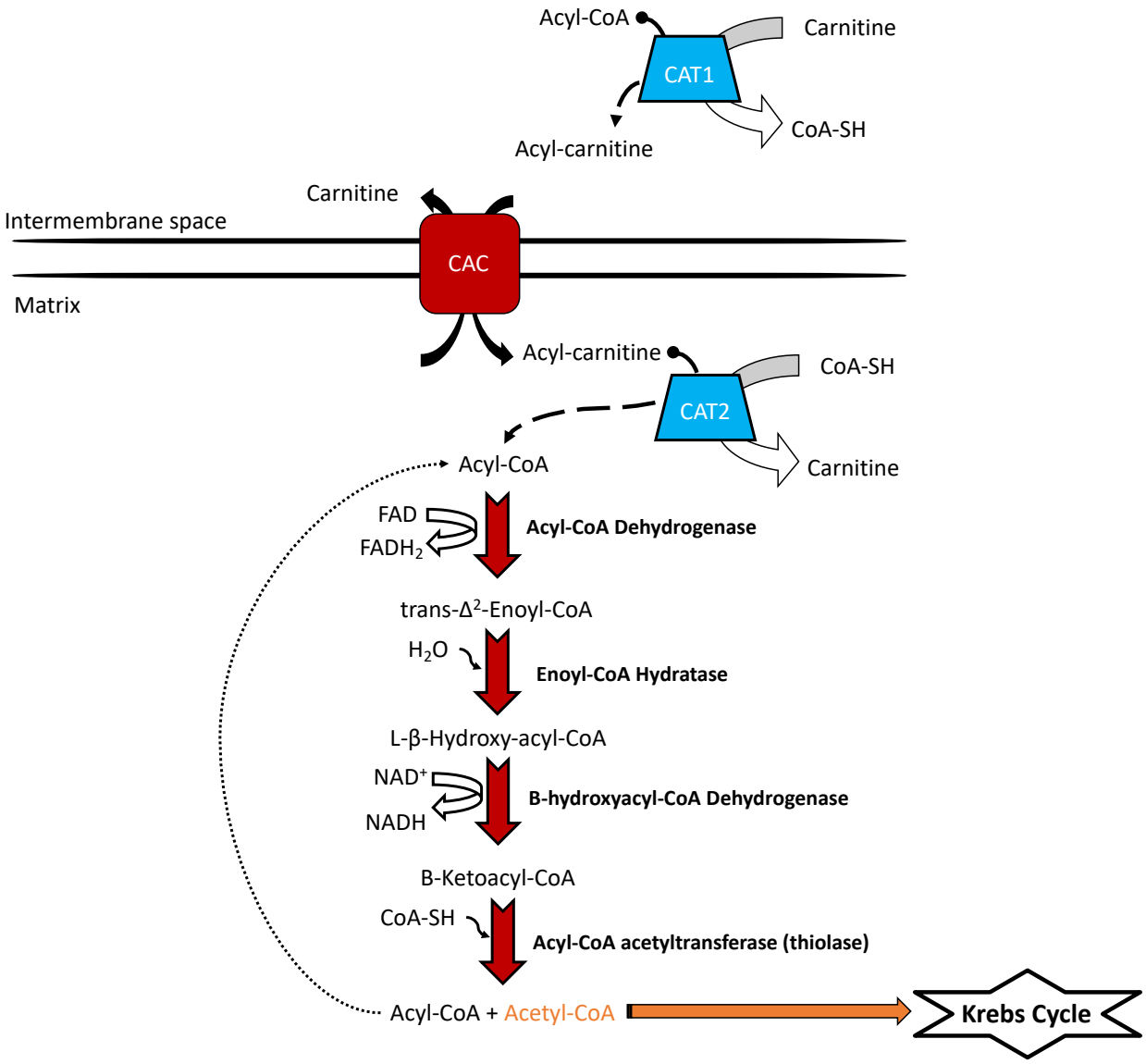

Figure 1.3: Acyl-CoA mitochondrial transport and β-oxidation pathway.

1.1.4 Oxidative Phosphorylation

It is crucial to note that up until this point, the production of electron carriers such as NADH and $FADH_2$ through different metabolic pathways has been discussed. These carriers neither are used as energy nor generate energy alone, but must donate their electrons to the ETC to produce a proton gradient. The action of these electrons "tunneling" down the ETC to prosthetic groups with a higher affinity for electrons (higher reducing potential) results in the release of free energy (1). This free energy can be coupled to the pumping of electrons from the mitochondrial matrix into the intermembrane space (1). Electron donating sites all converge on the ubiquinone (Q) pool forming ubiquinol (QH_2) before being passed along to complex IV resulting in the reduction of oxygen to water (8).

There are multiple pathways for the donation of electrons to the Q pool. NADH produced from the Krebs cycle and β-oxidation donate electrons directly to a flavin mononucleotide (FMN) subunit in complex I (NADH dehydrogenase) (1). Complex II (succinate dehydrogenase) through the action of converting succinate into fumarate accepts electrons to its flavin adenine dinucleotide (FAD) subunit (1). Other entry points into the Q pool include ETFQO, containing one FAD molecule and one Fe-S cluster, which has the capacity to accept electrons from many flavin-containing dehydrogenases, some of which catalyze the unsaturation step in β-oxidation (1,9). Two sites oriented towards the cytoplasm are *s,n*-glycerophosphate dehydrogenase and dihydroorotate dehydrogenase; the former is responsible for accepting electrons from cytoplasmic NADH, such as those created during glycolysis, and the latter is involved in pyrimidine biosynthesis (1).

A more detailed description of the pathway of electron "tunneling" is as follows. At complex I, NADH is oxidized by FMN, passing the electrons through 7 Fe-S clusters to 2

protein-bound semi-quinone molecules into the Q pool (8). Additionally, complex I is the largest mammalian ETC enzyme with 45 subunits (8). In complex II, succinate binds subunit A reducing FAD, then these electrons pass through 3 Fe-S clusters to ubiquinone (2). The electrons from ETFQO, *s,n*-glycerophosphate dehydrogenase, and dihydroorotate dehydrogenase are all passed to Q to reduce it to QH_2 requiring a 2 electron transfer (1). The reduction of complex III (ubiquinol-cytochrome c oxidoreductase) is performed by the Q-cycle, which involves the cyclic oxidation and reduction of QH_2/Q (1). This is accomplished through the transfer of a single electron to the Rieske Fe-S center which is then passed to cytochrome c_1 (2). Cytochrome c_1 then passes an electron to cytochrome c which dissociates from complex III and moves to complex IV (2). Complex IV receives 2 electrons from 2 cytochrome c molecules to reduce its binuclear center (2 Cu ions complexed with 2 Cys-SH groups) (2). Electrons then pass from heme a, to the heme a_3-Cu center (2). Oxygen then binds heme a_3 and is reduced to O_2^{2-}, which gets converted to 2 H_2O molecules with the passage of 2 more electrons (2). It should be noted that complex I pumps 4 protons across the membrane, complex III pumps 2, and complex IV pumps 4; these reactions are coupled to the release of free energy from the passing of electrons (1).

With the transfer of protons from the mitochondrial matrix into the intermembrane space, there is the generation of an electrochemical gradient, with the electrical gradient being the dominant component (1). Some proteins have the ability to tap into this potential energy to overcome unfavourable reactions such as the capacity of complex V (ATP synthase) to produce ATP. Complex V is composed of 2 subunits, F_o and F_1; the F_o subunit is membrane-bound and allows proton conductance back into the matrix (2). This is coupled to the rotation of subunit F_1 which binds ADP and P_i producing ATP (2). It is the three β subunits of F_1 that are responsible for the synthesis of ATP. While each of these subunits have the same amino acid sequence, it is

the conformation of these sites around the γ subunit, connected to F_1, that is attributed to their differences (2). As protons are passed through F_o down their gradient, the energy released is used to rotate this subunit along with the γ stalk, which passes through the 3 alternating α and β subunits (2). As the γ subunit turns, it is associated with only one of the three β subunits, changing it to the β-empty confirmation, releasing ATP from the complex (2). The other 2 neighbouring β subunits either retain a β-ADP confirmation (binds ADP and P_i) or a β-ATP confirmation (tightly binds and stabilizes ATP) (2). As the γ rotates 120^o, each of these subunits changes its conformation resulting in rotational catalysis of ATP (2). This ATP is then released into the cytoplasm for endergonic reactions through the adenine nucleotide transporter (ANT) in exchange for an ADP molecule entering the matrix (2).

Complex V is not the sole path protons can take to travel back into the matrix. Another important use of this gradient is the symport of phosphate ions as $H_2PO_4^-$, with H^+, to provide phosphate ions for the generation of ATP (1). Uncoupling proteins (UCP) also leak protons back into the matrix; for example, UCP1 (thermogenin) is responsible for thermogenesis in brown fat tissue, by coupling proton return to heat production (1). Another example of proton conductance back into the matrix is the formation of NADPH from NADH by nicotinamide nucleotide transhydrogenase (NNT), a reaction coupled to the return of protons through the protein (10).

1.2 Reactive Oxygen Species

1.2.1 Formation and sites of production

Reactive oxygen species (ROS) is a broad term that encompasses all oxyradicals and non-radicals, with a free radical defined as any molecule with 1 or more unpaired electrons (11). Molecular oxygen is a unique molecule as it has 2 unpaired electrons in its outer shell with the same electron spin quantum number, making it a bi-radical (11). Additionally, this property only

allows the transfer of one electron at a time to O_2 requiring it to pass through superoxide ($O_2^{\bullet-}$), allowing for the formation of hydrogen peroxide (H_2O_2) or the hydroxy radical (•OH) (9). ROS are known by-products of oxidative phosphorylation, but it should be noted that cytosolic sources such as NAD(P)H oxidases are also a significant ROS source (12). About 0.1 – 0.5% of electrons that are passed through electron carrying sites in mitochondria are leaked (Figure 1.4) (13). The specific amount is determined by factors such as the concentration of the reduced electron donor, concentration and type of substrate being oxidized, post-translational modifications, allosteric regulators, NADH availability, proton gradient, and the rate constant for the leak reaction (10,13).

ROS-producing sites have the ability to produce both $O_2^{\bullet-}$ and H_2O_2, which depends on flavin chemistry and how it reacts with di-oxygen (9). If a single electron is leaked to oxygen, then $O_2^{\bullet-}$ is formed, while if a pair of electrons are released together, then H_2O_2 is formed (14). Although $O_2^{\bullet-}$ was once considered the principal ROS formed by mitochondria, recent work has found H_2O_2 accounts for up to 75% of the ROS generated by sites of production (15). However, $O_2^{\bullet-}$ is formed nonetheless and must be rapidly cleared to preserve Fe-S cluster assemblies in mitochondria (9). Therefore, any $O_2^{\bullet-}$ formed is rapidly converted to H_2O_2 by superoxide dismutase (SOD). Thus, the dominant form of ROS generated by mitochondria is H_2O_2, occurring at a concentration in the nanomolar range compared to the picomolar range for $O_2^{\bullet-}$ (4).

To maintain a steady state concentration of ROS in the cell, there is constant regulation of its production and degradation. This allows the cell to maintain a redox homeostasis or the “golden

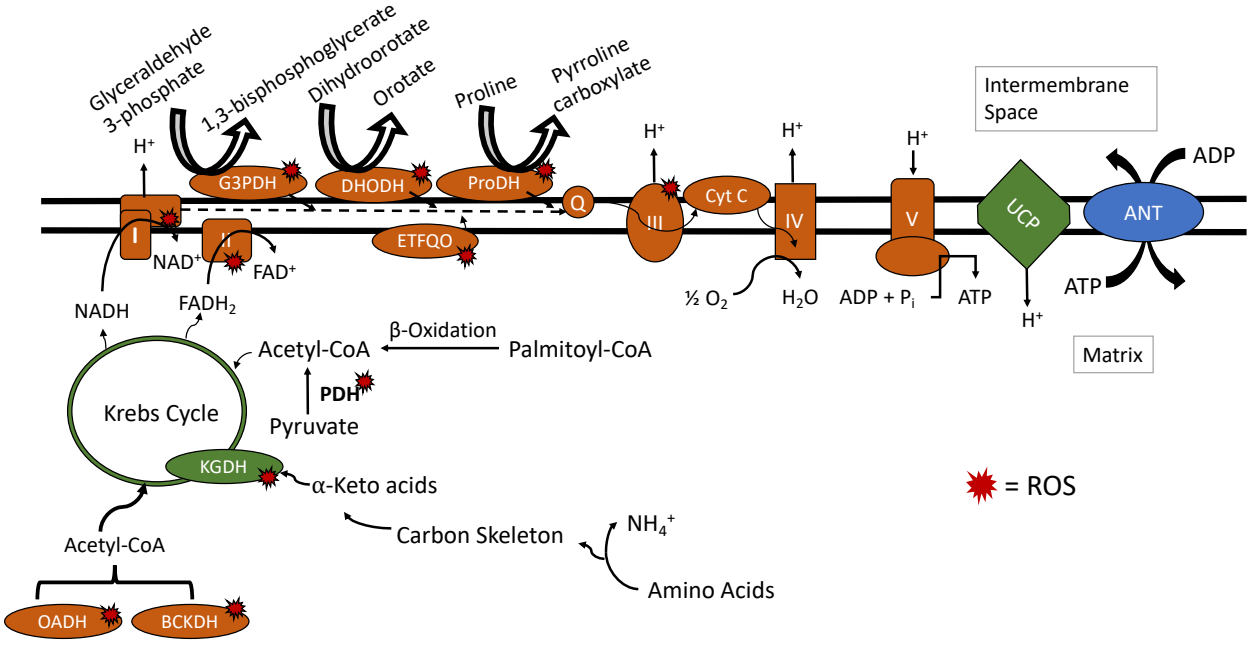

Figure 1.4: Sites of ROS production and carbon metabolism.

mean" as it is referred to in one such review, dispelling the notion that ROS is completely detrimental and instead, that the cell is in constant redox flux (16). Current research in the field has demonstrated that mitochondria can contain up to 12 sites of ROS production associated with fuel oxidation and the ETC (Figure 1.5). These sites are sub-categorized based on whether or not ROS genesis is linked to the oxidation and reduction of NAD or Q, the $NADH/NAD^+$ and QH_2/Q isopotential groups (10). The sources associated with the $NADH/NAD^+$ isopotential group include PDH, branched-chain keto acid dehydrogenase, 2-oxoadipate dehydrogenase, complex I (FMN site), and KGDH (10). Sources from QH_2/Q include complex I (Q binding site), complex II, complex III, ETFQO, *s,n*-glycerol-3-phopshate dehydrogenase, proline dehydrogenase, dihydroorotate dehydrogenase (10).

While all of these sites do contribute to overall mitochondrial ROS release into the cell, the individual contributions of these generators to total ROS produced can vary between tissue type and mouse strain. Indeed, this has been documented between C57BL/6N and C57BL/6J mice with the major sites being KGDH, PDH, and succinate dehydrogenase, respectively in 6N mice while, the major sources in 6J mice were 3-methyl-2-oxopentanoic acid, KGDH, and proline dehydrogenase, respectively (17). Similarly, our group has found that complex I and III are crucial for the production of ROS in cardiac mitochondria while KGDH and complex III are chief production sites in liver (18,19). The Brand lab has additionally shown that mitochondria from rat skeletal muscle produces $O_2^{\bullet-}/H_2O_2$ from complex III at twice the rate of any other site (13). This group has profiled production sites under different substrate oxidation finding orders of magnitude difference in sites of production (13,20).

With the discovery that H_2O_2 is an important intracellular signal transducer, the definition of oxidative stress had to be broken down into two categories: oxidative eustress and oxidative

distress. Oxidative eustress denotes a physiologically meaningful stress that serves a regulatory function (21). In this case, small but controlled bursts of H_2O_2 production results in the selective oxidation of cysteine switches on proteins, eliciting a change in cell behaviour (21). In contrast, oxidative distress is associated with excessive ROS production, which overwhelms antioxidant defenses and induces the non-selective oxidation of macromolecules, culminating with cell death (21). It should be noted that there is no fine line between oxidative eustress or distress, but instead a grey area that includes inflammation that could be considered beneficial or harmful to the cell (21).

Oxidative distress occurs when there is an imbalance between ROS production and degradation by antioxidants (21). This leads to toxic levels of oxidants that can oxidize lipids, DNA, and proteins leading to apoptosis (22). For example the base guanine is susceptible to oxidation resulting in 8-oxoguanine, causing mutations due to mispairing (23). Furthermore, lipid peroxidation results in lipid hydroxides such as 4-hydroxynonenal which are cytotoxic, linking them to pathological conditions (24). Proteins also have the potential for oxidation of their thiol groups, leading to their irreversible oxidation and loss of function (25). This has provided evidence for the foundation of the mitochondria theory of aging, in which some experts argue irreversible oxidation is the basis for human aging (25). Indeed, aging skeletal muscle mitochondria are marked by a decrease in ATP production and increase in oxidative stress, related to loss of muscle with aging (26). However, treatment of aged mice with SS-31, resulting in decreased oxidative stress and increased mitochondrial bioenergetics, leads to improved muscle function (26).

1.2.2 Hydrogen Peroxide Signalling

Hydrogen peroxide is now classified as a mitokine linking it to cellular signalling pathways. One of the best characterized signalling properties of H_2O_2 is the regulation of transcriptional factors. For example hypoxia-inducible factor-1α has been shown to require H_2O_2 originating from complex III to become stabilized and induce genes to enhance survival during hypoxia (27). Additionally, it has been demonstrated that H_2O_2 can affect the rate of transcription of activator protein-1 and tumor protein 53, while increasing the translation rate of NF-E2p45-related factor 2 (Nrf2) and specific protein 1 (21).

In the case of the Nrf2 pathway, increased stimulation of transcription is thought to occur due to stimulation of eukaryotic initiation factor 4F complex (eIF4F) phosphorylation through oxidation of Ser209 by H_2O_2 (28). H_2O_2 also has the capacity to oxidize Kelch-like ECH-associated protein 1 (KEAP1) preventing its binding to Nrf2 and preventing KEAP1 from initiating its ubiquitination and degradation (28). The upregulation of the Nrf2 pathway leads to increased antioxidant expression and the quenching of ROS. Additionally, high levels of ROS are indicative of oxidative damage in muscle, while pulsatile release of ROS due to repeated contractions is crucial for the adaptive and beneficial aspects of exercise (29). It is important to note that H_2O_2 has been linked to signalling via S-glutathionylation and is thought to prime these reactions by forming sulfenic acid (SOH), that can undergo spontaneous S-glutathionylation (discussed later) (4). Indeed, it has been found that metabolic stress in macrophages induces an increase in S-glutathionylation of up to 100 proteins and of these, 94 of them are S-glutathionylated by the addition of H_2O_2 (30).

1.3 Antioxidant Systems

Hydrogen peroxide plays a vital role as a secondary messenger but like any other signalling molecule, its levels need to be tightly regulated. This is crucial since it needs to be produced rapidly to change cell behaviour in response to environmental cues and then degraded thereafter to desensitize the signal. Additionally, its levels need to be tightly controlled since it can induce cell damage and apoptosis. The degradation of H_2O_2 and other ROS is facilitated by antioxidant defenses.

1.3.1 Peroxiredoxin

There are two main thiol-dependent antioxidant systems in mammals, the first being the thioredoxin (TRX)/peroxiredoxin (PRX) system and the other being the glutathione (GSH) system. The PRX system has the ability to remove H_2O_2, hydroperoxides (ROOH), and peroxynitrite utilizing a series of thiol disulfide exchange reactions (31). These reactions proceed by the PRX thiolate cysteine (Cys), in its active site, nucleophilicity attacking H_2O_2 via a S_N2 reaction yielding a SOH and H_2O (31). The C-terminal resolving Cys is then attacked by the SOH to form a disulfide bond, rendering PRX inactive (31). The intermolecular disulfide bridge in PRX is then reduced through a thiol disulfide exchange reaction with TRX, reactivating PRX (31). This deactivates TRX through the formation of a disulfide bridge which is then reduced by thioredoxin reductase (TR) utilizing the reductive power stored in NADPH (31). PRX/TRX systems are present in both the cytosol and matrix with the matrix-localized isoforms being PRX3 and PRX5, which catalyze reactions at 2×10^7 $M^{-1}s^{-1}$ and 3×10^5 $M^{-1}s^{-1}$ respectively (10). The reducing power of this system in the mitochondrial matrix comes from TXR2 and TR2 (10). It is important to note that TRX1 and 2 knockout is embryonically lethal in mice, demonstrating its important for cellular survival (32). Additionally, this system does not operate in isolation but

has been shown to crosstalk with the GSH antioxidant system due to is capability to reduce glutathione disulfide (GSSG) (32). GRX2 has also been observed to reduce TRX2 and its cytosolic isoform TRX1, an important discovery as TR is sensitive to inactivation by oxidation (32).

1.3.2 Glutathione

The GSH system has two distinguishing factors that make it a significant antioxidant system, the first being the high concentration it maintains in its reduced form and the second being the 1:2 ratio of GSH to glutathione disulfide (GSSG). Glutathione (also referred to as γ-L-glutamyl-L-cysteinylglycine) has a unique γ-carbonyl bond between the glutamate and cysteine making it resistant to most peptidases except γ-glutamyltranspeptidase (33). The synthesis of GSH follows a two-step reaction with ATP required for both enzymatic steps: 1) γ-glutamylcysteine is formed from glutamate and cysteine by glutamate-cysteine ligase, also referred to as the rate-determining step 2) GSH is formed from γ-glutamylcysteine and glycine with the help of glutathione synthase (33).

This system's ROS-quenching potential relies on the activity of two enzymes, glutathione peroxidase (GPX) and glutathione reductase (GR) along with NADPH as a cofactor. Key enzymes that contribute to maintaining the NADPH pool include malic enzyme, glutamate dehydrogenase, isocitrate dehydrogenase-2, NADH kinase, glucose-6-phosphate dehydrogenase, and nicotinamide nucleotide transhydrogenase (4). The reaction is initiated by the oxidation of the selenocysteine active site of GPX by H_2O_2, forming a selenic acid (SeOH) (4). This selenic acid group can then react with GSH forming a selenenyl-glutathione sulfide (Se-SG) which can further react with another GSH molecule to form a GSSG and return the GPX active site back to its reduced form (4). In order to regenerate the GSH, NADPH is utilized by GR to reduce the

GSSG back into 2GSH. The capacity of glutathione to act as a major mitochondrial redox buffer comes from the high GSH: GSSG ratio (~50-100) (22). The role of glutathione can be emphasized by dysfunction of glutamate-cysteine ligase, which when downregulated, results in hemolytic anemia, aminoaciduria, and spinocerebellar degeneration (34). Additionally the deletion of the gene that produces the catalytic subunit of glutamate ligase is embryonically lethal (34).

1.3.3 Other quenching systems

Two additional enzymes that are responsible for the removal of ROS are SOD and catalase. The SOD system works in conjunction with a metal enzyme to catalyze the reduction of $2O_2^{\bullet-}$ to O_2 and H_2O_2 through a two-step reaction at a rate of $1.8x10^9$ $M^{-1}s^{-1}$ (35). The rate of this reaction coincides with the rate of diffusion therefore rapidly removing $O_2^{\bullet-}$ from the cell medium and making it difficult to quantify.

Equation 1.5:

$$2O_2^{\cdot-} + 2H^+ \rightarrow H_2O_2 + O_2$$

The isoforms of SOD differ by the metal enzyme that they bind, with MnSOD present in the mitochondrial matrix and Cu/ZnSOD present in the cytosol (36). The importance of SOD can be displayed through the deletion of either MnSOD or Cu/ZnSOD. Indeed, deletion of MnSOD in mice leads to mortality within 10 days of birth with symptoms of dilated cardiomyopathy, metabolic acidosis, and increased lipid deposition in liver and muscle tissue (37). Whereas the deletion of Cu/ZnSOD is not lethal but leads to age-related pathologies such as accelerated Alzheimer's disease, muscle atrophy, and infertility (38).

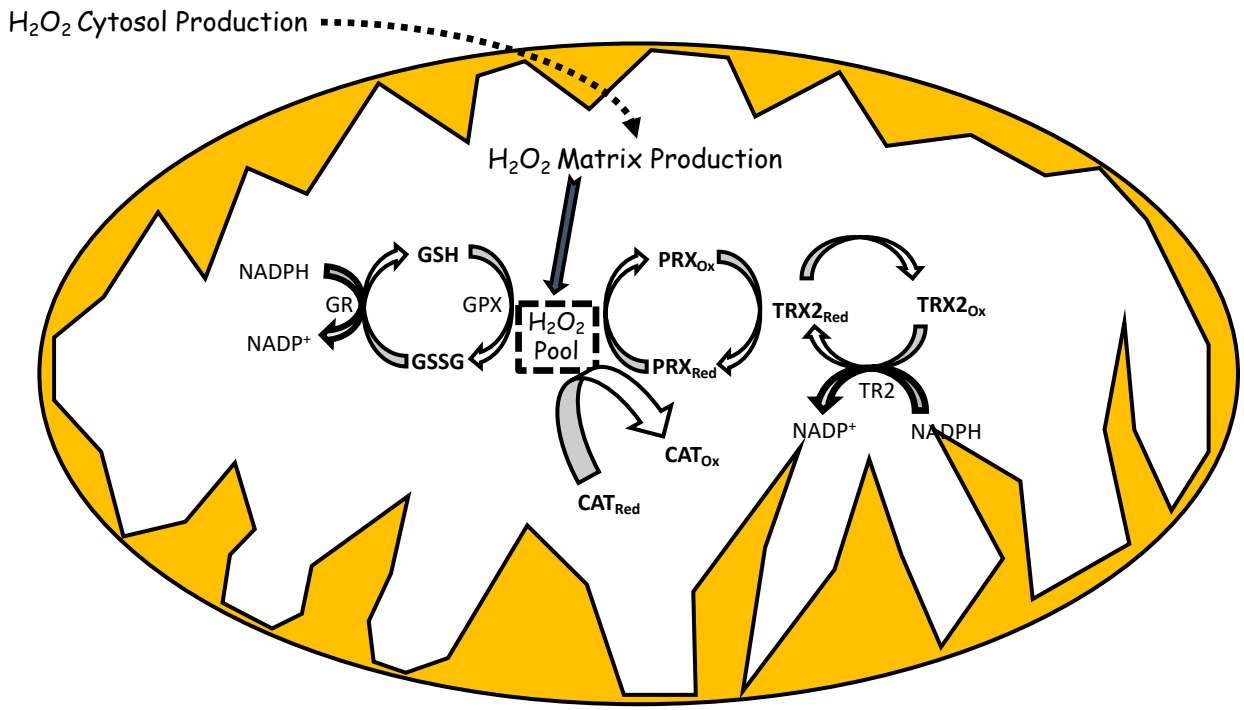

Figure 1.5: Antioxidant clearance of mitochondrial H_2O_2.

Catalase is thought to be a less significant antioxidant system by having a lower binding affinity than the other systems and playing a role only when ROS levels become high or another system has been compromised (39). Indeed, it has be shown that catalase plays an important role for ROS quenching in liver and heart mitochondria (19,39). This system relies on a heme prosthetic group for the reduction of H_2O_2 and therefore do not require a NADPH molecule for the regeneration of the reduced form.

Equation 1.6 (21)**:**

(1) Catalase-Fe^{3+} + H_2O_2 → Catalase-FeO^{3+} + H_2O

(2) Catalase-Fe^{3+} + H_2O_2 → Catalase-Fe^{3+} + O_2 + H_2O

or

Catalase-FeO^{3+} + AH_2 (Hydrogen donor) → Catalase-Fe^{3+} + A + H_2O

1.4 Protein S-glutathionylation

1.4.1 Reversible Reactions

As noted above, glutathione is a major antioxidant molecule that is required to safeguard cells from oxidative distress through the elimination of H_2O_2 and various electrophiles. However, glutathione also has the capacity to regulate protein functions. This is achieved through protein S-glutathionylation, a ubiquitous and reversible redox modification that involves the conjugation and removal of glutathione to and from a protein cysteine residue. These reactions can either be spontaneous or enzyme mediated (Figure 1.6). The spontaneous modification of protein cysteine thiols can occur by three mechanisms: 1) ionization of a protein thiol to a thiolate anion, which then nucleophilically attacks glutathione, 2) oxidation of a protein thiolate anion to a SOH by

H_2O_2 which can then nucleophilically attack glutathione, and 3) the formation of a thiyl radical, can proceed to form a protein thiyl radical-glutahionyl intermediate which can be resolved in the presence of O_2 to S-glutathionylation (4). However, spontaneous reactions are not typically favourable since most protein cysteine thiols have an equilibrium constant ~1 while the GSH: GSSG pool in the mitochondrial matrix is typically held at ~100 (4). There are exceptions to this such as C-Jun which has an equilibrium constant of ~15 allowing spontaneous glutathionylation to occur much more easily (4). Additionally, the pH of the mitochondria matrix is slightly alkaline, which promotes thiolate formation; therefore, during times of oxidative stress, this increases the likelihood of S-glutathionylation (40). Nevertheless, with all of these factors, spontaneous reactions are still very rare or occur under non-homeostatic conditions, such as during oxidative distress (4).

The enzyme-mediated reactions proceed by the action of GRX, for which there are two isoforms that carry out reactions. The isoform localized to the cytoplasm and mitochondrial intermembrane space is GRX1, while the GRX2 isoform consists of 3 sub-types: GRX2a, GRX2b, and GRX2c (4). The GRX2a isoform is localized to the mitochondrial matrix and GRX2b/GRX2c are localized to the nucleus, exclusively in testes (4). It is important to note the key differences that exist between GRX1 and GRX2. Firstly, GRX1 has only been shown to participate in deglutathionylation reactions with glutathionylation of proteins via GRX2 isolated to the mitochondrial matrix (4). Secondly, GRX2 is coordinated through a 2 Fe-S cluster to keep it in an inactive form; it is only upon disassembly by $O_2^{\bullet-}$ that the enzyme becomes active (41). As mentioned above, GRX2 also has the capacity to reoxidize TRX2 (32). While GRX1 and GRX2 have low homology with each other, common between them is the active site motif, CXXC, which is responsible for its thiol-disulfide exchange reaction. This reaction progresses in

two steps: 1) the N-terminal active site thiolate nucleophilic attacks the sulfur of the glutathionylated protein (PSSG), forming a GRX-SSG intermediate and releasing a reduced protein (PSH), and 2) a free GSH molecule can then attack the glutathionylated GRX and resolve it back to its reduced form and release a GSSG (40).

Alternatively, since this reaction is reversible, the GRX should theoretically glutathionylate proteins as well, for which evidence shows that GRX2 does proceed in this direction, but whether GRX1 does is still unknown (4). The catalytic cycle for which GRX2 completes this reaction requires firstly that the glutathione pool be in an oxidized state, through the quenching of H_2O_2 (42). The reaction commences with the addition of a GSH to one of the catalytic GRX2 cysteine residues, then through a thiol-disulfide exchange reaction, the GSH is conjugated to the target protein cysteine (42). This reaction proceeds via an S_N2 mechanism and is regulated through the ratio of GSH: GSSG, with a high ratio favouring the forward reaction and a low ratio favouring the reverse (4,42). This enzyme-mediated reversibility, along with being rapid, responding to the redox state of the cell, changing protein function, and there being specific protein motifs for this modification make S-glutathionylation a valid post-translational modification (4). As termed by Dean Jones, the capacity of S-glutathionylation to respond to the redox environment to modify and adapt protein function makes it a component of the redox code; allowing it to control "redox switches" in response to physiological cues such as high levels of H_2O_2 (43). It should be noted that in the cytosol and endoplasmic reticulum, glutathione S-transferase is responsible for catalyzing the addition of glutathione to target proteins (40,44).

1.4.2 Modulation of Respiratory Complexes

The respiratory complexes have multiple motifs for S-glutathionylation, one of the first discovered being complex I. It has since been found that there are 12 sites in complex I that can

undergo S-glutathionylation in response to the redox status of the glutathione pool (4,45). This modification has been discovered to occur in lens epithelia, heart, and muscle tissue as an adaptive response to increased ROS production, protecting the complex against irreversible oxidative damage (4). Two of the known sites of modification are the 51 kDa subunit that contains the NADH binding site and the 75 kDa subunit (45). S-glutathionylation of the 51 kDa subunit has been shown to occur on Cys^{531} and Cys^{704} reversibly by GRX2 (4). S-glutathionylation of complex I was found by the Murphy group to decrease its activity and increase $O_2^{\bullet -}$ emissions (45). Additionally, it has been found that S-glutathionylation of this complex reduces the ATP producing ability of these mitochondria (18,41).

In brain and liver mitochondria, it has been shown that complex V can be S-glutathionylated, reducing its ATP producing potential (46). This modification occurs on the α-subunit of the F_1 complex and is increased during fatiguing exercise (45,47). Furthermore, increases in oxidative stress in cardiac tissue, such as during heart failure, increases S-glutathionylation of complex V (48). Increased S-glutathionylation has a direct effect on dysregulation of complex V in cardiac tissue and cardiac resynchronization therapy has shown to reverse this (48). Complex II is unique as it is S-glutathionylated in its native state (49) The activity of complex II has been directly linked to the glutathionylation state of Cys^{90} in its 70 kDa flavin binding subunit (49). In the case of this complex it becomes basally S-glutathionylated to increase electron transfer efficiency and decrease electron leak from the complex (49). It was found that deglutathionylation of this complex can predispose it to oxidative stress in post-ischemic hearts (49).

1.4.3 Krebs Cycle

The Krebs cycle represents a major regulatory point for carbon metabolism and therefore requires fine-tuned regulation to ensure it maintains homeostasis in the cell. Many of the enzymes in this pathway are regulated by S-glutathionylation such as PDH, KGDH, isocitrate dehydrogenase, aconitase, succinyl-CoA transferase, malate dehydrogenase, and complex II (discussed above).

Two of the most studied of these enzymes are PDH and KGDH since they act as regulatory points in metabolic pathways due to the irreversibility of their activities. PDH is important for the commitment of pyruvate to acetyl-CoA and KGDH allows the entry of amino acid catabolism into the Krebs cycle (2). KGDH was first thought to be S-glutathionylated on its E2 subunit as a protective effect against irreversible oxidation by H_2O_2, with deglutathionylation restoring its activity when H_2O_2 was quenched (50). Further studies have concluded that S-glutathionylation not only plays a protective role for KGDH but regulates the enzymatic activity of both PDH and KGDH (51,52). Not only are KGDH and PDH sensitive to ROS they also are key sources, with PDH and KGDH producing 4x and 8x more ROS then complex I, respectively, in skeletal muscle (53). Both KGDH and PDH can undergo reversible modification by GRX2 in the E2 subunit and this modification influences their ROS production (51,52). Chemical induction of S-glutathionylation of KGDH and PDH was shown to diminish $O_2^{\bullet-}/H_2O_2$ production by ~90% under conditions of forward electron transfer but amplify production during reverse electron transfer (52). The role of S-glutathionylation with respect to these enzymes is tissue specific as deletion of GRX2 results in a decrease of $O_2^{\bullet-}/H_2O_2$ production in liver mitochondria but an increase in cardiac mitochondria (18).

S-glutathionylation is also linked to a 35% decrease in activity of aconitase due to S-glutathionylation of Cys^{126} and Cys^{385} close to its active site (54). While isocitrate dehydrogenase-2, succinyl-CoA transferase, and malate dehydrogenase have all been found to be S-glutathionylated, there is still debate on whether this alters their activities (4). Evidence exists to suggest that malate dehydrogenase is S-glutathionylated in skeletal muscle during fatiguing exercise (47). While isocitrate dehydrogenase-2 and succinyl-CoA transferase have both been shown to be sensitive to S-glutathionylation in brain tissue (48).

1.4.4 Solute Import and Proton Leak

As the MIM is only selectively permeable, it has an abundance of protein carriers to facilitate movement of substrates and molecules such as ATP and ADP in and out of the matrix. It is then no surprise that these proteins can be modified to regulate the uptake of substrates by mitochondria and that S-glutathionylation has been shown to be one of these regulatory measures. Indeed, a previous study in our lab showed that induction of S-glutathionylation was able to modulate mitochondrial pyruvate carrier 1 (MPC1) (41). In that study, chemical induction of S-glutathionylation via disulfiram was able to significantly decrease the pyruvate uptake in these mitochondria (41). In the same study, it was investigated if carnitine/acylcarnitine carrier (CAC) could undergo the same regulation. While our recent study was unable to show this result, a previous group had shown S-glutathionylation of Cys^{136} and Cys^{155} of CAC could be S-glutathionylated and could limit the activity of this transporter (55).

Another important group of proteins imbedded in the MIM that are S-glutathionylated include the uncoupling proteins (UCP). UCP2 is found in a variety of tissues and UCP3 is isolated to muscle and brown adipose tissue (56). These proteins facilitate the movement of protons back into the matrix, by-passing complex V, which uncouples the proton gradient from

ATP production. As indicated above, the strength of the potential of protons experienced across the MIM can have a powerful impact on the rate of mitochondrial ROS production. Indeed, $O_2^{\bullet-}$ /H_2O_2 generation has a non-Ohmic relationship with the proton gradient where a small increase in the PMF can induce a large increase in ROS production (4). The Brand lab were the first to propose the concept of UCP regulated by cellular redox changes, finding evidence that 4-hydroxy-2-nonenal and $O_2^{\bullet-}$ induced proton leaks through these proteins (57,58). However, these results could not be duplicated (56). It was later discovered that UCP2 and UCP3, but not UCP1, can be S-glutathionylated on Cys^{283} and Cys^{259} respectively, which are both located in the last loop region exposed to the mitochondrial matrix (4). These residues are surrounded by positively charged amino acids which makes them more amenable towards modification by S-glutathionylation (56). Surprisingly, when there is an increase in ROS, UCP3/2 become deglutathionylated and subsequently activated (56). In the case of UCP3, this diminishes the proton gradient and is thought to diminish ROS production (56). A recent study in our lab found that in the case of mice deficient in GRX2, there was a ~2-3 fold increase in proto n leak-dependent respiration that was due to increased activity of UCP3 and ANT (59). While mice with deletion of *Grx2* additionally show increased mitochondrial respiration, correlating to increases in UCP3-dependent proton leaks (60).

Another important solute anion carrier protein, ANT, also contains a modifiable cysteine in the last loop region and has been shown to be S-glutathionylated (4). ANT not only is responsible for the exchange of ADP for ATP at the MIM, it is thought to be a key in the assembly of the mitochondria permeability transition pore, resulting in apoptosis (61). There is, however, little knowledge on the effect of glutathionylation on ANT activity. A study by Queirga *et al.* determined that low levels of S-glutathionylation of ANT increased its ADP/ATP

translocase activity and prevented inner membrane permeability (62). Additionally, it has been recently found that in GRX2 deficient mice ANT's uncoupling activity is upregulated (59). This finding, along with leaks due to UCP, were found to be responsible for increased mitochondrial respiration and protection from DIO, indicating a link between weight gain and S-glutathionylation (59). This link is further supported by the evidence that liver and peri-renal adipose tissue from obese rats have significantly reduced protein S-glutathionylated content (63).

1.4.5 Other Protein Regulation

Protein S-glutathionylation reactions have the ability to govern fission and fusion of mitochondria, having a direct impact on metabolism and cell survival (64). The fusion of mitochondria can be induced due to cell stress and is shown to increase mitochondria efficiency (65). The regulation of mitochondrial fusion is achieved by specific GTPases, mitofusion 1 and 2 located in the mitochondrial outer membrane and autosomal dominant Optic Atrophy 1 located in the MIM. It has been shown that oxidized glutathione results in the fusion of mitochondria and that Cys^{684} of mitofusion 2 is the possible cysteine responsible for this reaction (65). Furthermore, a study found that addition of diamide, a S-glutathionylation catalyst, induced mitochondrial hyperfusion (66).

Furthermore, S-glutathionylation plays a vital role in skeletal muscle physiology, which can be underscored by a recent proteomic study that revealed ~2200 sites of modification in muscle and increased modification of 1290 of these sites after fatiguing exercise (47). Key sites involved in muscle contraction included ryanodine receptor-1, sarco/endoplasmic reticulum Ca^{2+}-ATPase-1 (SERCA), and titin (47). SERCA is a crucial Ca^{2+} pump that is responsible for relaxation of smooth, cardiac, and skeletal muscle. It has been shown that S-glutathionylation of Cys^{674} results in an increase of Ca^{2+} uptake and therefore muscle recovery from contraction (29). Titin is made

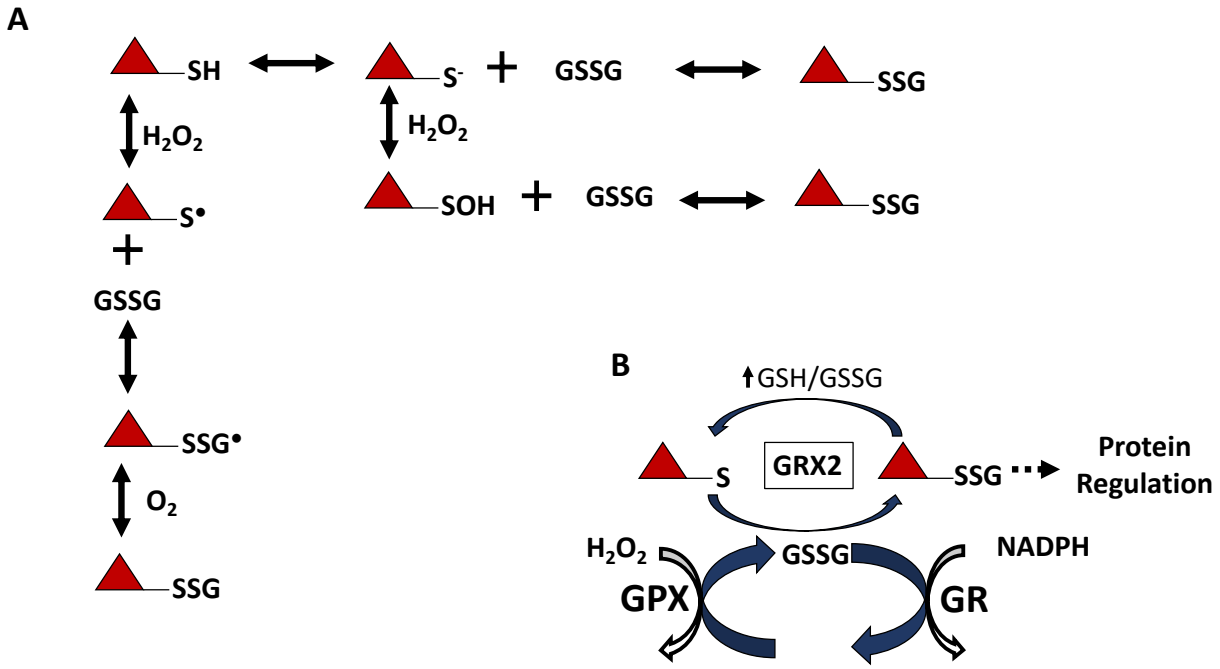

Figure 1.6: (A) Non-enzymatic S-glutathionylation reaction. (B) Grx2 medicated S-glutathionylation reaction.

up of folded immunoglobulin domains in its I band, all of which contain cysteine residues (67). It was found that the two cysteine residues in I91 are S-glutathionylated when they are in the unfolded state, preventing the band from refolding and increasing the elasticity of titin in cardiac tissue (67).

1.5 Metabolic Syndrome

The estimated economic burden of obesity in Canada is approximately 7 billion dollars, with half the population classified as either overweight or obese (68). Surveys in 2016/2017 from Statistics Canada indicates that 34% of Canadians are overweight with 27% classified as obese (69). Of all Canadians, Newfoundland and New Brunswick have the highest prevalence of overweight in the population at 38%, trends that are rising (69). Metabolic syndrome is defined by an accumulation of factors such as insulin resistance, hypertension, hepatic steatosis, dyslipidemia, glucose intolerance, and hyperinsulinemia, all of which result from an increase in adipose tissue (70). The World Health Organization (WHO) has officially classified metabolic syndrome as a world-wide epidemic.

For early mammals there was an evolutionary push to create modes of energy storage and more efficient mechanisms for ATP production. Those organisms who could survive longer without food and produce energy more efficiently would have had an evolutionary advantage. It is only in recent decades of human history that we see a shift from food scarcity to food surplus in developed countries. In today's Western society, technological advances have come with processed food and an ability to live sedentary lifestyles. This has led to an alarming amount of the population having a positive energy balance, leading to progression of obesity. As obesity is a form of low-grade inflammation, it has many adverse effects such as insulin resistance, type 2 diabetes mellitus, and atherosclerosis (71). More alarming is the fact that the current gold

standard of treatment for obesity is caloric restriction and exercise which has highly variable outcomes, as some individuals demonstrate resistance to weight loss and a tendency to regain their lost weight.

The result of an increase in nutrient supply to cells can alternatively lead to oxidative stress and progress to mitochondrial dysfunction (71). Indeed, it has been documented that obesity leads to oxidative stress (72). One such example is the finding that DIO leads to elevated levels of ROS in brain tissue in mice, leading to cognitive impairments (73). This now leads into the concept of mitochondrial dysfunction, which is another adverse effect of obesity, and in this context is defined as the maladaptive response of mitochondria to a surplus of nutrients (71). These dysfunctions can range from oxidative stress inducing mitophagy and decreasing mitochondria populations, to alterations in mitochondrial function such as lower energy generation capacities, less defined internal membranes, and lower fatty acid oxidation (71). It should be emphasized that these adaptations led to the further progression of obesity.

Furthermore, a surplus of nutrients can cause metabolic gridlock. In normal mitochondria, there is a constant switch between the selection of fuel to be used (70). This is defined as fuel portioning and is usually measured by the respiratory quotient (RQ) which usually ranges from 0.7-1.0 (70). Mitochondria are the organelle responsible for this fuel selection and typically oscillates between 0.7 (preference for fat oxidation) to 1.0 (preference for glucose oxidation) depending on circulating insulin levels (70). With the development of obesity, an inflexibility in this fuel selection was shown in a study by Kelley *et al.*, in which muscle from obese individuals showed resistance of the RQ when infused with insulin (74).

1.6 Sexual Dimorphisms

Early research lacked the insight to account for biological differences between sexes and instead research in male subjects was extrapolated to females. This flawed experimental design has led to a knowledge gap and the emergence of sex-specific claims. One example of the consequences of this blind spot are drugs like Zolpidem (sedative for insomnia), which dosage was found to result in twice the drug level in women due to differences in metabolism (75). The growing awareness of this issue in the scientific community can be seen by the funding of an Office of Women's Health by the FDA, which advocates for the participation of women in clinical research (75).

It is important to differentiate between a sex difference and gender difference. Sex differences are a direct result of the chromosomal identity of the organism, whereas gender differences are due to the cumulating factors of sex chromosome, sex hormone, and epigenetic interactions with the environment (76). It is therefore difficult to isolate these differences in a biological study and therefore in most cases, a sexual dimorphism is defined as a difference between a female or male organism, not differentiating whether its origin is sex- or gender-related (76). It is likely that it is a summation of all these factors that produces the sex-specific effects observed in organisms and herein, all reference to sexual dimorphisms will encompass the definition above.

The secretion of hormones likely plays a major role in sex differences in biology. One such study in skeletal muscle mitochondria points to elevated levels of 17-β estradiol to distinguish the differences observed in female mitochondria (77,78). Alternatively, it has been established that differences in the secretory patterns of growth hormone in rats and mice control sexual dimorphisms in liver gene expression (79). Indeed, the pulsatile release of growth hormone has

been established to regulate signal transducer and activation of transcription 5 (STAT5), a transcriptional regulator (79). Females exhibiting a slow steady rate of growth hormone secretion while male mice show a cyclic pulsatile release that may explain differential expression of genes between sexes and females' preference for oxidation of fatty acids (79). Furthermore, a study by Holloway *et al.* was able to determine that human female skeletal muscle mitochondria have decreased ADP sensitivity and greater sensitivity of CPT1 to inhibition by malonyl-CoA (80). This difference was determined to be due to differences in protein activity and not abundance of mitochondrial proteins (80).

It is important to note that mitochondria are maternally inherited and therefore the mtDNA is asymmetrically inherited. As a result, mtDNA has spent more time under natural selection in a female biological environment and is likely more equipped to function in females (81). With respect to mitochondrial bioenergetics, there have been definite sex dimorphisms observed. Indeed, it has been shown that women have more of a preference for fatty acids over carbohydrates and reduced AMP-activated kinase activity than males when exercising (82,83). Additionally, females display higher activities of Krebs cycle enzymes, such as citrate synthase and succinate dehydrogenase (81). In a study by Cardinale *et al.*, female and male human skeletal muscle mitochondria were directly compared. In this study, it was determined that women could produce the same rate of respiration as matched males, but with less mitochondria (84). This finding was attributed to female mitochondria having higher intrinsic respiration (84). The same study was also able to conclude that women had a lower oxygen affinity and increased proton leak when compared to men with equivalent maximal oxygen uptake (84). Furthermore, in animal models, it has been shown that female mitochondria produce less ROS and have higher oxidative capacity (81).

As for differences in redox signalling, it is known that female mitochondria have lower oxidative stress, lower oxidative stress biomarkers, produce less ROS, and have higher antioxidant potential than their male counterparts (81,85). Indeed, while female mitochondria are documented to have lower levels of GPX, they also have decreased ROS levels (85). It has been postulated that estrogen is the major factor for decreased ROS in female cells, due to the radical scavenging property of its phenolic hydroxy group (85). With this observation, it is implied that female mitochondria may be more efficient at maintaining ROS levels at optimal levels for redox signalling and preventing oxidative distress. This is supported by the fact that female mitochondria from brown adipose, white adipose, and skeletal muscle tissues show increased functionality compared to males (81). Additionally, rat brain tissue shows significantly lower oxidative damage in females than males (81). Furthermore, key signalling pathways of H_2O_2 such as the NRF2, Mfn2, and Sirt1 have been shown to be decreased in female mice, indicating a sex dimorphism in redox regulation of these proteins and signalling pathways (81).

1.7 Experimental Objectives and Hypotheses

1.7.1 Objectives

The primary objective of this project was to examine the metabolic response of female mice, on a C57BL/6N background, heterozygous for GRX2 ($GRX2^{+/-}$) and WT littermates fed a high-fat diet (HFD) compared to a control diet (CD). It was the goal of this research to ascertain the influence of a HFD on $GRX2^{+/-}$ mice in terms of:

1) Weight gain, the mass of liver, muscle, kidney, heart, and subcutaneous adipose tissue, and circulating blood glucose and triglycerides.
2) ROS production from different sites through the use of inhibitors and different carbon sources.

3) Mitochondrial respiration and proton leak.

A secondary objective was evaluating if there was any sexual dimorphisms observed in this study in comparison to a previous study measuring the same parameters in male mice (59).

1.7.2 Hypotheses

The broad hypothesis of this study was that female mice that are heterozygous for GRX2 would gain lower adiposity then WT mice when placed on a HFD. More specifically, I hypothesized:

1) Female $GRX^{-/+}$ mice on a HFD will demonstrate resistance to diet-induced weight gain.
2) Female $GRX^{-/+}$ mice will generate more ROS than their WT littermates due to an increase in mitochondrial respiration (i.e., specifically phosphorylating and proton leak respiration).

Chapter 2: Materials and Methods

2.1 Reagents

ADP (20398-34-9-A2754), antimycin A (1397-94-0-A8674), ATP (34369-07-8-A1852), Bradford reagent (B6916), diethyl malonate (105-53-3), dimethyl sulfoxide (DMSO) (67-68-5), ethylene glycol-bis (β-aminoethyl ether)-N,N,N',N'- tetraacetic acid (EGTA) (13368-13-3-E3889), fatty acid-free bovine serum albumin (BSA) (9048-46-8-A7030), HEPES sodium salt (75277-39-3-H7006), horseradish peroxidase (HRP) (9003-99-0-P8375), hydrogen peroxide (H_2O_2) (7722-84-1-216763), α-keto-beta-methyl-n-valeric acid (KMV) (24809-08-3-74414), L-carnitine hydrochloride (6645-46-1-C0283), magnesium chloride ($MgCl_2$) (7786-30-3-M8266), DL-malic acid (6915-15-7-240176), D-mannitol (69-65-8-M9647), monobasic potassium phosphate (7778-77-0-795488), myxothiazol (76706-55-3-T5580), oligomycin (579-13-5-75351), palmitoyl-carnitine chloride (18877-64-0-P1645), potassium chloride (KCl) (7447-40-7-P9333), REDExtract-N-Amp tissue PCR kit (XNATS), RIPA buffer (R0278), rotenone (83-79-4-R8875), sodium pyruvate (113-24-6-P2256), subtilisin A (9014-01-1-P5380), succinic acid (150-90-3-224731), sucrose (57-50-1-S7903), superoxide dismutase (SOD) (9054-89-1-S7571) were purchased from Sigma. Atpenin A5 (119509-24-9) and CPI-613 (95809-78-2) were purchased from Santa Cruz. Ethanol (64-17-5), hydrogen chloride (HCl) (7647-01-0), nuclease-free water (AM9935), SYBR Safe Gel stain (A45205), Tris borate EDTA (TBE) (B52), and 100 bp DNA ladder (15628050) were purchased from Thermo Fisher Scientific. Amplex UltraRed (AUR) (A36006) and UltraPure Agarose (LS16500500) were purchased from Invitrogen. 96 well plates (655076) were purchased from Greiner Bio-One. DNA primer sequences were purchased from Integrated DNA Technologies.

2.2 Animals

Female mice heterozygous for the *glutaredoxin-2* gene (*Grx2*$^{+/-}$) and wild type (WT) littermates were generated by breeding age-paired *GRX2*$^{+/-}$ mice housed in the animal care facility (~23 ºC and 12 hour (h) dark/ 12 h light cycle, lights on at 0700 hours). The *GRX2*$^{+/-}$ mouse line were a generous gift from Dr. Mary-Ellen Harper (University of Ottawa) and generated from the C57BL/6N mouse strain as described in Wu *et al.* (86). Deletion of the gene encoding GRX2 was originally conducted by the S-Y Ho lab through the deletion of exon 2 of the gene leading to a truncated mRNA gene product more predisposed to degradation (86). This truncated mRNA still possesses exons 1,3, and 4 resulting in a protein product with a mitochondrial translocation sequence but only 8 out-of-frame amino acids from exon 3 (86). Previous work in our lab found that mice heterozygous for the *Grx2* gene contain 50% less translational product compared to WT littermates (18). Additionally, total knockouts do not contain any GRX2 protein in the matrix of mitochondria (18). Breeding pairs were given free access to water and a standard chow diet (Teklad Global 18% protein rodent diet). New litters were weaned at three weeks of age and immediately ear notched for genotyping. Female WT and *GRX2*$^{+/-}$ littermates were fed a HFD (TD.06415) or matched CD (TD.06416) until 10 weeks of age (Table 2.1). Food and water consumption, body weight, and blood glucose measurements were taken weekly from week 4-10 weeks of age.

Blood glucose measurements were conducted as follows. Mice were restrained and the vein in the hind leg was exposed. The area below the knee was sterilized with 75% ethanol and then a small amount of petroleum jelly was applied to allow the blood to bead up. Pressure was applied to the great saphenous vein to engorge veins in the lower leg and then an exposed vein was pricked with an A26 gauge ½ inch hypodermic needle. The beaded blood was collected on a

blood glucose test strip (FreeStyle) and glucose levels were measured using a FreeStyle Lite blood glucose monitoring system. Animals were cared for in accordance with the principles and guidelines of the Canadian Council on Animal Care and the Institute of Laboratory Animal Resources (National Research Council). All procedures using mice were approved by the Animal Care and Use Committee of Memorial University of Newfoundland. At 10 weeks of age, mice were anesthetized with isoflurane at which time blood was collected by cardiac puncture leading to exsanguination of the mice. The total amount of animals utilized was 45 mice.

2.3 Genotyping

2.3.1 DNA Extraction

DNA was extracted from ear notches collected from mice right after weaning (3 weeks of age) using the REDExtract-N-Amp Tissue PCR Kit (Sigma-Aldrich). Each ear notch was placed in separate 1.5 mL microcentrifuge tubes labeled with the animal identification number. One hundred microliters of extraction solution and 25 μL of tissue prep solution was added to each tube. Samples were then incubated at room temperature for 10 minutes, followed by an incubation at 95 ^{o}C for 5 minutes. Samples were then allowed to cool down and 100 μL of neutralization solution was added to each tube. All pipette tips and microcentrifuge tubes used during this preparation were certified nuclease-free.

2.3.2 Polymerase chain reaction

Primers for *Grx2* were obtained from Integrated DNA Technologies. Primer sequences were provided by Dr. Mary-Ellen Harper (University of Ottawa) and were generated based on a previously published study by Wu *et al.* (86). In an Eppendorf PCR tube, 16 μL of primer mixture (1 μL of 0.5 μM *Grx2* forward primer, 1 μL of 0.5 μM *Grx2* reverse primer, 1μL of 0.5 μM *Grx2* neo primer, 3 μL nuclease free water, and 10 μL REDExtract-N-Amp PCR ReadyMix;

Table 2.1: Macromolecule/ingredient breakdown of HFD and matched CD (Teklad) (87).

Components	**TD.06415: High-Fat**	**TD.06416: Control**
Fat	**44.8% kcal (36 % saturated/47 % monounsaturated/17 % polyunsaturated)**	**10.2% kcal (29 % saturated/37 % monounsaturated/34 % polyunsaturated)**
Protein	**19% kcal**	**20% kcal**
Carbohydrate	**36.2% kcal**	**69.8% kcal**
Formula (g/kg)		
Casein	245.0	210.0
L-Cystine	3.5	3.0
Corn Starch	85.0	280.0
Maltodextrin	115.0	50.0
Sucrose	200.0	325.0
Lard	195.0	20.0
Soybean Oil	30.0	20.0
Cellulose	58.0	37.15
Mineral Mix	43.0	35.0
Calcium Phosphate, dibasic	3.4	2.0
Vitamin Mix	19.0	15.0
Choline Bitartrate	3.0	2.75
Food colour	0.1 (Red)	0.1 (yellow)

Table 2.2) and 4 μL of extracted DNA solution was added. DNA sequences were then amplified using an Eppendorf EP Gradient Mastercycler PCR system (Table 2.3).

2.3.3 Agarose gel electrophoresis

PCR samples were electrophoresed on a 1.5% (w/v) agarose gel which was made by dissolving 0.75 g of agarose powder (Fisher Scientific) in 0.5X Tris-Borate-EDTA (TBE, 10X solution diluted to 0.5X in analytical water) under heat. SYBR Safe DNA gel stain was added to the molten agarose (1/10,000 dilution), which was poured into a gel molding. The agarose was allowed to solidify and then set up in a Fisher Biotech Horizontal Electrophoresis System gel box. Five microliters of Trackit 100 base pair (bp) DNA Ladder (Fisher Scientific) was loaded into the first well to estimate DNA fragment size and 10 μL of the PCR products was loaded into the wells. Samples were electrophoresed for 40 minutes at 90 volts and nucleotide sequences corresponding to the amplified *Grx2* gene were visualized with an Alpha Innotech ChemiImager Ready System. WT mice produced a single nucleotide sequence that was 729 bp in size, $Grx2^{-/-}$ mice produced a fragment 510 bp in size, and $Grx^{+/-}$ mice contained both nucleotide fragments (Figure 2.1).

2.4 Buffer Preparation

2.4.1 Basic Medium

Basic medium (BM) was utilized for all experiments involving skeletal muscle. The medium was made fresh on a routine basis and stored at 4 ^{o}C for up to a month. BM consists of HEPES (20 mM) to buffer the solution, EGTA (1 mM) as a chelating agent to bind Ca^{2+} ions, $MgCl_2$ (5 mM) to stabilize ADP for phosphorylation, and KCl (140 mM) as an osmolyte. The pH of the buffer was adjusted to 7.0 using 2 M HCl.

Table 2.2: Primer sequences for amplification of *Grx2* gene.

Forward	**5'-GAC CTA GCC TAC CAG ACT TGG CTG AAA TTT ATT C-3'**
Reverse	**5'-CAT AGA CAC TCT TCA CTT TCA AGC CCA CCC TC-3'**
Neo	**5'- CCT ACA TTT TGA ATG GAA GGA TTG GAG CTA CGG G-3'**

Table 2.3: PCR protocol for amplification of *Grx2* gene.

Step 1	**94 ^{o}C for 5 minutes**
Step 2 (x30)	**94 ^{o}C for 30 seconds, 63 ^{o}C for 1 minute, 72 ^{o}C for 1 minute**
Step 3	**72 ^{o}C for 7 minutes**

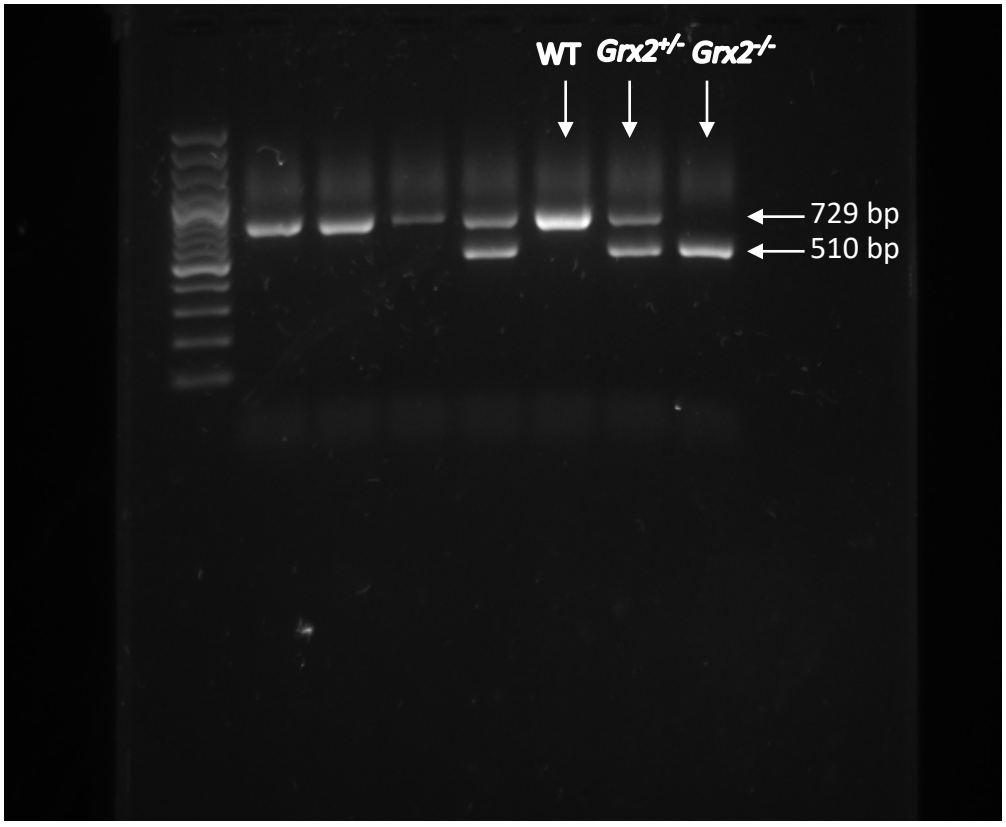

Figure 2.1: Agarose gel electrophoresis of PCR products to identify mouse genotype.

2.4.2 Homogenizing Medium

Muscle mitochondria were isolated in homogenizing medium (HM). The medium was made fresh on the day of experiments and kept on ice. HM consisted of BM containing 1 mM of ATP to promote myofiber depolymerization and the release of intramyofibrillar mitochondria, 1% (w/v) fatty acid free BSA to remove contaminating fatty acids and prevent the uncoupling of mitochondria, and 1 U subtilisin A, a protease required to digest myofibers. The amount of subtilisin A for muscle tissue homogenization was determined by the following:

Equation 2.1:

$$\boldsymbol{X\ uL\ of\ \frac{1mg}{mL}\ subtilisin\ A\ solution = \frac{muscle\ weight}{1\frac{mg}{mL}\ x\ 11.7\ mg/unit}}$$

2.4.3 Mannitol/EGTA/Sucrose/HEPES buffer

Mannitol/EGTA/sucrose/HEPES buffer (MESH) was utilized for all substrates and reagents pertaining to experiments with liver mitochondria. The medium was made fresh on a routine basis and stored at 4 ^{o}C for up to a month. MESH buffer consisted of 220 mM mannitol to quench hydroxyl radicals, 1 mM EGTA to chelate calcium ions, 70 mM sucrose to maintain osmolality, and 20 mM HEPES to buffer the solution. The pH was brought to 7.4 with 2 M HCl. MESH-B was utilized during mitochondrial isolation procedures and consisted of MESH and 0.5% (w/v) fatty acid-free BSA to remove contaminating fatty acids.

2.4.4 Respiration Medium

Respiration buffer was used for the polarographic measurement of oxygen consumption. For muscle mitochondria this medium consisted of basic medium supplemented with 10 mM

KH_2PO_4, to provide phosphate ions for ATP production and 0.5% (w/v) BSA to remove contaminating fatty acids. For liver mitochondria, this medium consisted of MESH-B supplemented with 10 mM KH_2PO_4 and 2 mM $MgCl_2$.

2.5 Histological Analysis

Haematoxylin and Eosin (H & E) and Periodic Acid-Schiff (PAS) staining was performed on isolated liver and muscle tissue and Oil Red O staining was performed exclusively on liver tissue. These were used for qualitative analysis of cell morphology, glycogen stores, and lipid accumulation respectively. Both were completed by the histology unit of the Medical Education and Laboratory Support Services at Memorial University's Faculty of Medicine. Tissue for H & E and PAS staining was prepared by emersion in 4% formalin upon isolation and Oil Red O liver sections were prepared by flash freezing in liquid nitrogen. Images were taken with an upright biological microscope equipped with a SPOT RT CCD Cool camera under bright field conditions.

2.6 Serum Biochemistry

Mice were heavily anesthetized with isoflurane at which time blood was collected by cardiac puncture leading to exsanguination of the mice. Cardiac puncture was performed with a heparinized (10,000 USP units/10 mL) 1 mL syringe with a 26-gauge, 1/2-inch needle. Once the mouse was heavily anesthetized a transverse incision was made exposing the mouse diaphragm and giving direct access to the heart. The needle was pushed through the diaphragm and into one of the heart ventricles and whole blood extracted until exsanguination. Whole blood was then transferred from the syringe into a 1.5 mL microcentrifuge tube on ice. Once remaining tissues were excised, whole blood was centrifuged at 2000 xg for 5 minutes to separate blood serum. Blood serum was decanted and placed in a separate 1.5 mL microcentrifuge tube and stored at

-80 ºC. Prior to each assay, frozen blood serum was removed from -80 ºC storage and allowed to thaw on ice.

2.6.1 Triglyceride levels

The L-type Triglyceride M assay kit from Wako Pure Chemical industries was utilized for determinations of serum triglyceride levels (Figure 2.2). Assays were conducted according to the manufacturer's instructions. A 5-point calibration curve was generated using the Wako Multi-Calibrator Lipids by addition of 4, 8, 12, and 16 µL of the calibrator lipid solution to separate wells in duplicate, corresponding to triglyceride concentrations of 100 mg/dL, 200 mg/dL, 300 mg/dL, and 400 mg/dL, respectively. Four microliters of analytical water (as a blank) and the unknown samples were also added to separate wells in duplicate. Ninety microliters of the R1 (colour A) solution were added to each well and mixed by gentle rotation at 37 ºC for 10 minutes. This solution contains the following:

- 50 U/mL glycerol kinase (GK)
- 8.0 mM ATP
- 5.6 U/mL Glycerol-3-phosphate oxidase (GPO)
- 150 U/mL Catalase
- 0.4 mM N-(3-isopropyl)-3methoxy-5-methylaniline (HMMPS)
- 2.0 U/mL ascorbate oxidase

The absorbance was measured at 600 nM using a SpectraMax M5 plate reader. This reading is established as the sample blank. Following this 30 µL of R2 (colour B) solution was added to each well and mixed by gentle rotation at 37 ºC for 10 minutes. This solution contains the following:

- 250 U/mL lipoprotein lipase (LPL)
- 25 U/mL horseradish peroxidase (HRP)
- 4.6 mM 4-aminoantipyrine

The absorbance is again read at 600 nm using a SpectraMax M5 plate reader. The final absorbance was calculated as the difference between the two absorbances and a standard curve generated to determine that concentration of triglycerides in the unknown samples.

2.6.2 Glutathione/ Glutathione Disulfide Pool

The glutathione assay kit from Sigma Aldrich was used to assess serum GSH and GSSG concentrations (Figure 2.3). Assays were conducted according to manufacturer's instructions. A 5-point standard curve was generated with the following nmoles GSH: 0.0312, 0.0625, 0.125, 0.25, 0.5. Twenty-five microliters of each serum sample were transferred to a new Eppendorf tube. Two hundred microliters of 5% 5-sulfosalicylic acid were added to each tube to deproteinize the sample. The samples were then vortexed vigorously and incubated at 4 ºC for 10 minutes followed by centrifugation at 10,000 x g for 10 minutes. Samples and standards provided in the kit were loaded into individual wells of a 96 well plate in duplicate. One hundred and fifty microliters of working mix (pH 7.0) containing potassium phosphate buffer (95 mM), EDTA (0.95 mM), 5,5'-dithiobis (2-nitrobenzoic acid) (DTNB; 0.031 mg/mL), glutathione reductase (0.115 U/mL), was added to each well and incubated for 5 minutes with agitation. Fifty microliters of the NADPH solution (0.038 mg/mL) was added to each well and the absorbance was read with a kinetic read at 412 nm at 1 minute intervals for 5 minutes using a SpectraMax M5 plate reader. The GSH standards were utilized to generate a standard curve. The GSH concentration in the unknown samples were interpolated from the standard curve.

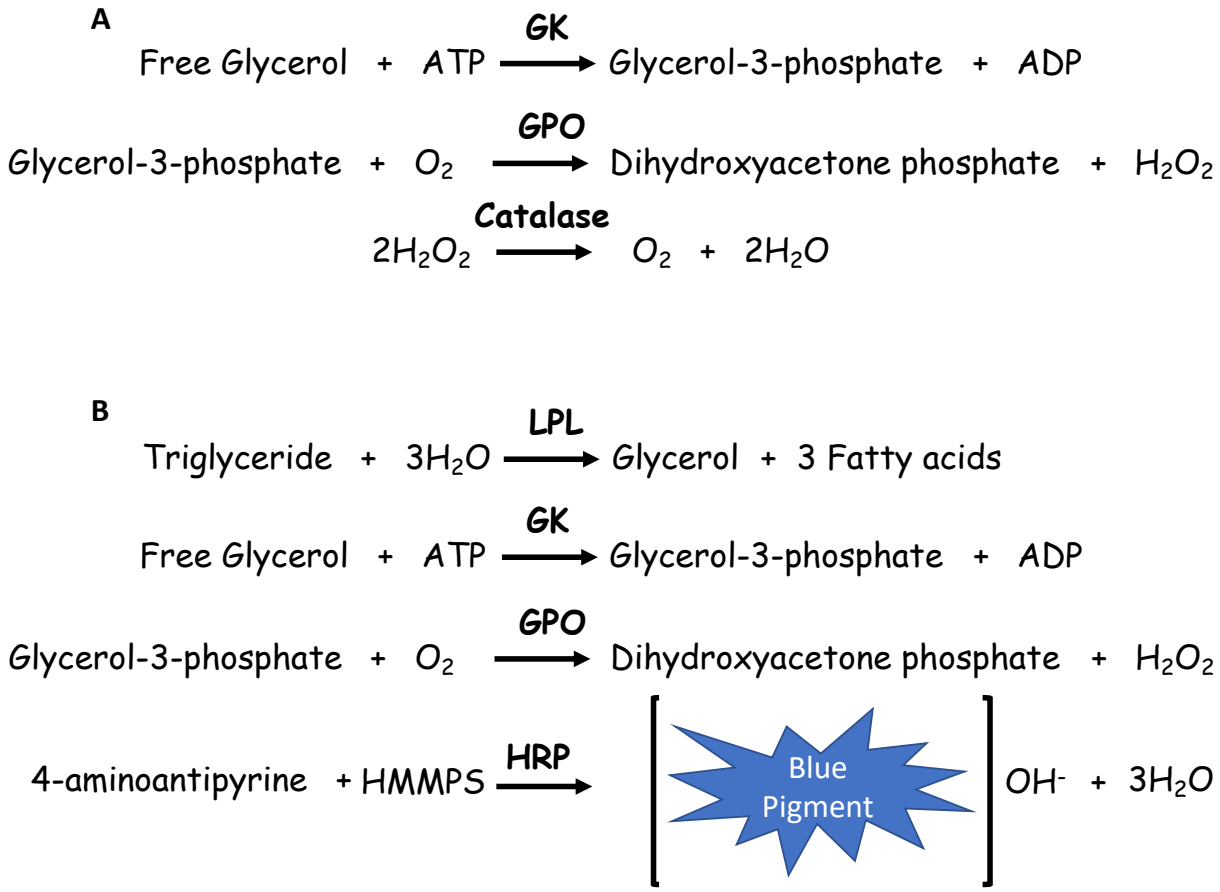

Figure 2.2: Principle of L-type Triglyceride Assay. (A) Glycerol kinase utilizes ATP to convert free glycerol to glycerol-3-phosphate which is subsequently converted to dihydroxyacetone phosphate coupled with the generation of H_2O_2 by the action of glycerol-3-phosphate oxidase. The H_2O_2 generated is neutralized to H_2O by the action of catalase. (B) Lipoprotein lipase cleaves triglycerides generating free fatty acids and glycerol. Glycerol is once again converted to dihydroxyacetone phosphate by glycerol kinase and glycerol-3-phosphate oxidase at the expense of ATP and coupled with the generation of H_2O_2. HMMPS and 4-aminoantipyrine undergo condensation to form a blue pigment in the presence of HRP and H_2O_2.

2.6.3 Protein Carbonyl Content Assay

The protein carbonyl content assay kit from Abcam was utilized to quantify protein carbonyls in mitochondrial samples. Protein carbonyl groups can be a biomarker for oxidative stress and the assay works by the derivatization of protein carbonyl groups with 2,4-dinitrophenylhydrazine (DNPH) leading to the formation of stable dinitrophenyl (DNP) hydrazine adducts that can be detected spectrophotometrically. Assays were conducted according to manufacturer's instructions. Mitochondrial samples for liver and muscle were diluted to 3 mg/mL in 100 µL of RIPA buffer in a 1.5 mL microcentrifuge tube. To remove nucleic acids that can interfere with the assay, 10 µL of Streptozocin was added to each sample, incubated for 15 minutes at room temperature, and centrifuged at 13,000 x g for 5 minutes. Supernatant from the previous step was placed in new tube and 100 µL of DNPH was added to each sample, vortexed, and incubated at room temperature for 5 minutes. Then 30 µL of 100% TCA was added, vortexed, and placed on ice for 5 minutes. Samples were then centrifuged at 13,000 x g for 2 minutes and supernatant removed. Pellets from previous step were washed twice by resuspension in 500 µL of cold acetone, vortexed for 30 seconds, incubated at -20 ^{o}C for 5 minutes, and then centrifuged at 13,000 x g for 2 minutes. Washed pellets were resolubilized in 200 µL of 6 M guanidine solution and 100 µL of each sample and a 100 µL H_2O blank were loaded into a 96 well plate in duplicate. The absorbance was read at 375 nm using a SpectraMax M5 plate reader and amount of carbonyl per well per mg protein was determined by:

Equation 2.2:

$$C = \frac{\frac{A_{372} - Blank}{6.364} x100}{0.3}$$

6.364 = millimolar extinction coefficient (22 $mM^{-1}cm^{-1}$) times path length (0.2893 cm)

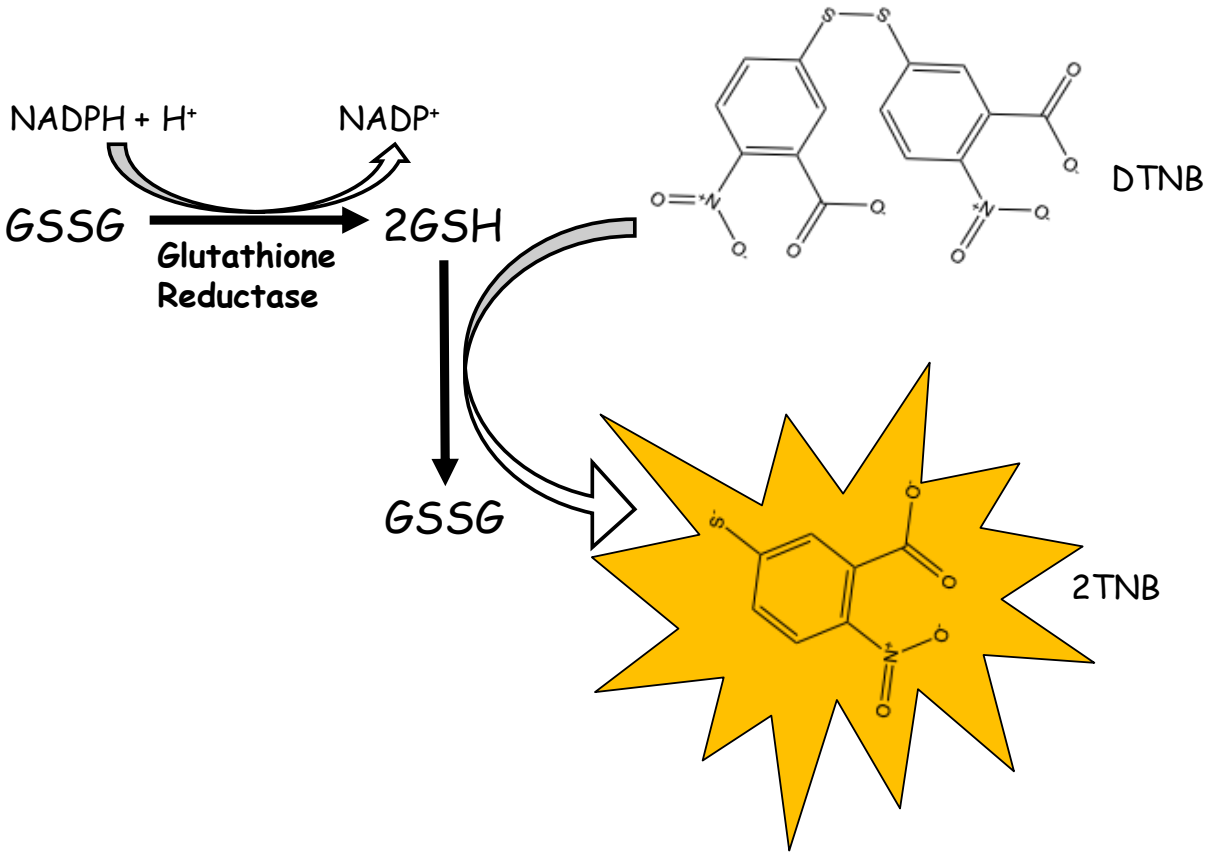

Figure 2.3: The GSH in this assay acts as a catalyst for the continuous reduction of DNTB to 5-thio-2-nitrobenzoic acid (TNB), a yellow substance. The GSSG formed is recycled by glutathione reductase and NADPH (GSSG present will also react to produce a positive value).

100 = total volume in well

0.3 = mg protein in well

2.7 Skeletal Muscle and Liver Mitochondria Isolation

All steps for tissue dissection and the isolation of mitochondria were carried out on ice or at 4 ^{o}C. At 10 weeks of age, mice were anesthetized with isoflurane and euthanized by cardiac puncture. Mice were then dissected and forelimb, hindlimb, and pectoral muscles were pooled in ice-cold BM while other organs were placed in MESH. All tissues were weighed and then pooled muscle and liver were placed in buffer. For the isolation of muscle mitochondria, connective tissue and fat were removed from the pooled samples, and then the tissue was dried and weighed to measure total tissue mass. Pooled muscles were minced on a Teflon watch glass using a steel razor. The minced tissue was then placed in 30 mL of homogenizing buffer. Tissue homogenization was carried out with a Glas-Col variable speed automatic tissue homogenizer (Cole-Palmer) for muscle. The tissue was completely homogeneous after ~6 to 10 passes with the Teflon pestle. Muscle homogenates were then centrifuged at 800 x g for 9 minutes. The supernatants were then collected and centrifuged at 12,000 x g for 9 minutes. The liquid was decanted, and the remaining pellet was resuspended in 1 mL of BM and incubated on ice for 5 minutes. Incubation of the resulting muscle pellet in BM promotes the repolymerization of any remaining myofibers allowing for their easy removal by low-speed centrifugation. After the incubation, 26 mL BM was added to each tube and the samples were centrifuged at 800 x g for 9 minutes to remove repolymerized myofibers. The supernatant was collected and then centrifuged at 12,000 x g for 9 minutes. The final mitochondria pellet was then resuspended in 200 μL of BM for muscle.

For liver mitochondria, tissues were minced on a Teflon watch glass and then homogenized using the Potter Elvejham method (~20 passes). The homogenate was then centrifuged at 800 x g for 9 minutes to pellet undisrupted material. The supernatant was collected and then centrifuged at 12,000 x g for 9 minutes. The solution was decanted and the sides of the centrifuge were carefully cleaned with a Kimwipe to remove excess fat. The pellet was suspended in 1 mL of MESH-B and then topped up to 26 mL with MESH-B and centrifuged at 12,000 x g for 9 minutes. The solution was decanted and the pellet was resuspended in 500 μL MESH. All centrifugations were performed with a Thermo Sorvall RC6+ centrifuge. Mitochondria were then stored on ice and used immediately for assays. Any remaining mitochondria were stored at -80 ^{o}C for later use.

2.8 Bradford Assay

2.8.1 Protein concentration

Protein equivalents to mitochondria was determined using the Bradford assay. This assay works under the principle that protein molecules (namely basic amino acids residues) bind to Coomassie dye under acidic conditions resulting in a pigment change of brown to blue. One microliter of mitochondria was diluted in 999 μL of analytical grade water. Samples were then vortexed vigorously and 50 μL of the diluted mitochondria was added to 200 μL of Bradford reagent. Then 750 μL of analytical water was added and the mixture vortexed vigorously. Two hundred microliters of the Bradford mixture was loaded into a black 96 well plate in duplicate and the absorbance was read at 595 nm using a SpectraMax M5e plate reader (Molecular Devices) and Softmax pro software (version 5.4.6). Protein concentration equivalent to mitochondria was then calculated using a standard curve.

2.8.2 Standard Curve

The standard curve was constructed by mixing increasing concentrations of BSA (0-1.875 μg/mL) with Bradford reagent and diluting with analytical water, precisely as described above. Changes in absorbance were then measured and values plotted on the y-axis while the corresponding concentrations plotted on the x-axis (Figure 2.4). This allowed unknown protein concentrations to be determined from their absorbance. The final concentration of proteins equivalent to mitochondria was ~7-20 mg/mL for muscle and ~15-40 mg/mL for liver.

2.9 Amplex UltraRed Assay

The Amplex UltraRed (AUR) assay was used to quantify the rate of $O_2^{\bullet-}$ / H_2O_2 production by isolated mitochondria. AUR is a non-fluorescent molecule which reacts with H_2O_2 in the presence of horseradish peroxidase (HRP) to form fluorescent resorufin, as depicted in Figure 2.5. For these assays, mitochondria were first diluted to 1.5 mg/mL (skeletal muscle) in BM or 3.0 mg/mL (liver) in MESH, respectively. Samples were then diluted to 0.15 mg/mL or 0.3 mg/mL, respectively, in the wells of a black 96 well plate. Mitochondria were then incubated for 5 minutes at 25 ^{o}C. Fifty micromolar carnitine was included in the incubation medium for experiments using palmitoyl-carnitine. Wells were then incubated for 10 minutes at 25 ^{o}C either in the presence or absence of various site specific $O_2^{\bullet-}$ / H_2O_2 inhibitors (Figure 2.5). The inhibitors served as a negative control to ensure that changes in resorufin fluorescence was associated with the detection of H_2O_2 by mitochondria and not due to non-specific auto-oxidation. Additionally, inhibitors were chosen based on the substrate that was being oxidized during our measurements and concentrations based on previous literature (19,52). The inhibitors used were as follows; CPI-613 (150 μM; Pyruvate/Liver), KMV/Rotenone (10 mM/4 μM; Pyruvate/Muscle), Malonate (5 mM; Succinate), Roteone/Mxothiazol/Aptein A5 (4 μM/4 μM/40

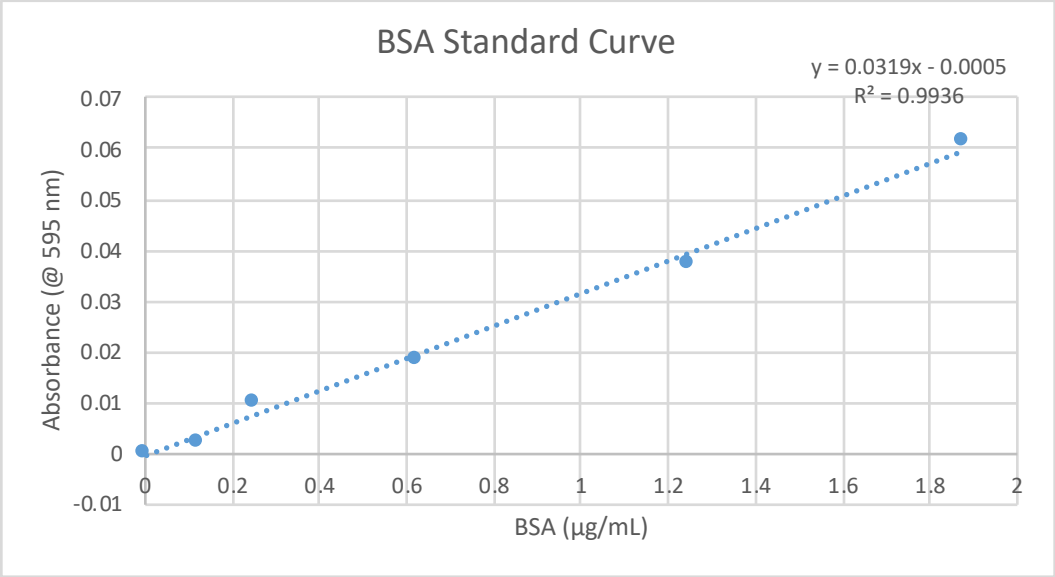

Figure 2.4: BSA standard curve for which the equation of the line of best fit was utilized to determine mitochondria protein concentration.

μM; Palmitoyl-carnitine)(Figure 2.5). After the incubation, SOD (25 U/mL), HRP (3 U/mL), and AUR (10 μM) were added to the samples and the reaction initiated by the addition of substrate (50 μM Pyruvate/50 μM Succinate/50 μM palmitoyl-carnitine).

For this assay the concentration of AUR is kept low at 10 μM due to the ability of AUR to inhibit mitochondrial respiration at higher concentrations. For the concentration of substrates chosen, these substrate concentrations represent physiological levels that produce maximal $O_2^{\bullet-}$/ H_2O_2 (88). Furthermore, exogenous addition of SOD preserves the accuracy of $O_2^{\bullet-}$/ H_2O_2 measurement by limiting peroxynitrite formation by $O_2^{\bullet-}$, which has the capacity to react with AUR (89). Additionally, the reaction of HRP and H_2O_2 forms a compound (Compound I) responsible for the equimolar formation of resorufin, compound I reacts with fluxes of $O_2^{\bullet-}$ (89). Dual wavelength fluorescence changes were then measured over 5 minutes at 30 second intervals using a Spectramax M5 plate reader set to an excitation/emission 565 nm:600 nm (AUR) and 376 nm:450 nm (NAD(P)H). Values of resorufin fluorescence were converted into $O_2^{\bullet-}$/ H_2O_2 produced using a H_2O_2 standard curve, generated from using 0, 20, 50, 200, 500, and 1000 nM H_2O_2 stock solution. To determine rate of $O_2^{\bullet-}$/ H_2O_2 production the following equation was used to get a rate as per min/mg protein:

Equation 2.3:

$$\frac{\boldsymbol{Final\ Concentration - Inital\ Concentration}}{\mathbf{5}\ \boldsymbol{minutes}} \div \boldsymbol{mitochondial\ concentration\ in\ well}$$

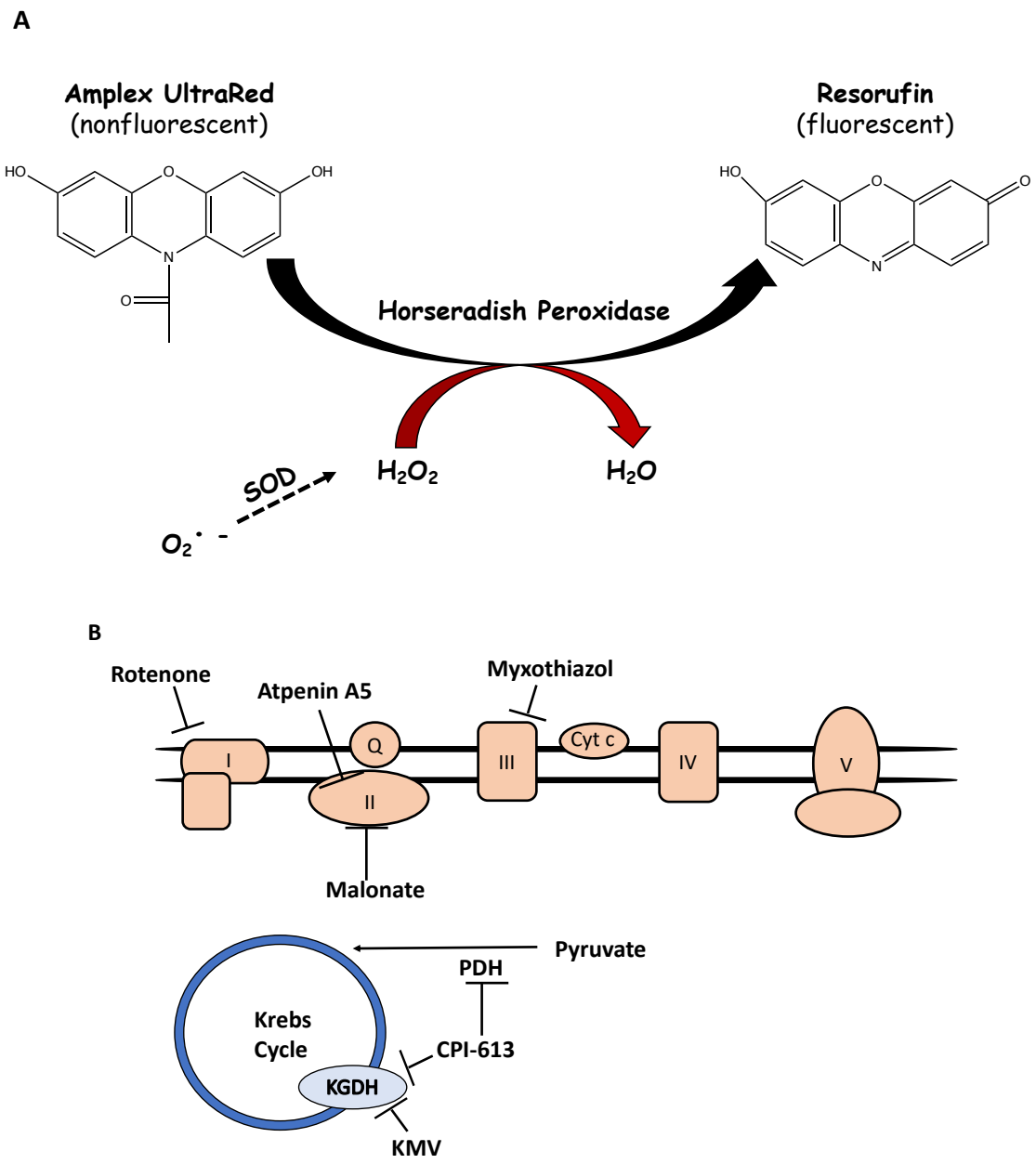

Figure 2.5: (A) Depiction of Amplex UltraRed reaction with horseradish peroxidase and hydrogen peroxide. Superoxide dismutase (SOD) supplementation ensures any superoxide present is converted to hydrogen peroxide. (B) Site-specific inhibition of $O_2^{\bullet -}$/ H_2O_2 for the chemicals used as controls for Amplex UltraRed Assay.

2.10 Polarographic Measurement of Mitochondrial Respiration

The mitochondrial health index can be measured by monitoring the different states of respiration. This was achieved using an Oxytherm electrode system (Hansatech) (Figure 2.6). The Oxytherm chamber measures the partial pressure of O_2 using a platinum anode and silver cathode that are separated by a KCl solution. Molecular oxygen from the chamber diffuses through the PVDF membrane, making contact with the silver cathode where it is reduced forming H_2O_2. The resulting H_2O_2 is then oxidized by the platinum anode creating a current that is proportional to the partial pressure of O_2 in the chamber. Therefore, the rate of O_2 consumption measured by a population of mitochondria is inversely proportional to the amperage traveling through the anode. Mitochondrial were diluted to 0.2 mg/mL (muscle) or 0.5 mg/mL (liver) in the reaction chamber containing respiration medium. State 2 respiration was then induced by the addition of substrates malate (2 mM)/pyruvate (10 mM) or succinate (5 mM). State 2 respiration was induced once a stable O_2 baseline level was reached, mitochondria respired under these conditions for a few minutes to establish a PMF. This was followed by the addition of ADP (1 mM) to induce state 3 (phosphorylating respiration). This effectively completes the respiratory chain by allowing proton return from the intermembrane space into the mitochondrial matrix through complex V, driving up respiration. Once ADP was completely exhausted from the reaction chamber, oligomycin (4 μg/mL) was added to the reaction chamber to measure state 4 respiration (proton leak-dependent respiration associated with the return of protons to the matrix using complex V-independent systems). Oligomycin serves as a complex V inhibitor but also prevents the metabolism of ATP back to ADP by any contaminating ATPases. Therefore, addition of oligomycin ensures that respiration associated with leaks is accurately

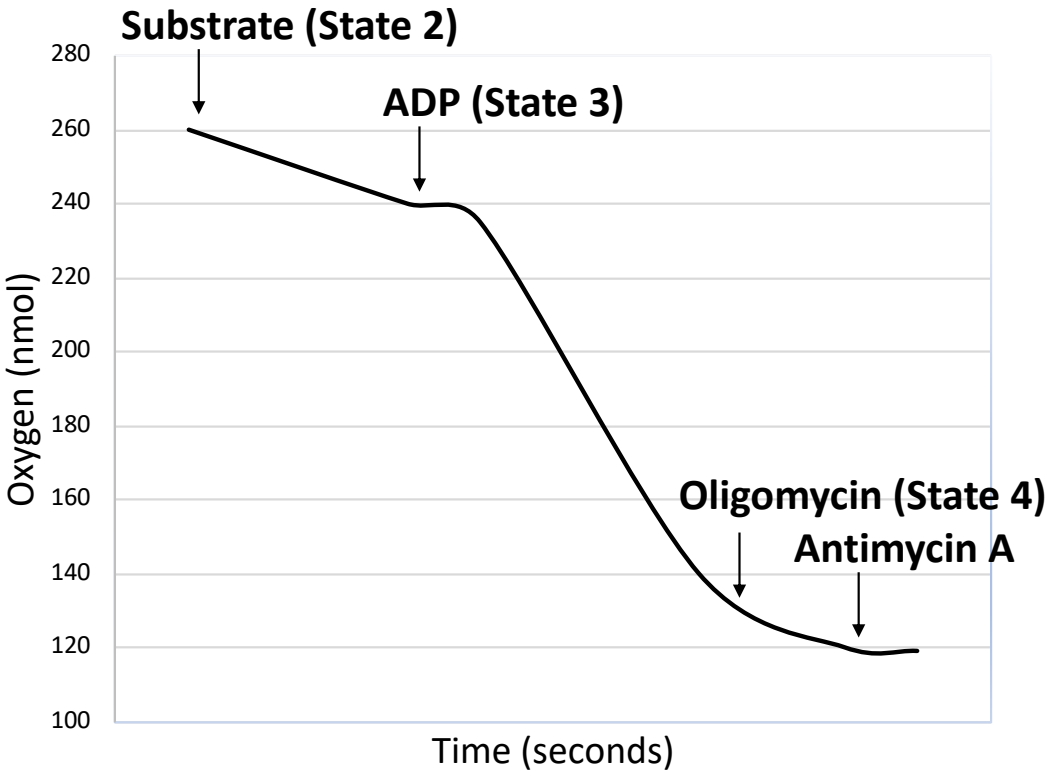

Figure 2.6: Trace of oxygen concentration during the different states of respiration in an Oxytherm Clark-type electrode.

measured. Final volume in the reaction chamber was 1 mL and reactions were halted by the addition of antimycin A (4 μM), a complex III inhibitor. Respiratory control ratio (RCR) values were calculated as the state 3 to state 4 respiration and is a proxy measure of the ATP producing potential of mitochondria.

2.11 Data Analysis

Graphpad Prism 6 software was utilized for all statistical analysis. Data are represented either as the mean ± standard error of the mean (SEM) or mean ± standard deviation (SD) with n ≥ 4. Two-way ANOVA repeated measures was utilized to determine significance when comparing repeated measures over time. Two-way ANOVA with a Tukey's post-hoc test was utilized to determine significance when comparing two variables between groups. Statistical significance was represented as the following:

*/#	$P \leq 0.05$
**/##	$P \leq 0.01$
***/###	$P \leq 0.001$
****/####	$P \leq 0.0001$

Chapter 3: Results

3.1 Deleting the *Grx2* gene does not alter the response of mice towards high-fat feeding.

3.1.1 Deleting the Grx2 gene does not alter the weight gain profile of mice fed a HFD.

Our group observed previously that the male C57BL/6N mice containing a deletion for the gene encoding GRX2 did not display any alterations in weight gain, adipose tissue mass, or circulating insulin and triglyceride levels and were protected from intrahepatic lipid accumulation and preserved liver glycogen levels (59). This was in contrast to male WT littermates where high-fat feeding induced weight gain, insulin resistance, and fatty liver disease (59). In the present thesis, we conducted a similar study except on female mice containing a deletion for *Grx2*. To examine the role that GRX2 protein plays in female metabolism, a whole body *Grx2* deficient mouse model was generated from a heterozygous *GRX2* breeding pair.

From 3 to 10 weeks of age, there was no diet or genotypic differences in mouse weight-gain profiles (Figure 3.1A). Indeed, it was observed that *Grx2* $^{+/-}$ mice on CD and HFD had the same weight-gain trend as WT littermates on both diets. This observation was independent of food and water consumed over the 7-week diet (Figure 3.1B-C). These data are in contrast to the male study in which it was observed that WT mice on a HFD gained significantly more mass than the WT mice on matched CD (59). Indeed, male WT mice had a significant increase in weight gain as early as 4 weeks when fed a HFD in the WT, while *Grx2* $^{+/-}$ mice displayed a weight gain profile that was identical to the control group (59). Additionally, male WT mice fed a HFD also displayed a significant increase in circulating triglycerides and insulin, an effect that was not observed in the male *Grx2*$^{+/-}$ littermates (59). Here, however, I observed no statistically significant changes in circulating glucose (Figure 3.2A) or triglycerides (Figure 3.2B) in female mice fed either CD or HFD. Furthermore, no genotype effect was observed in WT and *Grx2* $^{+/-}$

mice fed a HFD. It should be noted here that the CD and HFD used in the female study were identical to those in the male study.

At ~10 weeks of age, mice were euthanized and subcutaneous abdominal fat pads were excised and weighed as a proxy for mouse obesity. Compatible with mouse body weight data there was no significant difference in mouse adipose tissue mass between groups (Figure 3.3A). This result contrasts with male mice where a significant increase in the mass of the abdominal fat pad was observed in the WT mice on a HFD, an effect that was absent from *Grx2*$^{+/-}$ littermates (59). This contrast shows a distinct resistance to DIO in WT female mice that is absent in male mice. Furthermore, these findings indicate that deleting the gene encoding GRX2 does not have the same metabolic effects on female mice as observed in the male counterparts. Organ weights were also not significantly different for muscle, kidney, and heart in female mice between genotype or diet (Figure 3.3B-D). However, there was a significant diet effect on liver mass in both the WT and *Grx2* $^{+/-}$ female mice fed an HFD. Indeed, liver mass was significantly lower in mice fed a HFD when compared to the control groups (Figure 3.3E). Additionally, there was a significant difference between WT and *Grx2* $^{+/-}$ mice on HFD, with WT mice displaying increased liver mass (Figure 3.3A).

3.1.2 Increased Liver Fat Deposition and Increased Glycogen Storage

Next, we conducted histological analyses on liver and muscle tissue to determine if diet and genotype affected the overall morphology of hepatocytes or differentiated polynucleated muscle fibers. H & E staining of hepatocytes determined that there was no observable difference in the overall morphology of these cells (Figure 3.4). Similar observations were made with muscles – there was no diet or genotype effect on the overall morphology of the muscle fibers (Figure 3.4). Oil Red O staining was also performed on hepatocytes to determine if there was any

difference in intrahepatic lipid accumulation in mice fed both diets. There appeared to be an increase in the size of lipid droplet stains in WT/HFD mice and to a smaller extent *Grx2* $^{+/-}$/CD mice when compared to WT/CD mice (Figure 3.5). There also appeared to be an increase in lipid staining in liver sections from the *Grx2* $^{+/-}$ mice fed a HFD, but this staining does not appear to correlate to increased size of lipid droplets but instead an increase in abundance of droplets (Figure 3.5).

Intrahepatic glycogen content was evaluated using a Periodic Acid-Schiff (PAS) stain. Stains were conducted on samples treated with amylase as a control, a glycoside hydrolase that degrades polysaccharides into their corresponding monosaccharide units. PAS non-specifically stains polysaccharides, including cell surface polysaccharides on glycoproteins. Therefore, treating samples with amylase is an important control since it allows one to discern how much of the overall stain is associated with glycogen granules housed in the intrahepatic environment. This staining revealed that glycogen appears to have increased deposits in the WT mice on an HFD when compared to the other three groups (Figure 3.6). It also appears that there is more glycogen storage in *Grx2* $^{+/-}$ mice compared to the WT/CD mice (Figure 3.6). The results from Oil Red O and PAS staining appears to reveal that the difference in liver masses observed was due to differences in lipid accumulation and glycogen storage in hepatocytes. However, it is not possible to determine whether it is lipid or glycogen storage that is the dominant factor.

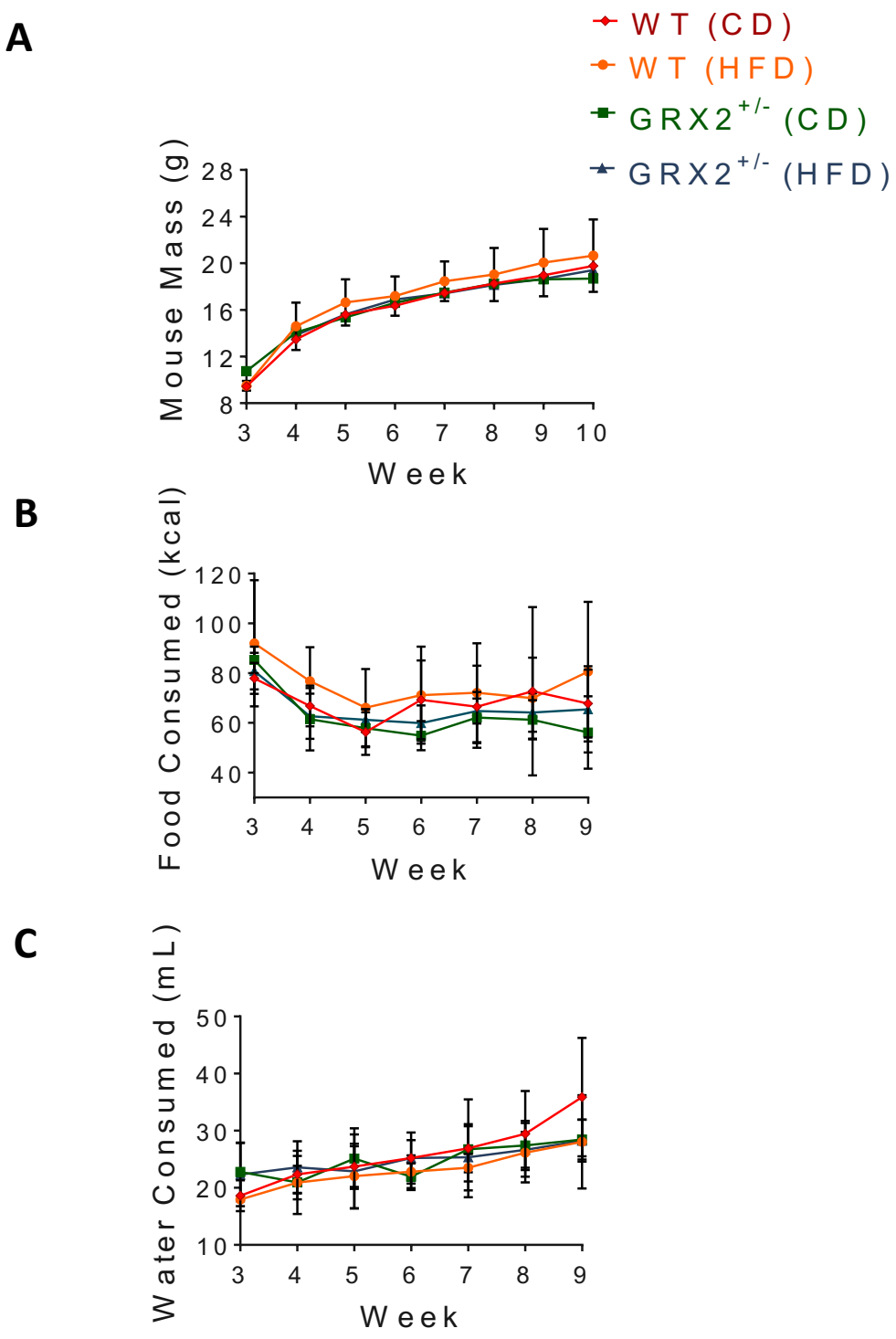

Figure 3.1: Mouse measurements taken from 3 to 10 weeks of age (A) Mouse mass (B) Food consumption (C) Water consumption. n = 4-8, mean ± SD, two-way repeated measures ANOVA.

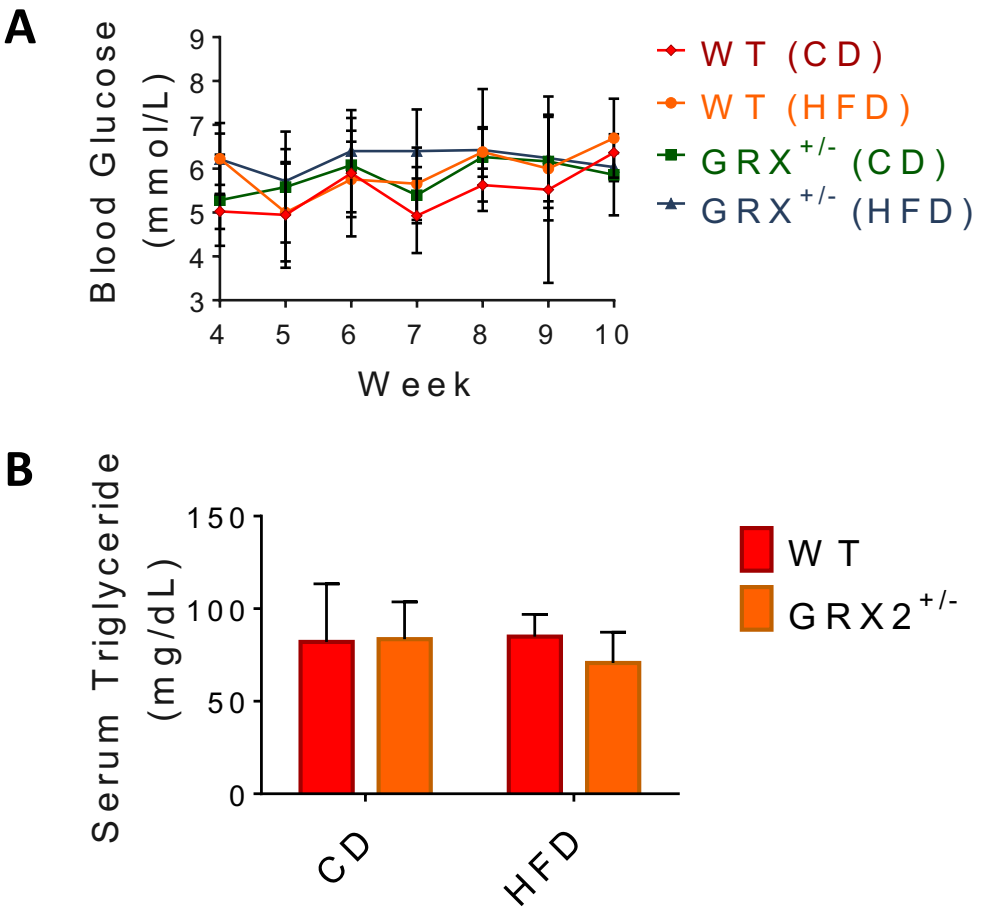

Figure 3.2: (A) Non-fasted mouse blood glucose levels taken ~18:00 h weekly from 4 to 10 weeks. WT (n = 4), *GRX2*$^{+/-}$ (n=5); mean ± SD, two-way repeated measures ANOVA.

(B) Mouse triglyceride levels in blood serum collected by cardiac puncture on non-fasted mice, n = 4, mean ± SEM, two-way ANOVA.

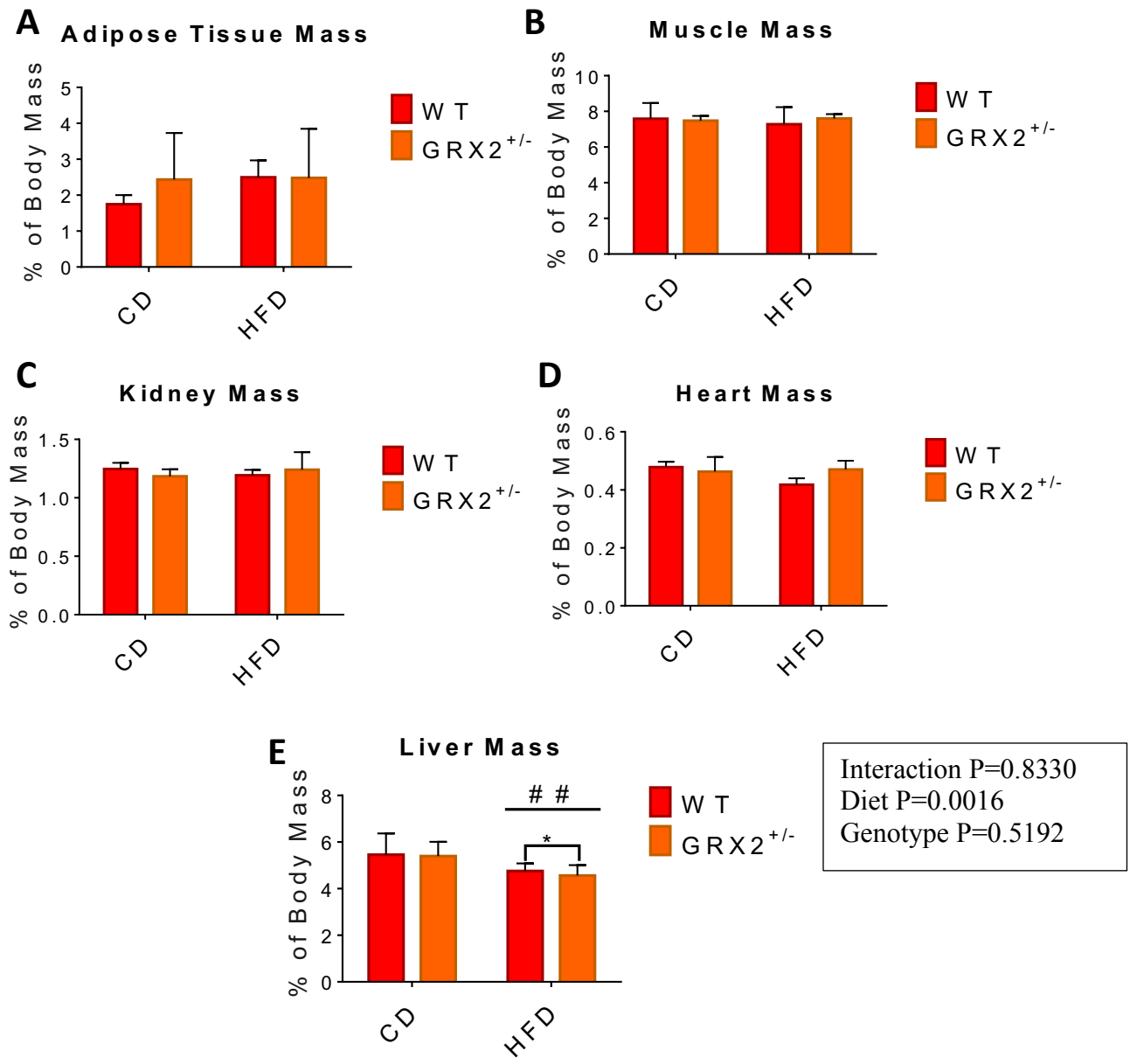

Figure 3.3: Mouse organ mass corrected to mouse body mass (A) Adipose tissue (B) Muscle (C) Kidney (D) Heart (E) Liver. WT(CD) n = 6, WT(HFD) n = 7, *GRX2*$^{+/-}$(CD) n = 9, *GRX2*$^{+/-}$ (HFD) n = 9; mean ± SD, two-way ANOVA with Tukey's post-hoc test. * represents genotypic differences while # represents differences between diet.

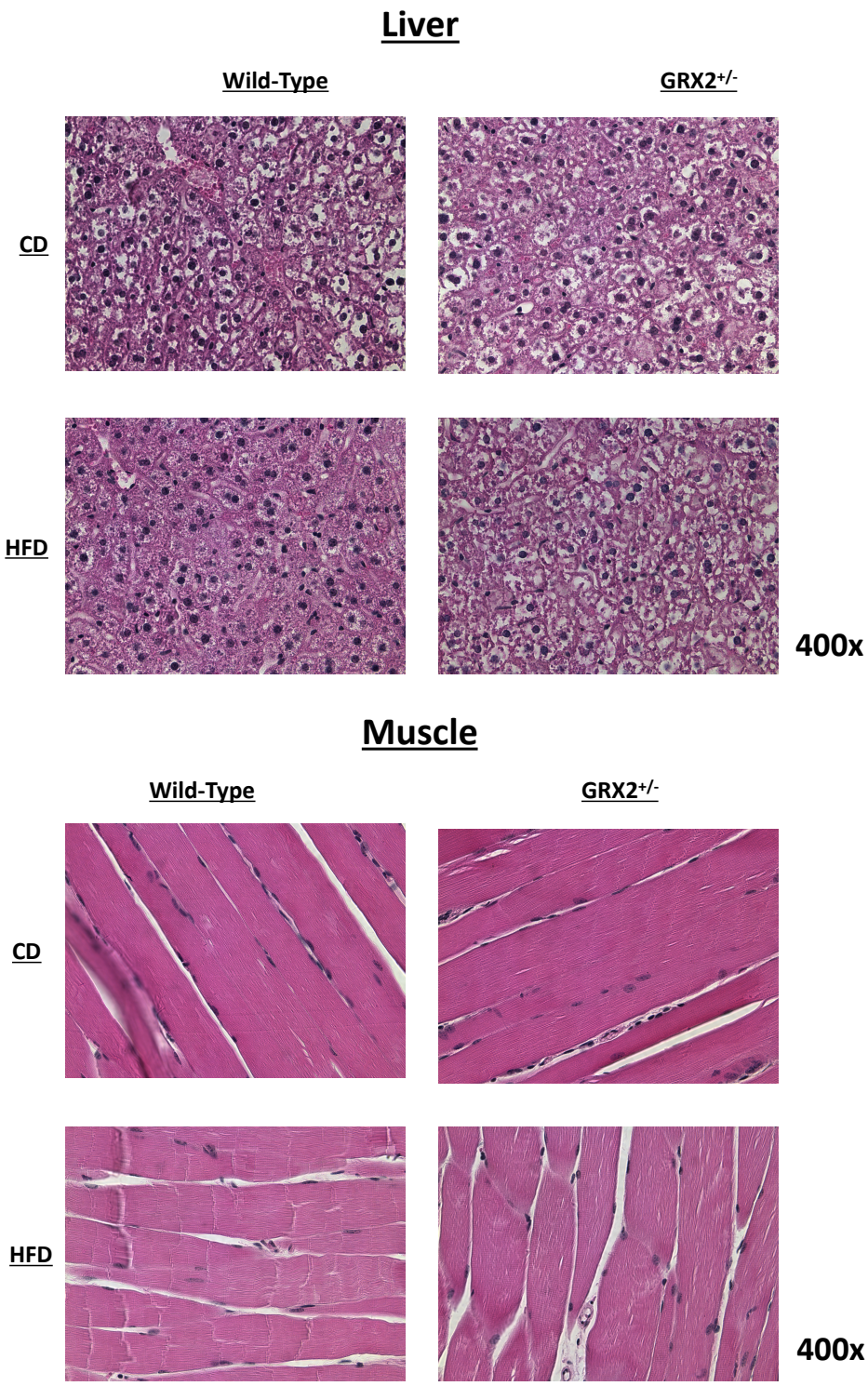

Figure 3.4: Hematoxylin and Eosin staining of liver (top) or gastrocnemius muscle (bottom) sections prepared from 10 week old *Grx2*$^{+/-}$ mice and littermates fed a CD or HFD, to determine if diet or genotype had effect on overall morphology (n = 3).

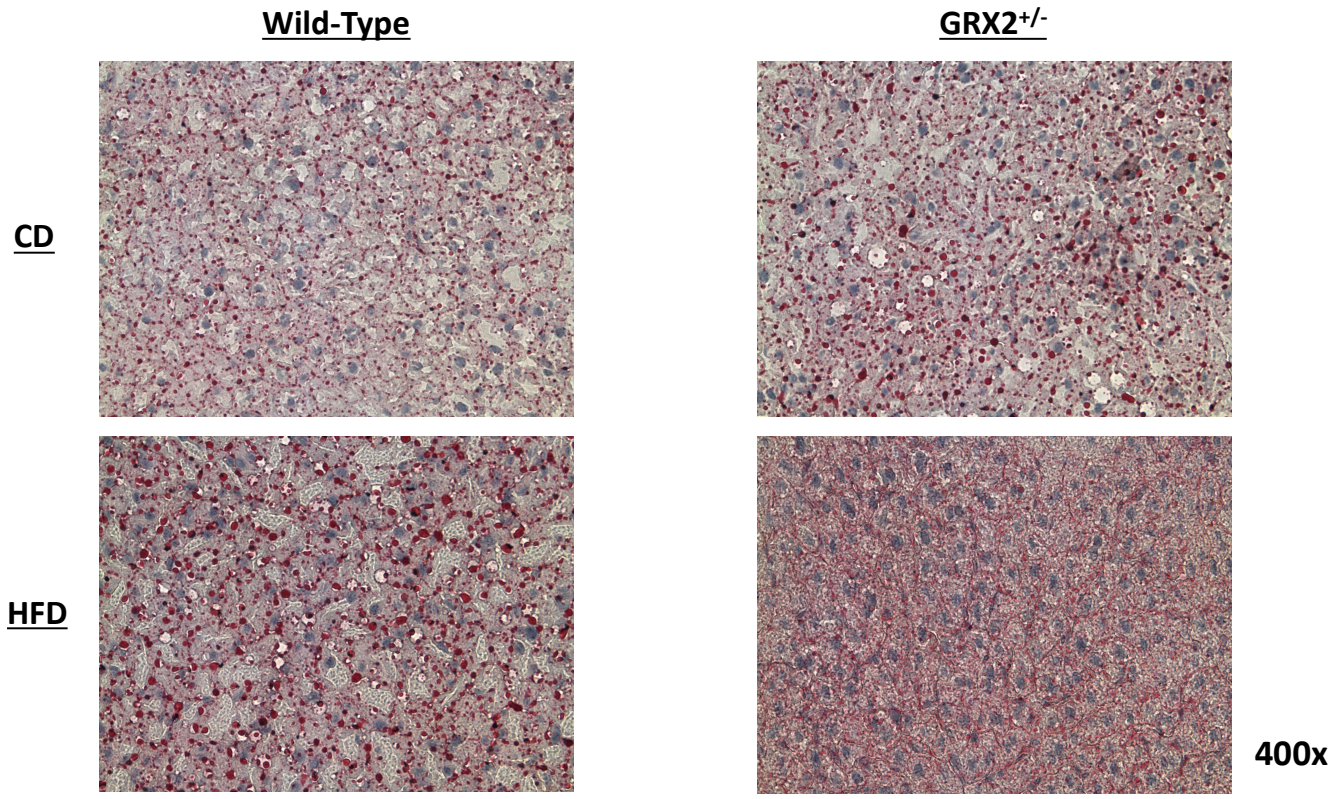

Figure 3.5: Oil Red O staining of liver sections prepared from 10 week old *Grx2*$^{+/-}$ mice and littermates fed a CD or HFD, to determine differences in intrahepatic lipid accumulation, lipid droplets represented as red staining (n = 3).

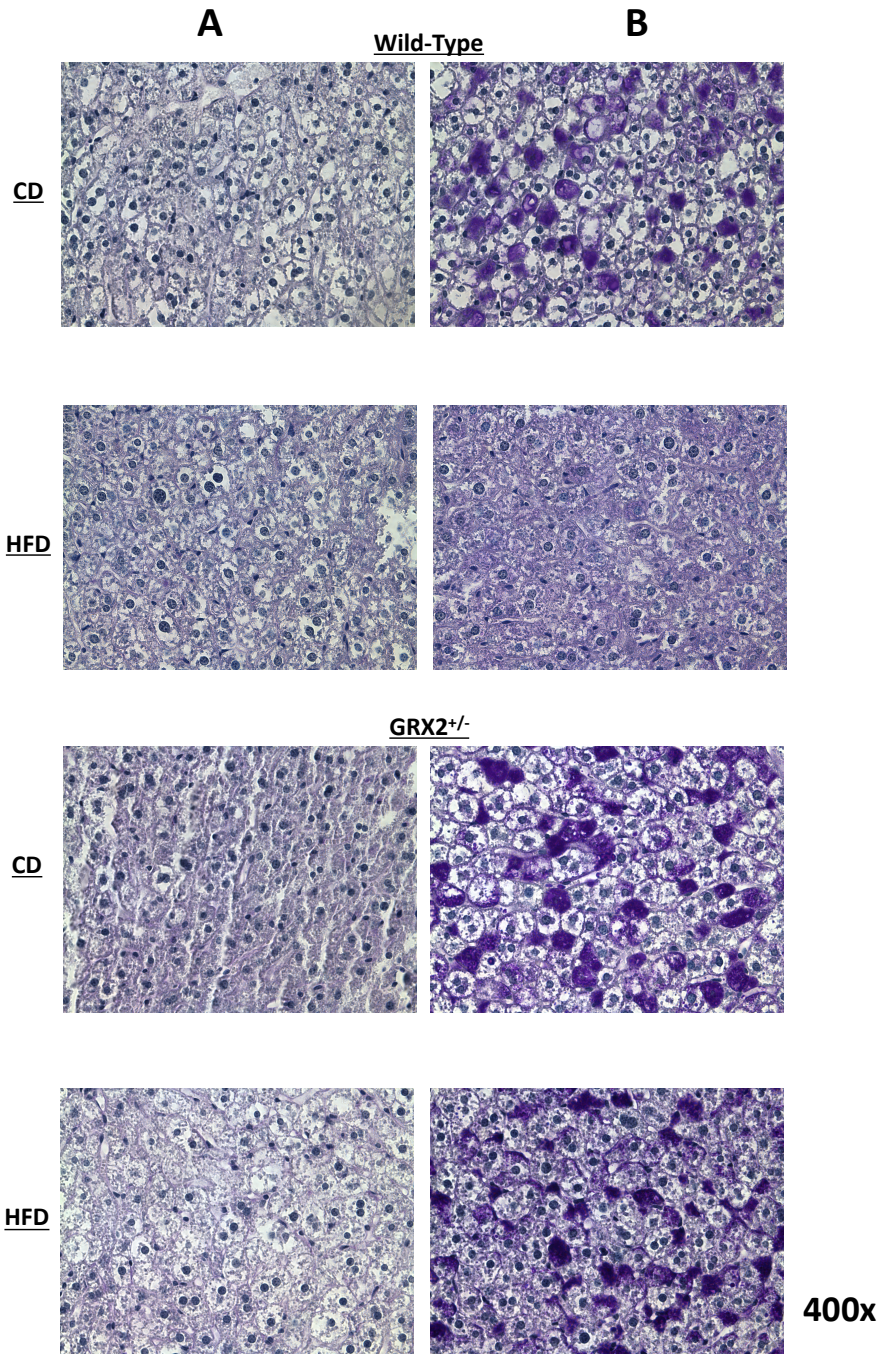

Figure 3.6: Periodic acid-Schiff stain of liver sections prepared from 10 week old *Grx2*$^{+/-}$ mice and littermates fed a CD or HFD, purple stain represents staining of polysaccharides, mucus substances, and basement membranes. (A) Amylase positive slides, which digests carbohydrates and represents glycogen absent staining. (B) Amylase-negative slides, represents total staining (n = 3).

3.2 Impact of Deleting *Grx2* Gene on $O_2^{\bullet-}/H_2O_2$ Production

3.2.1 Liver Mitochondria ROS Production

The rate of $O_2^{\bullet-}/H_2O_2$ release by mitochondria energized with pyruvate/malate revealed a genotype difference in production between WT and *Grx2*$^{+/-}$ littermates fed a HFD (Figure 3.7A). Indeed, when challenged with a HFD, *Grx2*$^{+/-}$ mice had elevated levels of $O_2^{\bullet-}/ H_2O_2$ compared to WT littermates fed the same diet. However, I observed no statistically significant diet-dependent effects for liver mitochondria isolated from WT and *Grx2*$^{+/-}$ mice (Figure 3.7A). Reaction chambers were also supplemented with CPI-613, a keto acid dehydrogenase inhibitor, to confirm that the change in resorufin fluorescence was associated with ROS produced by mitochondria oxidizing pyruvate. CPI-613 is a lipoic acid analog and thus inhibits keto acid dehydrogenase activity by forming covalent adducts with the vicinal protein thiols in the E2 subunit of the enzyme complex. This curtails substrate oxidation and the transfer of electrons from lipoic acid in the E2 subunit to the FAD center in the E3 subunit, which happens to be the source of ROS in keto acid dehydrogenases like PDH or KGDH (52). Treatment with the inhibitor induced a significant decrease in $O_2^{\bullet-}/H_2O_2$ production by liver mitochondria isolated from WT and *Grx2*$^{+/-}$ mice fed either diet, confirming that changes in resorufin fluorescence were due to mitochondrial ROS production (Figure 3.7A). When liver mitochondria were supplemented with succinate or palmitoyl-carnitine there was no genotypic or diet differences observed (Figure 3.7B-C). Malonate, which competes for the succinate binding site in complex II, was used as a control when succinate served as the electron donor. Inclusion of malonate induced a significant decrease in $O_2^{\bullet-}/H_2O_2$ production (Figure 3.7B). For palmitoyl-carnitine driven ROS production, a combination of rotenone, myxothiazol, and atpenin A5 was added as the control. Unlike the other controls, addition of this combination of inhibitors significantly

elevated $O_2^{\bullet-}/H_2O_2$ production (Figure 3.7C). This is an expected outcome since these inhibitors block complex I, II, and III causing increased reduction of ETFQO and long chain fatty acid dehydrogenase, enzymes required for fatty acid oxidation which happen to serve as ROS sources (90).

3.2.2 Muscle Mitochondria ROS Production

$O_2^{\bullet-}/H_2O_2$ production by muscle mitochondria was profiled with no significant differences with pyruvate/malate, succinate, or palmitoyl-carnitine oxidation (Figure 3.8). The same controls as liver were used except for pyruvate/malate. While inhibition with CPI-613 was attempted in this case, it was not successful at reducing $O_2^{\bullet-}/H_2O_2$ emission (data not shown). To correct this, the concentration of CPI-613 was doubled (300 μM) which was also unsuccessful at reducing ROS production (data not shown). Due to this lack of effect, we next attempted to inhibit ROS production using KGDH inhibitor, KMV and rotenone, a complex I inhibitor. Surprisingly, a combination of KMV and rotenone did not elicit an effect either (Figure 3.8A). Additionally, including KMV and rotenone induced a trend (P=0.1699) for an increase in ROS production, although this was not significant. PDH has been shown to be a potent ROS producer in muscle mitochondria from mouse, rat, and human myofibers (14,91,92). Thus, it is possible that these inhibitor combinations were not effective simply because PDH is a highly effective ROS generator in muscle tissue. The use of malonate during succinate oxidation showed significant reduction in $O_2^{\bullet-}/H_2O_2$ production (Figure 3.8B). Addition of an inhibitor cocktail comprised of rotenone, atpenin A5, and myxothiazol to muscle mitochondria oxidizing palmitoyl-carnitine abolished $O_2^{\bullet-}/H_2O_2$ emission (Figure 3.8C). This is not surprising since the main ROS sources in muscle mitochondria oxidizing palmitoyl-carnitine are complexes I, II, and III, with ETFQO making a negligible contribution (13).

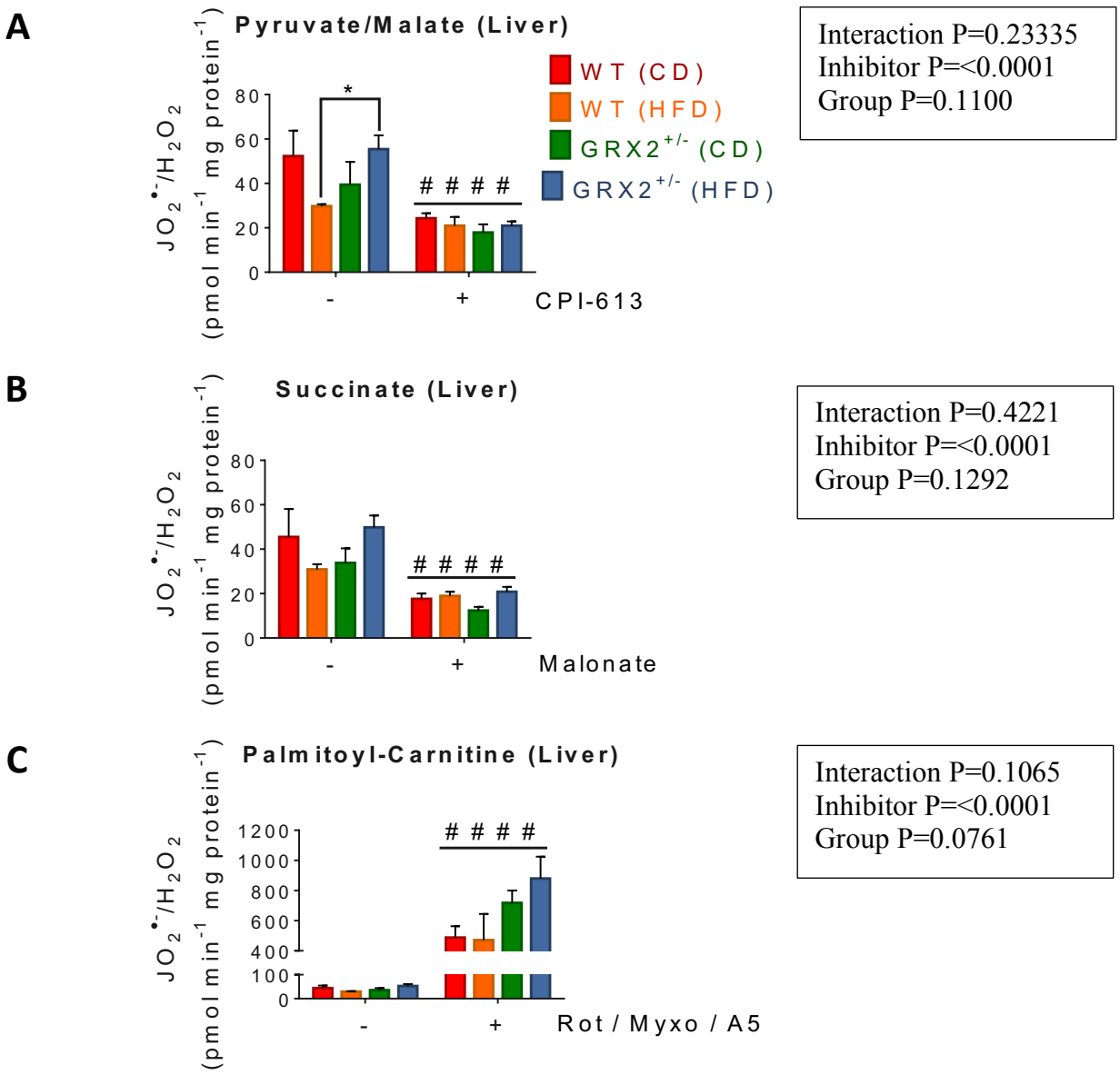

Figure 3.7: Rates of $O_2^{\bullet-}/H_2O_2$ production by liver mitochondria supplemented with (A) Pyruvate (50 µM)/malate (50 µM) (B) Succinate (50 µM) (C) Carnitine (50 µM)/palmitoyl-carnitine (50 µM). Mitochondria were diluted to 0.3 mg/mL in reaction wells with or without inhibitors (A) CPI-613 (150 µM) (B) Malonate (5 mM) (C) Rotenone (4 µM)/myxothiazol (4 µM)/aptenin A5 (40 µM) and changes in ROS production were then measured. n = 4, mean ± SEM, two-way ANOVA with Tukey's post-hoc test. * represents genotypic difference while # represents difference between diets.

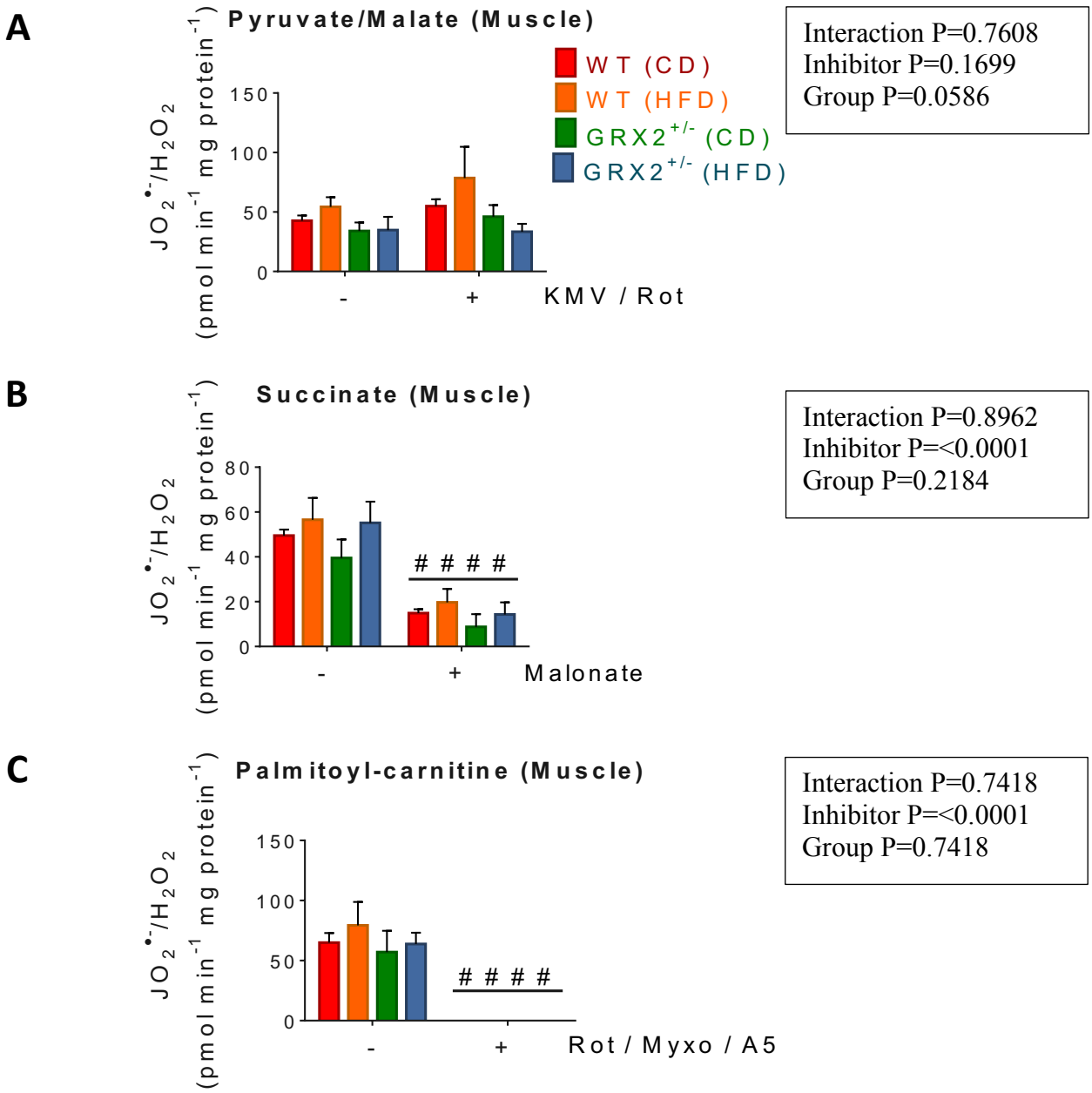

Figure 3.8: Rates of $O_2^{\bullet-}/H_2O_2$ production by muscle mitochondria supplemented with (A) Pyruvate (50 µM)/malate (50 µM) (B) Succinate (50 µM) (C) Carnitine (50 µM)/palmitoyl-carnitine (50 µM). Mitochondria were diluted to 0.15 mg/mL in reaction wells with or without (A) Rotenone (4 µM)/KMV (10 mM) (B) Malonate (5 mM) (C) Rotenone (4 µM)/myxothiazol (4 µM)/aptenin A5 (40 µM) and changes in ROS production were then measured. n = 4, mean ± SEM, two-way ANOVA with Tukey's post-hoc test. # represents difference between diets.

3.3 High-fat Diet and *Grx2* Deficiency Decreases Protein Oxidation Without Impacting Total Glutathione Levels

Since liver mitochondrial $O_2^{\bullet-}/H_2O_2$ profiling revealed a genotypic difference in ROS production when oxidizing pyruvate, a protein carbonyl assay was performed to determine if there was any alteration in the redox state of the mitochondrial environment. A protein carbonyl assay is a simple and accurate way to quantify carbonyl groups, biomarkers for oxidative stress. Quantification of protein carbonyl content of liver mitochondria revealed that there was a significant decrease in WT/HFD mice along with *Grx2*$^{+/-}$ mice on both diets, compared to the WT/CD mice (Figure 3.9A). Quantification of protein carbonyls in muscle mitochondria revealed no significant diet or genotypic differences (Figure 3.9B).

Next, we assessed total circulating glutathione and the redox state of the glutathione pool in the blood stream to determine if diet and genotype affected redox buffering capacity. It can be seen in figure 3.9C that there is no significant difference in total amount of glutathione in the blood serum, suggesting that there is no change in glutathione biosynthesis or degradation. However, calculation of the reduction potential of the pool, represented as the ratio of reduced to oxidized glutathione, revealed that challenging mice from either genotype with an HFD led to a significant oxidation of circulating glutathione (Figure 3.9D).

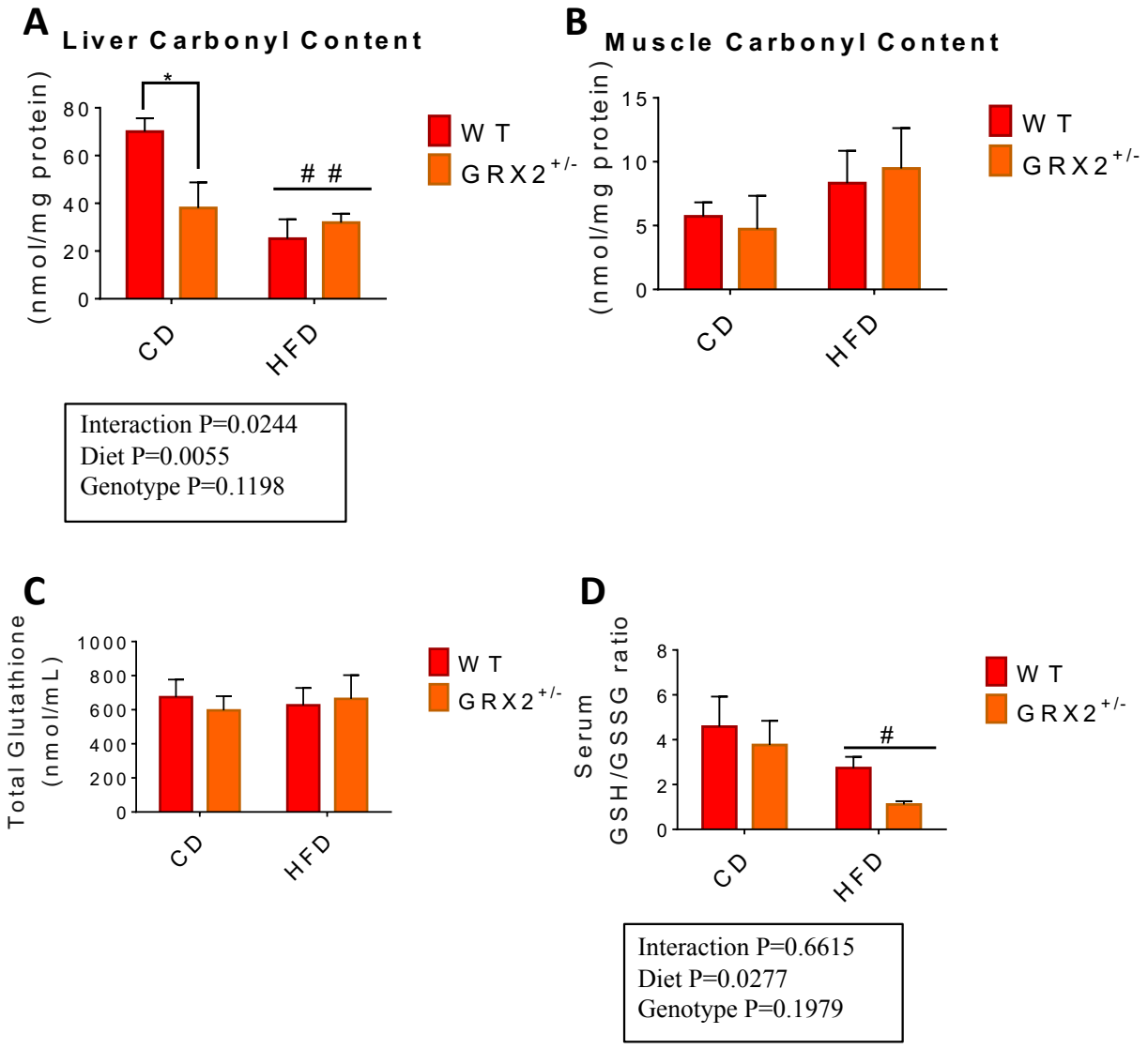

Figure 3.9: Protein carbonyl content in (A) Liver mitochondria (B) Muscle mitochondria. Amount of (C) Total glutathione (D) Reduced to oxidized glutathione ratio. n = 4, mean ± SEM, two-way ANOVA with Tukey's post-hoc test. * represents genotypic difference while # represents difference between diet.

3.4 Evaluation of *Grx2*$^{+/-}$ Mitochondrial Respiration When Challenged with a HFD

3.4.1 Liver Mitochondria

As noted above, no differences in mitochondrial ROS production by liver mitochondria oxidizing pyruvate, succinate, or palmitoyl-carnitine were observed. This prompted us to examine the impact of diet and genotype on mitochondrial bioenergetics. Evaluation of mitochondrial bioenergetics was conducted using a Clark-electrode, allowing validation of mitochondrial function and health (93). The different respiratory steady-states are defined based on the typical addition of substrates. State 1 respiration refers to O_2 consumption by mitochondria alone and is minimal since there is a lack of fuel. State 2 respiration is O_2 consumption after addition of a substrate (pyruvate/malate or succinate in this case) and reflects the basal rate of proton conductance back into the matrix. Addition of ADP primes state 3 respiration, allowing formation of ATP by complex V, coupled to proton return into the matrix. Oxygen consumption therefore reflects regeneration of the proton gradient during this state. State 4 respiration reflects O_2 consumption under non-phosphorylating conditions, once all ADP has been converted to ATP. Oligomycin is added during this state controlling for possible contaminating ATP synthases that could work in reverse, allowing an accurate measure of proton leak-dependent respiration. The use of pyruvate allows measurement of the rate of O_2 consumption from electrons donated to complex I, while succinate supplementation results in rates from donation of electrons to complex II. Note that rotenone is added to succinate-driven respiration to prevent reverse electron transfer to complex I, allowing an accurate measure of O_2 consumption from complex II-linked substrates.

Rates of oxygen consumption by liver mitochondria revealed no significant effect of diet or genotype on the states of respiration (Figure 3.10A-B). Indeed, no significant differences in

phosphorylating and non-phosphorylating respiration were observed with liver mitochondria energized with either pyruvate or succinate. There was a large amount of error in my measurements, which I attributed to succinate serving as a poor substrate for respiration. Next, I calculated the respiratory control ratio (RCR), a proxy measure for the efficiency of ATP production, using the state 3 and state 4 respiration rate data. Results for RCR in liver mitochondria followed the same trend as rates of O_2 consumption with no significant genotypic or diet effect observed (Figure 3.10C-D). Additionally, the high RCR when pyruvate served as the substrate indicates that the mitochondrial population being studied is well-coupled and thus healthy. However, succinate was not a good driver for respiration or ATP production, as indicated by the variable RCR and low state 3 respiration. When compared to pyruvate metabolism, state 3 respiration during succinate oxidation is ~85% lower. These findings are consistent with a previous study published by our group (88).

3.4.2 Muscle Mitochondria

Muscle tissue undergoes repeated cycles of contraction and relaxation powering the energetically expensive process of locomotion. Therefore, muscle mitochondria are required to produce an abundance of ATP. This can be observed when you evaluate the state 3 respiration between liver and muscle mitochondria (Figure 3.11-3.12). The consumption of oxygen is clearly higher in muscle mitochondria (~20 to 25 nmol min^{-1} mg^{-1}) compared to liver mitochondria (~12 nmol min^{-1} mg^{-1}), when evaluating pyruvate metabolism. Additionally, there was a significant increase in *Grx2*$^{+/-}$ mice challenged with a CD when metabolizing succinate (Figure 3.11B). No other significant differences in rate of O_2 were found when mitochondria were supplemented with malate/pyruvate or succinate (Figure 3.11A-B). Furthermore, no significant difference in RCR for muscle mitochondria was observed (Figure 3.11C-D). It is

important to note that in male mice, it was determined that muscle mitochondria had significantly increased state 3 and state 4 respiration during malate/pyruvate- and succinate-driven respiration for *Grx2* $^{+/-}$ mice (59). It was determined that this increased respiration led to the DIO protective effect displayed in those mice and further experimentation uncovered that the increase in state 4 respiration was due to enhanced proton leak through UCP3 (59). These results were not reproducible in female *Grx2* $^{+/-}$ mice.

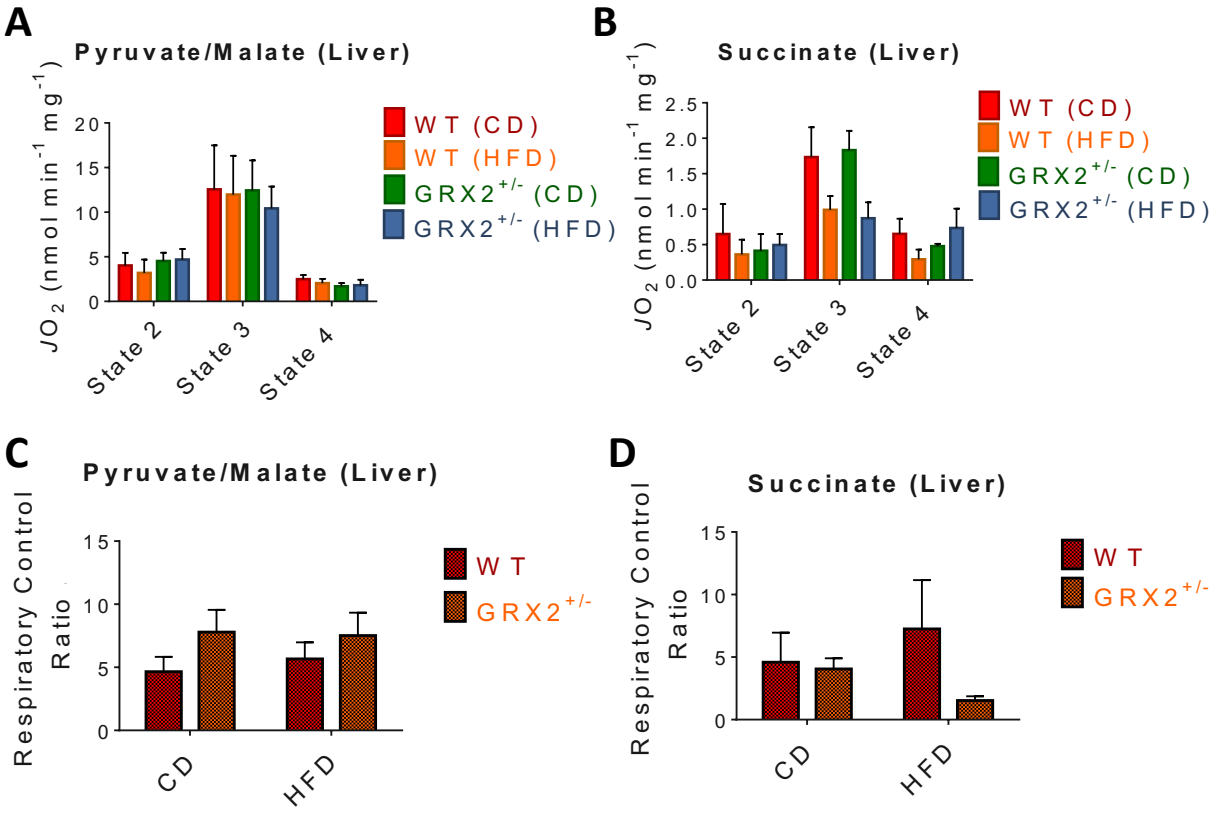

Figure 3.10: Rates of oxygen consumption by liver mitochondria supplemented with (A) Pyruvate (10 mM)/malate (2 mM) (B) Succinate (2 mM)/rotenone (4 µM) (C-D) Respiratory control ratios, represented as state 3/state 4. Mitochondria were diluted to 0.5 mg/mL in the reaction chamber and state 2 respiration initiated by addition of substrate, state 3 (phosphorylating respiration) initiated by addition of ADP (1 mM), state 4 (leak-dependent respiration) initiated by addition of oligomycin (4 µg/mL), and baseline of oxygen consumption was determined by addition of antimycin A (4 µM); for which all O_2 consumption values were corrected. n = 4-6, mean ± SEM, two-way ANOVA.

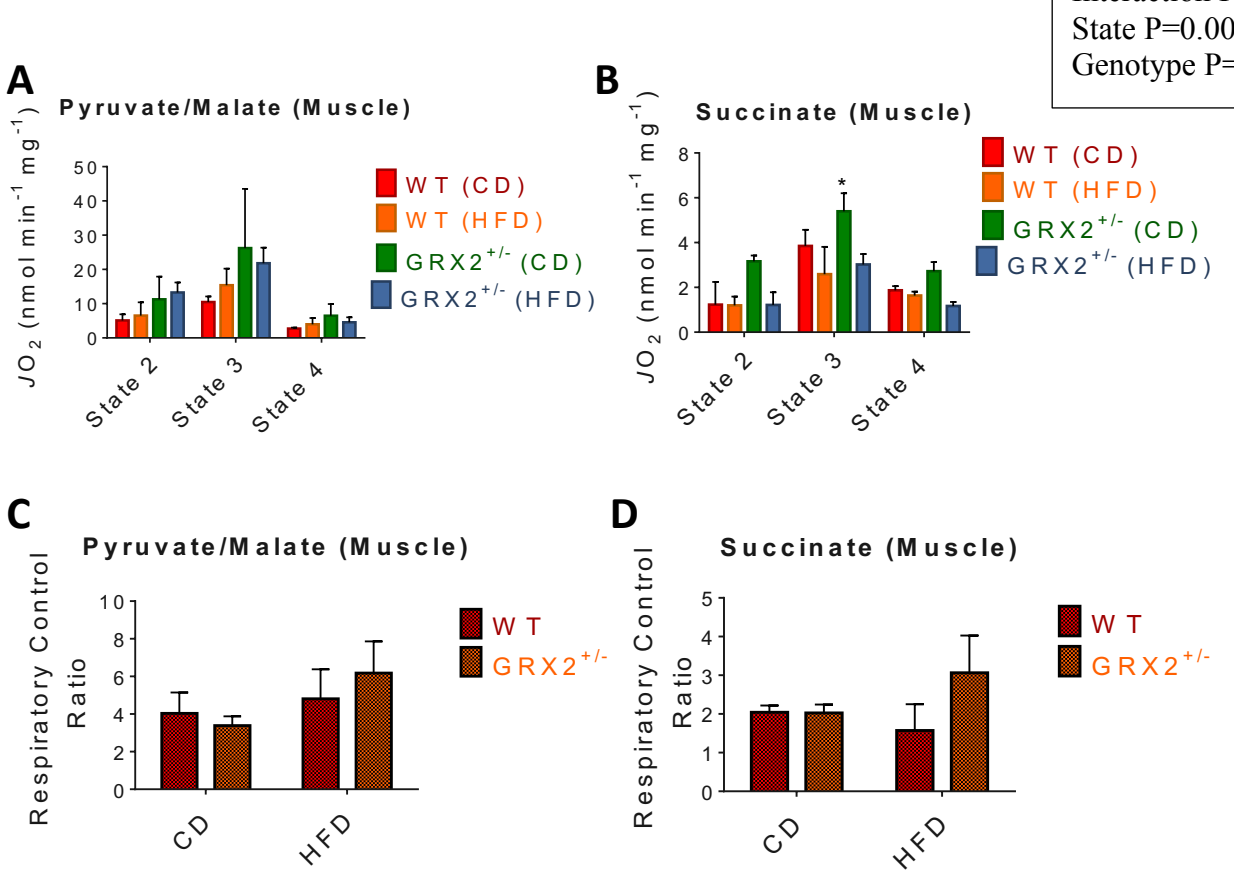

Figure 3.11: Rates of oxygen consumption by muscle mitochondria supplemented with (A) Pyruvate (10 mM)/malate (2 mM) (B) Succinate (2 mM)/rotenone (4 μM) (C-D) Respiratory control ratios, represented as state 3/state 4. Mitochondria were diluted to 0.2 mg/mL and state 2 respiration initiated by addition of substrate, state 3 (phosphorylating respiration) initiated by addition of ADP (1 mM), state 4 (leak-dependent respiration) initiated by addition of oligomycin (4 μg/mL), and baseline of oxygen consumption was determined by addition of antimycin A (4 μM); for which all O_2 consumption values were corrected. Pyruvate n = 3-5, Succinate n = 2-4 (n = 2 for WT/CD); mean ± SEM, two-way ANOVA with Tukey's post-hoc test. * represents difference within state from WT (CD).

Chapter 4: Discussion

4.1 Summary

The first discovery of a metabolic difference in *GRX2* deficient mice was observed in a study by Mailloux *et al.* in 2013 (60). In that study, it was found that total body and lower gonadal white adipose tissue mass was significantly lower in male $GRX2^{-/-}$ mice (60). These phenotypic changes in mass due to the deletion of the *Grx2* gene correlated strongly with an increase in overall energy metabolism and proton leaks in muscle (60). Recently, our group evaluated if the $Grx2^{+/-}$ phenotype could protect male mice from DIO and the development of related disorders. It was found that male WT mice subjected to a HFD gained weight rapidly, which was associated with hypertrophy of white fat, higher circulating levels of triglycerides, intrahepatic lipid accumulation, and depletion of liver glycogen stores (59). However, male mice heterozygous for the *Grx2* gene fed a HFD displayed a weight gain profile similar to the control group (59). This was associated with increased muscle fuel metabolism, proton leaks, and protection from oxidative stress in muscle (59).

Measurement of body and adipose mass, food and water consumption, and serum triglyceride levels revealed that female WT mice were resistant to DIO. These results are in contrast to male WT mice, which showed significant increases in total body and adipose mass, and circulating triglycerides and insulin (59). Furthermore, measurement of organ masses found that livers from female mice fed a HFD had lower mass compared to their CD counterparts, an observation even more apparent in $Grx2^{+/-}$ mice. Previous work in the lab utilizing male mice showed no alteration in liver mass of $Grx2^{+/-}$ or $Grx2^{-/-}$ mice compared to WT littermates (18).

Measurement of the rate of $O_2^{\bullet-}/H_2O_2$ production by liver and muscle mitochondria revealed an augmentation of $O_2^{\bullet-}/H_2O_2$ production in $Grx2^{+/-}$/HFD mice when liver mitochondria were supplemented with pyruvate/malate. It has been documented that PDH is a high-capacity site for

$O_2^{\bullet-}/H_2O$ production in liver mitochondria (52,92). It has been shown that $O_2^{\bullet-}/H_2O_2$ production by PDH and KGDH is modulated by GRX2 and S-glutathionylation reactions (41,52). Therefore, it is not surprising that there is augmented ROS in the *Grx2*$^{+/-}$ mice challenged with a HFD. However, it was surprising to only observe this in liver, as muscle mitochondria were resistant to any augmentation but found to be augmented by *Grx2* deletion in males (59).

Evaluation of the oxidative state of liver mitochondria with a protein carbonyl assay revealed that there was significantly less protein oxidation in *Grx2*$^{+/-}$ mice and mice challenged with a HFD. There also was a decrease in the GSH: GSSG ratio when mice were challenged with a HFD, indicating a higher level of oxidized glutathione during high-fat feeding. These findings suggest an increase in oxidative stress resulting in upregulation of antioxidant pathways when mice are challenged with a HFD or deficiency in *Grx2*. Work by Yang *et al*. support these findings as they demonstrated a significant increase of liver $O_2^{\bullet-}/H_2O_2$ production in male ob/ob C57BL/6 mice that had developed obesity and fatty liver (94). Subsequently this group was able to show a significant upregulation of enzymatic activity of SOD2 and catalase in these obese mice (94).

Results from mitochondrial respiration experiments suggest no alteration in mitochondrial respiration between WT and *Grx2*$^{+/-}$ mice when oxidizing complex I or II substrates. However, there was a small increase in respiration of *Grx2*$^{+/-}$ mice on a CD when supplemented with ADP and succinate. Whereas in the male study, there was a ~2-fold increase in state 3 and state 4 respiration for both pyruvate and succinate driven respiration (59).

4.2 Female Obesity

The chromosomal make-up that determines biological sex in a fetus occurs during embryonic development and due to the paternal inheritance of either an X or Y chromosome. The default

sex of a developing fetus is female (XX), which can be switched to male differentiation following the expression of the sex-determining region Y (SPY) gene on the Y-chromosome (95). This gene encodes a transcription factor for testis development that alters hormone secretion and the fate of the embryo towards male (XY) development (95). In the present study, there is an inherent protection against obesity in female mice on a HFD. This is not unexpected as health issues such as cardiovascular disease, interstitial cystitis, and stroke show distinct sex differences in symptoms and onset (95,96). For example a conservative estimate for the prevalence of interstitial cystitis is 8:2 for female to male, a 4-fold sex difference (96). Additionally, there is an increase incidence of abdominal fat accumulation, hyperlipidemia, insulin resistance, and cardiovascular disease in post-menopausal women, correlating to a drastic decrease in estrogen secretion (95).

The estrogen-related receptor family of transcription factors have been found to regulate metabolic genes, as both the nucleus and mitochondrial membranes have estrogen receptors (81). Indeed 17-β estradiol has a direct link to promotion of genes regulating lipid metabolism and mitochondria function (76,80). Estrogen additionally has been shown to influence the browning of adipose tissue, the process of turning white adipose tissue into brown adipose tissue. This is achieved through increases the metabolic activity of these tissues by increasing mitochondrial abundance and upregulation of UCP1 (97). Estrogen through estrogen receptor-α can regulate brain-derived neurotrophic factor, which is linked to inducing browning (97). Estrogen increases atrial natriuretic peptide and brain natriuretic peptide which has been linked to white adipose tissue browning (97). The eating patterns in female mice have similarly been shown to be cyclic with ovarian cycles with food consumption at its peak during estrus, when estradiol is lowest (97).

Obesity is classified as an inflammatory disease and with 80% of autoimmune diseases occurring in women, inflammation seems to be strongly sex-linked (95). Female mice have a lot of physiological similarities to humans and reach sexual maturity at 6 to 8 weeks, making them a good experimental model to evaluate sex differences in research (98). Indeed, in mice there are differences between sexes observed in inflammatory markers when fed a HFD (95). One difference being that male adipocytes are infiltrated by M1 macrophages and they express higher levels of inflammatory cytokines, while female adipocytes are infiltrated by M2 macrophages (95). There is also a sexual dimorphism with fat disposition, as males are more likely to accumulate visceral fat, while females have a tendency to accumulate subcutaneous fat (95). This sex difference in fat deposits is due to differential rates of fatty acid uptake by adipocytes in these regions (95).

Likewise, there is a sex difference observed in the onset of obesity in mice, as male mice show increased weight gain during juvenile age (~ six weeks), while females are more predisposed to weight gain later in their life cycle (~31 weeks of age) (99). This correlates well with observations in this study, as female mice did not show overall body or adipose tissue mass gain from 3 to 10 weeks of age on a HFD. Additionally, these mice did not show elevated triglyceride levels while on a HFD. This finding is supported by literature demonstrating pre-menopausal women typically have higher HDL and lower LDL levels, allowing for better free fatty acid clearance than males (95). Altogether, this may highlight a limitation to the current study, as the sample of mice used was 3 to 10 weeks of age. There may have been more pronounced differences found if female mice from later stages in life (~31 weeks) were utilized, as they would have been more predisposed to developing DIO.

4.3 Importance of Female Based Studies

4.3.1 Differences to Male Study

This study highlights the importance of including female animals in study designs and the inability to generalize male studies to female populations. Indeed, there are distinct sex differences between the preceding male study and this study in female littermates under similar experimental parameters. The most noticeable difference is the resistance in female mice to overall body and adipose mass gain when fed a HFD. However, this has been reported before in LDL receptor null mice, where a HFD induced both body and adipose mass increases in the male mice but failed to do so in females (30). Females, however still developed hypercholesterolemia in that study, due to their inability to uptake cholesterol via LDL receptors (30). Furthermore, sex differences in mice body mass gain when on a HFD was abolished by performing ovariectomies, indicating a hormonal influence (97).

A few studies have focused on whether or not sex differences affect cell redox signalling pathways. In regard to the role of S-glutathionylation in regulating mitochondrial functions, studies have mostly focused on rodent models (18,41,59,88). Recently, our group found that male mice carrying a deletion for *Grx2* are protected from DIO and the development of related disorders (59). This was associated with increased muscle fuel combustion and ROS generation, the latter of which plays an important role in muscle physiology (59). The increase in fuel combustion was associated with increased proton leaks through UCP3 and ANT, resulting in increased muscle O_2 consumption (59). Differences in S-glutathionylation profiles have been discovered between female and male mice, but very few studies have narrowed in on sex differences in S-glutathionylation and its impact on redox signalling (30). For example in a large scale proteomic study of macrophages, 47 proteins in female mice vs 17 in male were

exclusively S-glutathionylated when challenged with a HFD for 10 weeks (30). Also in this study, they assessed the cellular pathways most affected by S-glutathionylation. The pathways most affected in females were for cell differentiation and inflammatory response, while for males the top pathways were H_2O_2 metabolism and response to stress (30). The 2-fold increase in response to cellular stress in females along with there not being a need to upregulate antioxidant or stress response pathways, indicate female mice are better equipped to deal with metabolic stress.

In terms of oxidative stress, when comparing the measurements of protein carbonyls in muscle mitochondria between both the male and female studies I see a stark difference. In the previous male study, the protein carbonyl content in *Grx2*$^{+/-}$ mice was the same as the control, regardless of whether they were placed on a HFD (59). The WT mice on HFD, however, showed a greater then 2-fold increase in protein carbonyls (59). The protection from oxidative stress in male *Grx2*$^{+/-}$ mice was accompanied by higher serum total glutathione levels along with a more reduced glutathione pool (59). In males, this demonstrated an adaptive response of the *Grx2*$^{+/-}$ mice to deal with oxidative stress by enhancing antioxidant capacity. In female mice there is no alteration of the protein carbonyl content in muscle of either group. Additionally, there was no change in the level of total glutathione, but there was instead a higher content of oxidized glutathione for the *Grx2*$^{+/-}$ mice on a HFD. This possibly demonstrates a more efficient capacity for female muscle mitochondria to deal with oxidative stress without having to compensate with upregulating antioxidants. On the other hand, this could be due to the fact that female mitochondria produce less ROS than their male counterparts. Indeed, this has been shown for female mouse brain mitochondria as they have lower levels of H_2O_2 and decreased oxidative stress than male brains (81). Additionally, as stated above, one of the key pathways S-

glutathionylated, in response to stress, in macrophages of male mice was H_2O_2 metabolism (30). Evidently, the processes for H_2O_2 metabolism were found to have a significant decrease in S-glutathionylation in female macrophages (30).

In female liver mitochondria, there are contradictory protein carbonyl findings as there was a significant decrease in protein carbonyl content for WT mice on a HFD and *Grx2*$^{+/-}$ mice on either diet. Unfortunately, the previous male study did not isolate liver mitochondria and therefore, a comparison could not be made; however, a similar comparison was conducted by another group. A key study by Yamamoto *et al.* compared the antioxidant capacity in livers of female and male rats, under sedentary or active conditions (100). They determined that in the active mice (oxidative stress-inducing conditions), GSH levels were elevated in female rats compared to males (100). Additionally, they found that the activities of GPX, GR, and γ-glutamyltranspeptidase (an enzyme initiating the membrane-crossing transport of GSH) were 2-fold higher in female rat livers under both sedentary and active conditions (100). Also relevant to our study is the fact that GPX activity of female rats increased from the sedentary to active groups, while there was no adaptive response in the male rats (100). These findings support the possibility of an antioxidant adaptation to the HFD in female mice, but a lack of adaptation in males.

4.3.2 Altered Female ROS production

The results presented herein support other findings by our group that demonstrate that sex has an impact on ROS production by liver and muscle mitochondria (88). Indeed, a recent study in our lab supports no genotypic alteration in liver $O_2^{\bullet-}/H_2O_2$ production when oxidizing pyruvate, α-ketoglutarate, and succinate in mice with a partial or full deletion of *Grx2* (88). Additionally, this previous study did not show any genotypic difference in $O_2^{\bullet-}/H_2O_2$ production

for skeletal muscle mitochondria (88). In male mice, however, a significant increase in $O_2^{\bullet-}/H_2O_2$ generation in liver and cardiac muscle was found with deletion of *Grx2* (18). Production of $O_2^{\bullet-}/H_2O_2$ in liver mitochondria with a deletion or deficiency of *Grx2* resulted in decreased $O_2^{\bullet-}/H_2O_2$ release when oxidizing pyruvate and α-ketoglutarate, but the reverse was observed when oxidizing succinate (18). Alternatively, in cardiac mitochondria deletion or deficiency of *Grx2* augmented $O_2^{\bullet-}/H_2O_2$ production with these 3 substrates (18). A similar trend was observed in male skeletal muscle mitochondria as *Grx2* deficiency results in augmented $O_2^{\bullet-}/H_2O_2$ production when oxidizing pyruvate, succinate, and palmitoyl-carnitine (59). The current study, while observing a small genotypic difference for liver mitochondria supplemented with pyruvate, observed no significant difference between WT and $Grx2^{+/-}$ mice for muscle or liver, which is in line with what was previously observed (88).

Furthermore, when comparing rates of $O_2^{\bullet-}/H_2O_2$ production between sexes, female mice produced significantly less $O_2^{\bullet-}/H_2O_2$ when supplemented with pyruvate and α-ketoglutarate but more when supplemented with succinate in liver mitochondria, compare to males (88). However, when oxidizing these substrates in muscle mitochondria females produced significantly more $O_2^{\bullet-}/H_2O_2$, with a ~6-fold increase for pyruvate (88). Comparing rates of $O_2^{\bullet-}/H_2O_2$ production from this study with those previously observed in males, WT/CD mice have a 2-fold increase when supplemented with pyruvate or succinate, but about the same production when oxidizing palmitoyl-carnitine, consistent with current literature (59). With PDH, KGDH, and complex II ROS-generating abilities regulated by S-glutathionylation, these results suggest sexual dimorphic regulation of ROS production by S-glutathionylation.

This sex difference in ROS production has been a focus of study by the Neufer group (77,78). Studies by this lab have been able to highlight that 17β-estradiol localizes to the MIM

and influences microviscosity of the MIM and ETC function (78). Taken further, they were able to determine that knockdown of 17β-estradiol causes increased H_2O_2 production by complex I in skeletal muscle (77). Interestingly, this effect was not observed in liver mitochondria, but instead treatment of 17β-estradiol decreased state 3 respiration (78). This supports other findings in liver mitochondria that show a reduced state 3 respiration in females compared to males (88). This further explains why a decline in 17β-estradiol, such as during menopause in women, correlates to an increased risk of obesity, insulin resistance, and cardiovascular disease (77). It may be 17β-estradiol that is responsible for the metabolic sexual dimorphisms observed for differential ROS generation and better mitochondrial coupling observed in females (80).

4.3.3 Role of GRX2

The deletion of *Grx2* has serious effects such as heart disease, hypertension, cataract formation, and hindering embryonic development (4). It is for these reasons that in the following study, heterozygous mice for the *Grx2* gene were utilized to avoid any extraneous variables influencing the study outcomes. Comparisons of the $Grx2^{+/-}$ mouse model between sexes show a 2-fold increase in liver $O_2^{\bullet-}/H_2O_2$ production in male mice compared to female mice supplemented with succinate (18). When comparing pyruvate oxidation between male and female *Grx2* deficient mice, again a 2-fold increase in production was observed in males. This augmented $O_2^{\bullet-}/H_2O_2$ production in males was also seen in muscle mitochondria (59). It has been observed that in male skeletal muscle mitochondria that S-glutathionylation reactions regulate complex I through the NDUFS1 subunit and regulate pyruvate influx by inhibiting MPC (41). Also, GRX2 has been shown to form part of the redox interface by modulating $O_2^{\bullet-}/H_2O_2$ production, as complex II requires GRX2 to reduce ROS when oxidizing succinate (18).

However the results from this study indicate that GRX2 is not required from female mice to maintain either $O_2^{\bullet-}/H_2O$ or mitochondrial bioenergetics and ATP production. This indicated a possible difference in the role of GRX2 for female mice. However, to my knowledge, this is the first time the role of GRX2 has been investigated in females and therefore requires more work to be done to elucidate the role of GRX2 in females. This sex-specific role of GRX2 does not come as a surprise since it has been shown that GRX2 has a tissue-specific effect (18).

4.3.4 Altered Fuel Combustion

In a previous study comparisons among WT, *Grx2*$^{+/-}$, and *Grx2*$^{-/-}$ female mice liver and muscle mitochondria were made. It was found that liver mitochondria has significant increases in state 3 respiration for *Grx2*$^{+/-}$ and *Grx2*$^{-/-}$ mice when oxidizing pyruvate and increased state 4 respiration when oxidizing succinate (88). These results were not reproduced in this thesis as there was no significant difference in liver mitochondrial bioenergetics observed. It should be emphasized, that in the study cited above, mice were not subjected to dietary manipulation (88). Indeed, it has been documented that mitochondria from mice fed different diets can display alterations in bioenergetics (30,59). In terms of skeletal muscle mitochondria, there was no changes in state 3 respiration when fuelled by complex I or II substrates, which is also confirmed in this thesis (88). However, there was a significant increase in state 3 respiration in female *Grx2*$^{+/-}$ mice on a CD when supplemented with succinate and ADP. Additionally in our previous study a significant decrease in proton leak-dependent respiration was observed in *Grx2* deficient mice when supplemented with succinate (88). This observation was absent here as there was no change in proton leak in liver or muscle mitochondria for pyruvate or succinate fuel metabolism.

When overall fuel combustion is compared between male and female studies, results show lower fuel oxidation in female mitochondria in all groups oxidizing succinate and pyruvate (59).

These findings might be considered to be surprising since the Broushel group has shown that human female skeletal muscle requires a smaller population of mitochondria to achieve the same respiratory output as males (84). This disparity is linked to female mitochondria having a higher intrinsic respiration capacity and increased O_2 affinity (84). This group postulated that this could be due to a higher cristae density, which has been observed to occur in endurance athletes, or a higher abundance of supercomplexes and respirasomes (84). My results, do not support their findings as when I matched mitochondrial content for male and female studies, we did not see a higher respiration rate in female mice muscle or liver mitochondria. The Broushel group also found a 2-fold higher intrinsic proton leak in human female skeletal muscle mitochondria, a finding also not supported by our results (84). As mitochondrial ROS production and bioenergetics have been found to be both animal- and strain-dependent, and because our study was conducted in mice, these differences could be explained by differences in models. Also, the Broushel study looked a specific section of the vastus lateralis muscle while our preparations utilized total muscle from pectoral, hindlimb, and forelimb (84). The type of muscle fibre does influence the bioenergetics of the mitochondria isolated from it.

In this study, we observed a distinct reduction in the capacity of female mitochondria to utilize succinate as a substrate. When comparing WT male and female mice, succinate oxidation was 10-fold higher in state 3 respiration in males. Similar results were found in a previous study in our lab where direct comparison showed a 3x increase in succinate driven state 3 respiration in male liver mitochondria compared to female (88). These are not surprising findings since it has been documented that complex II in vastus lateralis muscle is less active in females (101). It has also been documented that glycolytic enzyme activities for females are significantly lower than for males (101). Moreover, a more recent study found higher levels of succinic acid in urine

samples of females, indicating a failure to metabolize this metabolite (96). This is not surprising as women have a greater abundance of type I muscle fibres and a preference for oxidation of fatty acids (84,102). This difference in muscle fibres underlines another limitation of this study as the type of muscle fibre from which the mitochondria were isolated was not controlled in my study, nor was mitochondrial respiration performed with a fatty acid source such as palmitoyl-carnitine.

4.4 Conclusions

To conclude, this study showed that female WT mice were completely resistant to DIO, unlike their male WT littermates. Additionally while the ROS generation and redox environment in liver mitochondria seem to be altered between WT and *Grx2*$^{+/-}$ mice, this trend does not hold true for muscle mitochondria. Lastly, bioenergetics data suggest no genotypic difference between these mice when fueled by complex I or II substrates. These results collectively indicate an alteration in the role for GRX2 in female mice. Therefore, this study suggests that a sexual dimorphism exists for mitochondrial redox signalling through the GRX2 pathway.

4.5 Future Directions

Future work to build off previous research in the lab and this study will further investigate the role of GRX2 in mice and the sexual dimorphisms present. This will include:

1. Completing fatty acid fuel mitochondrial respiration in female GRX2 deficient mice challenged with a HFD.
2. Further investigation of the GRX2 deficient mouse model with muscle specific knockouts of *Grx2*.
3. Investigate sexual dimorphisms of S-glutathionylation between male and female mice and how these differences alter $O_2^{\bullet-}/H_2O_2$ production and redox signalling.

Citations:

1. Nicholls DG, Ferguson SJ (Stuart J.) Bioenergetics, 2013 419 p.
2. Nelson DL (David L, Cox MM, Lehninger AL. Lehninger principles of biochemistry. W.H. Freeman and Company; 2013.
3. Ballard JWO, Whitlock MC. The incomplete natural history of mitochondria. Mol Ecol. 2004;13(4):729–44.
4. Young A, Gill R, Mailloux RJ. Protein S-glutathionylation: The linchpin for the transmission of regulatory information on redox buffering capacity in mitochondria. Chem Biol Interact. 2019;299:151–62.
5. Cárdenas ML, Cornish-Bowden A, Ureta T. Evolution and regulatory role of the hexokinases. Biochim Biophys Acta - Mol Cell Res. 1998;1401(3):242–64.
6. Bricker DK, Taylor EB, Schell JC, Orsak T, Boutron A, Chen Y-C, et al. A mitochondrial pyruvate carrier required for pyruvate uptake in yeast, *Drosophila* , and humans. Science. 2012;337(6090):96–100.
7. Birsoy K, Festuccia WT, Laplante M. A comparative perspective on lipid storage in animals. Journal of Cell Science. 2013;126:1541-1552.
8. Papa S, Martino PL, Capitanio G, Gaballo A, De Rasmo D, Signorile A, et al. The Oxidative Phosphorylation System in Mammalian Mitochondria. In Springer, Dordrecht. 2012. p. 3–37.
9. Mailloux RJ. Teaching the fundamentals of electron transfer reactions in mitochondria and the production and detection of reactive oxygen species. Redox Biol. 2015;4:381–98.
10. Mailloux RJ. Mitochondrial antioxidants and the maintenance of cellular hydrogen peroxide levels. Oxid Med Cell Longev. 2018;2018:1–10.

11. Turrens JF. Mitochondrial formation of reactive oxygen species. J Physiol. 2003;552(2):335–44.

12. Sorescu D, Weiss D, Lassègue B, Clempus RE, Szöcs K, Sorescu GP, et al. Superoxide production and expression of Nox family proteins in human atherosclerosis. Circulation. 2002;105(12):1429–35.

13. Brand MD. Mitochondrial generation of superoxide and hydrogen peroxide as the source of mitochondrial redox signaling. Free Radic Biol Med. 2016;100:14–31.

14. Goncalves RLS, Quinlan CL, Perevoshchikova I V, Hey-Mogensen M, Brand MD. Sites of superoxide and hydrogen peroxide production by muscle mitochondria assessed ex vivo under conditions mimicking rest and exercise. J Biol Chem. 2015;290(1):209–27.

15. Starkov AA, Fiskum G, Chinopoulos C, Lorenzo BJ, Browne SE, Patel MS, et al. Mitochondrial -ketoglutarate dehydrogenase complex generates reactive oxygen species. J Neurosci. 2004;24(36):7779–88.

16. Ursini F, Maiorino M, Forman HJ. Redox homeostasis: The golden mean of healthy living. Redox Biol. 2016;8:205–15.

17. Oldford C, Kuksal N, Gill R, Young A, Mailloux RJ. Estimation of the hydrogen peroxide producing capacities of liver and cardiac mitochondria isolated from C57BL/6N and C57BL/6J mice. Free Radic Biol Med. 2019;135:15–27.

18. Chalker J, Gardiner D, Kuksal N, Mailloux RJ. Characterization of the impact of glutaredoxin-2 (GRX2) deficiency on superoxide/hydrogen peroxide release from cardiac and liver mitochondria. Redox Biol. 2018;15:216–27.

19. Slade L, Chalker J, Kuksal N, Young A, Gardiner D, Mailloux RJ. Examination of the superoxide/hydrogen peroxide forming and quenching potential of mouse liver

mitochondria. Biochim Biophys Acta - Gen Subj. 2017;1861(8):1960–9.

20. Quinlan CL, Perevoshchikova I V., Hey-Mogensen M, Orr AL, Brand MD. Sites of reactive oxygen species generation by mitochondria oxidizing different substrates. Redox Biol. 2013;1(1):304–12.

21. Sies H. Hydrogen peroxide as a central redox signaling molecule in physiological oxidative stress: Oxidative eustress. Redox Biol. 2017;11:613–9.

22. Kuksal N, Chalker J, Mailloux RJ. Progress in understanding the molecular oxygen paradox - function of mitochondrial reactive oxygen species in cell signaling. Biol Chem. 2017;398(11):1209–27.

23. Sies H, Berndt C, Jones DP. Oxidative Stress. Annu Rev Biochem. 2017; 86:715-748.

24. Ayala A, Muñoz MF, Argüelles S. Lipid peroxidation: production, metabolism, and signaling mechanisms of malondialdehyde and 4-hydroxy-2-nonenal. Oxid Med Cell Longev. 2014;2014:360438.

25. Dai D-F, Chiao YA, Marcinek DJ, Szeto HH, Rabinovitch PS. Mitochondrial oxidative stress in aging and healthspan. Longev Heal. 2014;3:6.

26. Campbell MD, Duan J, Samuelson AT, Gaffrey MJ, Merrihew GE, Egertson JD, et al. Improving mitochondrial function with SS-31 reverses age-related redox stress and improves exercise tolerance in aged mice. Free Radic Biol Med. 2019;134:268–81.

27. Chandel NS, McClintock DS, Feliciano CE, Wood TM, Melendez JA, Rodriguez AM, et al. Reactive oxygen species generated at mitochondrial complex III stabilize hypoxia-inducible factor-1alpha during hypoxia: a mechanism of O2 sensing. J Biol Chem. 2000;275(33):25130–8.

28. Marinho HS, Real C, Cyrne L, Soares H, Antunes F. Hydrogen peroxide sensing,

signaling and regulation of transcription factors. Redox Biol. 2014;2:535–62.

29. Kramer PA, Duan J, Qian W-J, Marcinek DJ. The Measurement of Reversible Redox Dependent Post-translational Modifications and Their Regulation of Mitochondrial and Skeletal Muscle Function. Front Physiol. 2015;6:347.

30. Ullevig SL, Kim HS, Short JD, Tavakoli S, Weintraub ST, Downs K, et al. Protein S-Glutathionylation mediates macrophage responses to metabolic cues from the extracellular environment. Antioxid Redox Signal. 2016;25(15):836–51.

31. Lu J, Holmgren A. The thioredoxin antioxidant system. Free Radic Biol Med. 2014;66:75–87.

32. Zhang H, Du Y, Zhang X, Lu J, Holmgren A. Glutaredoxin-2 reduces both thioredoxin-2 and thioredoxin-1 and protects cells from apoptosis induced by auranofin and 4-Hydroxynonenal. Antioxid Redox Signal. 2014;21(5):669–81.

33. Lu SC. Glutathione synthesis. Biochim Biophys Acta. 2013;1830(5):3143–53.

34. Franklin CC, Backos DS, Mohar I, White CC, Forman HJ, Kavanagh TJ. Structure, function, and post-translational regulation of the catalytic and modifier subunits of glutamate cysteine ligase. Mol Aspects Med. 2009;30(1–2):86–98.

35. Tainer JA, Getzoff ED, Richardson JS, Richardson DC. Structure and mechanism of copper, zinc superoxide dismutase. Nature. 1983;306:284.

36. Guan T, Song J, Wang Y, Guo L, Yuan L, Zhao Y, et al. Expression and characterization of recombinant bifunctional enzymes with glutathione peroxidase and superoxide dismutase activities. Free Radic Biol Med. 2017;110:188–95.

37. Li Y, Huang T-T, Carlson EJ, Melov S, Ursell PC, Olson JL, et al. Dilated cardiomyopathy and neonatal lethality in mutant mice lacking manganese superoxide

dismutase. Nat Genet. 1995;11(4):376–81.

38. Watanabe K, Shibuya S, Ozawa Y, Nojiri H, Izuo N, Yokote K, et al. Superoxide dismutase 1 loss disturbs intracellular redox signaling, Resulting in Global Age-Related Pathological Changes. 2014;140165:1-10

39. Rindler PM, Cacciola A, Kinter M, Szweda LI. Catalase-dependent H_2O_2 consumption by cardiac mitochondria and redox-mediated loss in insulin signaling. Am J Physiol - Hear Circ Physiol. 2016;311(5):H1091–6.

40. Zhang J, Ye Z-W, Singh S, Townsend DM, Tew KD. An evolving understanding of the S-glutathionylation cycle in pathways of redox regulation. Free Radic Biol Med. 2018;120:204–16.

41. Gill RM, O'Brien M, Young A, Gardiner D, Mailloux RJ. Protein S-glutathionylation lowers superoxide/hydrogen peroxide release from skeletal muscle mitochondria through modification of complex I and inhibition of pyruvate uptake. PLoS One. 2018;13(2):e0192801.

42. Gallogly MM, Starke DW, Mieyal JJ. Mechanistic and kinetic details of catalysis of thiol-disulfide exchange by glutaredoxins and potential mechanisms of regulation. Antioxid Redox Signal. 2009;11(5):1059–81.

43. Jones DP, Sies H. The Redox Code. Antioxid Redox Signal. 2015;23(9):734–46.

44. Ye Z-W, Zhang J, Ancrum T, Manevich Y, Townsend DM, Tew KD. Glutathione *S*-Transferase P-mediated protein S-glutathionylation of resident endoplasmic reticulum proteins influences sensitivity to drug-induced unfolded protein response. Antioxid Redox Signal. 2017;26(6):247–61.

45. Taylor ER, Hurrell F, Shannon RJ, Lin T-K, Hirst J, Murphy MP. Reversible

glutathionylation of complex I increases mitochondrial superoxide formation. J Biol Chem. 2003;278(22):19603–10.

46. Garcia J, Han D, Sancheti H, Yap LP, Kaplowitz N, Cadenas E. Regulation of mitochondrial glutathione redox status and protein glutathionylation by respiratory substrates. J Biol Chem. 2010;285(51):39646–54.

47. Kramer PA, Duan J, Gaffrey MJ, Shukla AK, Wang L, Bammler TK, et al. Fatiguing contractions increase protein S-glutathionylation occupancy in mouse skeletal muscle. Redox Biol. 2018;17:367–76.

48. Wang S-B, Foster DB, Rucker J, O'Rourke B, Kass DA, Van Eyk JE. Redox regulation of mitochondrial ATP synthase: implications for cardiac resynchronization therapy. Circ Res. 2011;109(7):750–7.

49. Chen Y-R, Chen C-L, Pfeiffer DR, Zweier JL. Mitochondrial complex II in the post-ischemic heart: oxidative injury and the role of protein S-glutathionylation. J Biol Chem. 2007;282(45):32640–54.

50. Applegate MAB, Humphries KM, Szweda LI. Reversible inhibition of α-ketoglutarate dehydrogenase by hydrogen peroxide: glutathionylation and protection of lipoic acid †. Biochemistry. 2008;47(1):473–8.

51. Mailloux RJ, Craig Ayre D, Christian SL. Induction of mitochondrial reactive oxygen species production by GSH mediated S-glutathionylation of 2-oxoglutarate dehydrogenase. Redox Biol. 2016;8:285–97.

52. O'Brien M, Chalker J, Slade L, Gardiner D, Mailloux RJ. Protein S-glutathionylation alters superoxide/hydrogen peroxide emission from pyruvate dehydrogenase complex. Free Radic Biol Med. 2017;106:302–14.

53. Quinlan CL, Goncalves RLS, Hey-Mogensen M, Yadava N, Bunik VI, Brand MD. The 2-oxoacid dehydrogenase complexes in mitochondria can produce superoxide/hydrogen peroxide at much higher rates than complex I. J Biol Chem. 2014;289(12):8312–25.

54. Han D, Canali R, Garcia J, Aguilera R, Gallaher TK, Cadenas E. Sites and mechanisms of aconitase inactivation by peroxynitrite: modulation by citrate and glutathione. Biochemistry. 2005;44(36):11986–96.

55. Giangregorio N, Palmieri F, Indiveri C. Glutathione controls the redox state of the mitochondrial carnitine/acylcarnitine carrier Cys residues by glutathionylation. Biochim Biophys Acta - Gen Subj. 2013;1830(11):5299–304.

56. Mailloux RJ, Seifert EL, Bouillaud F, Aguer C, Collins S, Harper M-E. Glutathionylation acts as a control switch for uncoupling proteins UCP2 and UCP3. J Biol Chem. 2011;286(24):21865–75.

57. Echtay KS, Esteves TC, Pakay JL, Jekabsons MB, Lambert AJ, Portero-Otín M, et al. A signalling role for 4-hydroxy-2-nonenal in regulation of mitochondrial uncoupling. EMBO J. 2003;22(16):4103–10.

58. Talbot DA, Lambert AJ, Brand MD. Production of endogenous matrix superoxide from mitochondrial complex I leads to activation of uncoupling protein 3. FEBS Lett. 2004;556(1–3):111–5.

59. Young A, Gardiner D, Kuksal N, Gill R, O'Brien M, Mailloux RJ. Deletion of the glutaredoxin-2 gene protects mice from diet-induced weight gain which correlates with increased mitochondrial respiration and proton leaks in skeletal muscle. Antioxid Redox Signal. 2019;ars.2018.7715.

60. Mailloux RJ, Xuan JY, Beauchamp B, Jui L, Lou M, Harper M-E. Glutaredoxin-2 is

required to control proton leak through uncoupling protein-3. J Biol Chem. 2013;288(12):8365–79.

61. Queiroga CSF, Almeida AS, Martel C, Brenner C, Alves PM, Vieira HLA. Glutathionylation of adenine nucleotide translocase induced by carbon monoxide prevents mitochondrial membrane permeabilization and apoptosis. J Biol Chem. 2010;285(22):17077–88.

62. Queiroga CSF, Almeida AS, Martel C, Brenner C, Alves PM, Vieira HLA. Glutathionylation of adenine nucleotide translocase induced by carbon monoxide prevents mitochondrial membrane permeabilization and apoptosis. J Biol Chem. 2010;285(22):17077–88.

63. Picklo Sr MJ, Idso JP, Jackson MI. S-Glutathionylation of hepatic and visceral adipose proteins decreases in obese rats. Obesity (Silver Spring). 2013;21(2):297-305.

64. Shutt T, Geoffrion M, Milne R, McBride HM. The intracellular redox state is a core determinant of mitochondrial fusion. EMBO Rep. 2012;13(10):909–15.

65. Thaher O, Wolf C, Dey P, Pouya A, Wullner V, Tenzer S, Methner A. The thiol switch C684 in Mitofusin-2 mediates redox-induced alterations of mitochondrial shape and respiration. Neurochem Int. 2018;117:167–73.

66. Redpath CJ, Bou Khalil M, Drozdzal G, Radisic M, McBride HM. Mitochondrial hyperfusion during oxidative stress is coupled to a dysregulation in calcium handling within a C2C12 cell model. PLoS One. 2013;8(7):e69165.

67. Alegre-Cebollada J, Kosuri P, Giganti D, Eckels E, Rivas-Pardo JA, Hamdani N, et al. S-glutathionylation of cryptic cysteines enhances titin elasticity by blocking protein folding. Cell. 2014;156(6):1235–46.

68. Obesity and overweight [Internet]. [cited 2019 Jul 31]. Available from: *https://www.who.int/news-room/fact-sheets/detail/obesity-and-overweight*

69. Stats Canada [Internet]. {cited 2019 July 2]. Available from: *https://www150.statcan.gc.ca/n1/pub/82-625-x/2017001/article/14830-eng.htm#moreinfo*

70. Muoio DM. Metabolic inflexibility: when mitochondrial indecision leads to metabolic gridlock. Cell. 2014;159(6):1253–62.

71. de Mello AH, Costa AB, Engel JDG, Rezin GT. Mitochondrial dysfunction in obesity. Life Sci. 2018;192:26–32.

72. McMurray F, Patten DA, Harper M-E. Reactive oxygen species and oxidative stress in obesity-recent findings and empirical approaches. Obesity. 2016;24(11):2301–10.

73. Freeman LR, Zhang L, Nair A, Dasuri K, Francis J, Fernandez-Kim S-O, et al. Obesity increases cerebrocortical reactive oxygen species and impairs brainfunction. Free Radic Biol Med. 2013;56:226–33.

74. Kelley DE, Goodpaster B, Wing RR, Simoneau J-A. Skeletal muscle fatty acid metabolism in association with insulin resistance, obesity, and weight loss. Am J Physiol Metab. 1999;277(6):E1130–41.

75. Liu KA, Mager NAD. Women's involvement in clinical trials: historical perspective and future implications. Pharm Pract (Granada). 2016;14(1):708.

76. Sugiyama MG, Agellon LB. Sex differences in lipid metabolism and metabolic disease risk. Biochem Cell Biol. 2012;90(2):124–41.

77. Torres MJ, Ryan TE, Lin C-T, Zeczycki TN, Neufer PD. Impact of 17β-estradiol on complex I kinetics and H2O2 production in liver and skeletal muscle mitochondria. J Biol Chem. 2018;293(43):16889–98.

78. Torres MJ, Kew KA, Ryan TE, Pennington ER, Lin CT, Buddo KA, et al. 17β-Estradiol directly lowers mitochondrial membrane microviscosity and improves bioenergetic function in skeletal muscle. Cell Metab. 2018;27(1):167-179.e7.

79. Lichanska AM, Waters MJ. How growth hormone controls growth, obesity and sexual dimorphism. Trends Genet. 2008;24(1):41–7.

80. Miotto PM, McGlory C, Holloway TM, Phillips SM, Holloway GP. Sex differences in mitochondrial respiratory function in human skeletal muscle. Am J Physiol Integr Comp Physiol. 2018;314(6):R909–15.

81. Ventura-Clapier R, Moulin M, Piquereau J, Lemaire C, Mericskay M, Veksler V, et al. Mitochondria: a central target for sex differences in pathologies. Clin Sci. 2017;131(9):803–22.

82. Tarnopolsky MA. Gender differences in substrate metabolism during endurance exercise. Can J Appl Physiol. 2000;25(4):312–27.

83. Roepstorff C, Thiele M, Hillig T, Pilegaard H, Richter EA, Wojtaszewski JFP, et al. Higher skeletal muscle α_2 AMPK activation and lower energy charge and fat oxidation in men than in women during submaximal exercise. J Physiol. 2006;574(1):125–38.

84. Cardinale DA, Larsen FJ, Schiffer TA, Morales-Alamo D, Ekblom B, Calbet JAL, et al. Superior intrinsic mitochondrial respiration in women than in men. Front Physiol. 2018;9:1133.

85. Kander MC, Cui Y, Liu Z. Gender difference in oxidative stress: a new look at the mechanisms for cardiovascular diseases. J Cell Mol Med. 2017;21(5):1024-1032.

86. Wu H, Lin L, Giblin F, Ho Y-S, Lou MF. Glutaredoxin 2 knockout increases sensitivity to oxidative stress in mouse lens epithelial cells. Free Radic Biol Med. 2011;51(11):2108–

17.

87. Diet induced obesity | Envigo [Internet]. [cited 2019 Jul 11]. Available from: *https://www.envigo.com/products-services/teklad/laboratory-animal-diets/custom-research/diet-induced-obesity/*

88. Mallay S, Gill R, Young A, Mailloux RJ. Sex-dependent Differences in the Bioenergetics of liver and muscle mitochondria from mice containing a deletion for glutaredoxin-2. Antioxidants (Basel). 2019;8(8):E245.

89. Dikalov SI, Harrison DG. Methods for detection of mitochondrial and cellular reactive oxygen species. Antioxidants & redox signalling. 2014;20(2):372-382.

90. Zhang Y, Bharathi SS, Beck ME, Goetzman ES. The fatty acid oxidation enzyme long-chain acyl-CoA dehydrogenase can be a source of mitochondrial hydrogen peroxide. Redox Biol. 2019;26:101253.

91. Anderson EJ, Lustig ME, Boyle KE, Woodlief TL, Kane DA, Lin C-T, et al. Mitochondrial H2O2 emission and cellular redox state link excess fat intake to insulin resistance in both rodents and humans. J Clin Invest. 2009;119(3):573–81.

92. Quinlan CL, Goncalves RLS, Hey-Mogensen M, Yadava N, Bunik VI, Brand MD. The 2-oxoacid dehydrogenase complexes in mitochondria can produce superoxide/hydrogen peroxide at much higher rates than complex I. J Biol Chem. 2014;289(12):8312–25.

93. Perry CGR, Kane DA, Lanza IR, Neufer PD. Methods for assessing mitochondrial function in diabetes. Diabetes. 2013;62(4):1041–53.

94. Yang S, Zhu H, Li Y, Lin H, Gabrielson K, Trush MA, et al. Mitochondrial adaptations to obesity-related oxidant stress. Arch Biochem Biophys. 2000;378(2):259–68.

95. Zore T, Palafox M, Reue K. Sex differences in obesity, lipid metabolism, and

inflammationd A role for the sex chromosomes? Mol Metab. 2018;15:35–44.

96. Fan S, Yeon A, Shahid M, Anger JT, Eilber KS, Fiehn O, et al. Sex-associated differences in baseline urinary metabolites of healthy adults. Sci Rep. 2018;8(1):11883.

97. Palmer BF, Clegg DJ. The sexual dimorphism of obesity. Mol Cell Endocrinol. 2015;0:113–9.

98. Perlman RL. Mouse models of human disease An evolutionary perspective. Evolution (N Y). 2016;170–6.

99. Salinero AE, Anderson BM, Zuloaga KL. Sex differences in the metabolic effects of diet-induced obesity vary by age of onset. Int J Obes. 2018;42(5):1088–91.

100. Yamamoto T, Ohkuwa T, Itoh H, Sato Y, Naoi M. Effect of gender differences and voluntary exercise on antioxidant capacity in rats. Comp Biochem Physiol C Toxicol Pharmacol. 2002;132(4):437–44.

101. Green HJ, Fraser IG, Ranney DA. Male and female differences in enzyme activities of energy metabolism in vastus lateralis muscle. J Neurol Sci. 1984;65(3):323–31.

102. Haizlip KM, Harrison BC, Leinwand LA. Sex-based differences in skeletal muscle kinetics and fiber-type composition. Physiology (Bethesda). 2015;30(1):30–9.